

ISSN 2579-2784 (Print)
ISSN 2538-2788 (Online)

**MATHEMATICAL
PROBLEMS
OF COMPUTER
SCIENCE**

LXIII

**Yerevan
2025**

Հայաստանի Հանրապետության Գիտությունների ազգային ակադեմիայի
Ինֆորմատիկայի և ավտոմատացման պրոբլեմների ինստիտուտ
Институт проблем информатики и автоматизации Национальной академии наук
Республики Армения
Institute for Informatics and Automation Problems of the National Academy of
Sciences of the Republic of Armenia

**Մոմայուտերային գիտության
մաթեմատիկական խնդիրներ**

**Математические проблемы
компьютерных наук**

**Mathematical Problems of Computer
Science**

LXIII

ՀՐԱՏԱՐԱԿՎԱԾ Է ՀՀ ԳԱԱ ԻՆՖՈՐՄԱՏԻԿԱՅԻ ԵՎ ԱՎՏՈՄԱՏԱՑՄԱՆ
ՊՐՈԲԼԵՄՆԵՐԻ ԻՆՍՏԻՏՈՒՏԻ ԿՈՂՄԻՑ
ОПУБЛИКОВАНО ИНСТИТУТОМ ПРОБЛЕМ ИНФОРМАТИКИ И
АВТОМАТИЗАЦИИ НАН РА
PUBLISHED BY THE INSTITUTE FOR INFORMATICS AND AUTOMATION
PROBLEMS OF NAS RA

Կոմպյուտերային գիտության մաթեմատիկական խնդիրներ, LXIII

Կոմպյուտերային գիտության մաթեմատիկական խնդիրներ պարբերականը հրատարակվում է տարեկան երկու անգամ ՀՀ ԳԱԱ Ինֆորմատիկայի և ավտոմատացման պրոբլեմների ինստիտուտի (ԻԱՊԻ) կողմից: Այն ընդգրկում է տեսական և կիրառական մաթեմատիկայի, ինֆորմատիկայի և հաշվողական տեխնիկայի ժամանակակից ուղղությունները:

Այն ընդգրկված է Բարձրագույն որակավորման հանձնաժողովի ընդունելի ամսագրերի ցանկում:

Տպագրվում է Խմբագրական խորհրդի 2025թ. մայիսի 23-ի N 23-05/2 նիստի որոշման հիման վրա

ԽՄԲԱԳՐԱԿԱՆ ԽՈՐՀՈՒԲԴ

Գլխավոր խմբագիր

Յու. Շուքուրյան *Գիտությունների ազգային ակադեմիա, Հայաստան*
Գլխավոր խմբագրի տեղակալ

Մ. Հարությունյան *ՀՀ ԳԱԱ ԻԱՊԻ, Հայաստան*
Խմբագրական խորհրդի անդամներ

- Ս. Աղայան *Նյու Յորքի քաղաքային համալսարան, ԱՄՆ*
- Հ. Ավետիսյան *ՌԳԱ Համակարգային ծրագրավորման ինստիտուտ, Ռուսաստան*
- Լ. Ասլանյան *ՀՀ ԳԱԱ ԻԱՊԻ, Հայաստան*
- Հ. Ասցատրյան *ՀՀ ԳԱԱ ԻԱՊԻ, Հայաստան*
- Մ. Դայդե *Թուրուզի համակարգչային գիտությունների հետազոտական համալսարան, Ֆրանսիա*
- Ա. Դեգտյարյով *Սանկտ Պետերբուրգի պետական համալսարան, Ռուսաստան*
- Ե. Զորյան *Սինոփսիս, Կանադա*
- Յու. Հակոբյան *Երևանի պետական համալսարան, Հայաստան*
- Գ. Մարգարով *Հայաստանի ազգային պոլիտեխնիկական համալսարան, Հայաստան*
- Հ. Մելաձե *Վրաստանի տեխնիկական համալսարան, Վրաստան*
- Հ. Շահումյան *Դուբլինի համալսարանական քոլեջ, Իռլանդիա*
- Ս. Շուքուրյան *Երևանի պետական համալսարան, Հայաստան*
- Է. Պողոսյան *ՀՀ ԳԱԱ ԻԱՊԻ, Հայաստան*
- Վ. Սահակյան *ՀՀ ԳԱԱ ԻԱՊԻ, Հայաստան*

Պատասխանատու քարտուղար

Փ. Հակոբյան *ՀՀ ԳԱԱ ԻԱՊԻ, Հայաստան*

ISSN 2579-2784 (Print)

ISSN 2738-2788 (Online)

© Հրատարակված է ՀՀ ԳԱԱ Ինֆորմատիկայի և ավտոմատացման պրոբլեմների ինստիտուտի կողմից, 2025

Математические проблемы компьютерных наук, LXIII

Журнал **Математические проблемы компьютерных наук** издается два раза в год Институтом проблем информатики и автоматизации НАН РА. Он охватывает современные направления теоретической и прикладной математики, информатики и вычислительной техники.

Он включен в список допустимых журналов Высшей квалификационной комиссии.

Печатается на основании решения N 23-05/2 заседания
Редакционного совета от 23 мая 2025г.

РЕДАКЦИОННЫЙ СОВЕТ

Главный редактор

Ю. Шукурян Национальная академия наук, Армения

Зам. главного редактора

М. Арутюнян Институт проблем информатики и автоматизации, Армения

Члены редакционного совета

А. Аветисян Институт системного программирования РАН, Россия

С. Агаян Городской университет Нью-Йорка, США

Л. Асланян Институт проблем информатики и автоматизации, Армения

Г. Асцатрян Институт проблем информатики и автоматизации, Армения

Ю. Акопян Ереванский государственный университет, Армения

М. Дайде Тулузский научно-исследовательский институт компьютерных наук,
Франция

А. Дегтярев Санкт-Петербургский государственный университет, Россия

Е. Зорян Синописис, Канада

Г. Маргаров Национальный политехнический университет Армении, Армения

Г. Меладзе Грузинский технический университет, Грузия

Э. Погосян Институт проблем информатики и автоматизации, Армения

В. Саакян Институт проблем информатики и автоматизации, Армения

А. Шаумян Дублинский университетский колледж, Ирландия

С. Шукурян Ереванский государственный университет, Армения

Ответственный секретарь

П. Акопян Институт проблем информатики и автоматизации, Армения

ISSN 2579-2784 (Print)

ISSN 2738-2788 (Online)

© Опубликовано Институтом проблем информатики и автоматизации НАН РА, 2025

Mathematical Problems of Computer Science, LXIII

The periodical **Mathematical Problems of Computer Science** is published twice per year by the Institute for Informatics and Automation Problems of NAS RA. It covers modern directions of theoretical and applied mathematics, informatics and computer science.

It is included in the list of acceptable journals of the Higher Qualification Committee.

Printed on the basis of decision N 23-05/2 of the session of the Editorial Council dated May 23, 2025.

EDITORIAL COUNCIL

Editor-in-Chief

Yu. Shoukourian National Academy of Sciences, Armenia

Deputy Editor

M. Haroutunian Institute for Informatics and Automation Problems, Armenia

Members of the Editorial Council

S. Aгаian City University of New York, USA
A. Avetisyan Institute for System Programming of the RAS, Russia
L. Aslanyan Institute for Informatics and Automation Problems, Armenia
H. Astsatryan Institute for Informatics and Automation Problems, Armenia
M. Dayde Institute for Research in Computer Science from Toulouse, France
A. Degtyarev St. Petersburg University, Russia
Yu. Hakopian Yerevan State University, Armenia
G. Margarov National Polytechnic University of Armenia, Armenia
H. Meladze Georgian Technical University, Georgia
E. Pogossian Institute for Informatics and Automation Problems, Armenia
V. Sahakyan Institute for Informatics and Automation Problems, Armenia
A. Shahumyan University College Dublin, Ireland
S. Shoukourian Yerevan State University, Armenia
E. Zoryan Synopsys, Canada

Responsible Secretary

P. Hakobyan Institute for Informatics and Automation Problems, Armenia

ISSN 2579-2784 (Print)

ISSN 2738-2788 (Online)

© Published by the Institute for Informatics and Automation Problems of NAS RA, 2025

CONTENTS

D. Asatryan, L. Andreasyan, and G. Sazhumyan Full-Reference Image Quality Assessment Procedure Based on Rice Distribution Model	7
M. Haroutunian, J. Santosyan and P.Hakobyan Reliability Criteria in Source Coding Problem with Secret Component	14
M. Haroutunian and G. Gharagyozyan Information Theory Tools and Techniques to Overcome Machine Learning Challenges	25
A. Nahapetyan Fractal Geometry and Quantitative Evolution of the Aesthetic Appeal of Ancient Armenian Architecture Monuments	42
R. Chitchyan Regularly Varying of Normalizing Constants in Theorem of Convergence to Positive Stable Distribution	54
L. Tatli and P. Stevenson A Quantum Diophantine Equation Solution Finder	60
A. Atashyan, A. Lazyan and D. Hayrapetyan Implementation of Automata Mechanism for a Self-Organizing Swarm of Drones Platform	71
V. Altunyan FlashRMSD: An Effective Approach for Symmetry-Corrected RMSD Calculation with Extensive Benchmark Analysis	81

UDC 529.6

Full-Reference Image Quality Assessment Procedure Based on Rice Distribution Model

David G. Asatryan^{1,2}, Liana K. Andreasyan³ and Grigor S. Sazhumyan²

¹Institute for Informatics and Automation Problems of NAS RA, Yerevan, Armenia

²Russian-Armenian University, Yerevan, Armenia

³National Polytechnic University of Armenia, Yerevan, Armenia

e-mail: dasat@iiap.sci.am, landreasyan@yahoo.com, grigorsazhumyan@gmail.com

Abstract

The problem of full-reference image quality assessment is considered based on the application of the mathematical model of the Rice distribution. The gradient field of an image is adequately described by the Weibull distribution, which allows one to effectively analyze image properties, evaluate their similarity, classify them by quality, etc. In this paper, an attempt is made to solve similar problems using the above-mentioned model, relying, in particular, on additional properties of the Rice distribution associated with the normal approximation of the latter. It is shown that the structural similarity measure used in different problems is also applicable to the case of the Rice gradient field model. In particular, images from the TID2013 database are experimentally studied. The modeling results obtained from both the Weibull and Rice distribution models were compared using the mean square and structural similarity measures, as well as the Mean Opinion Score (MOS) values. It is shown that the types of distortions in these indicators are in complete agreement, while for some other types, the Rice distribution model shows better results.

Keywords: Gradient magnitude, Weibull distribution, Rice distribution, Parameter estimation, Image similarity, MOS.

Article info: Received 29 January 2025; sent for review 6 February 2025; accepted 28 April 2025.

1. Introduction

Creating effective quality assessment methods is one of the most popular and applied tasks in the field of image processing. The existing quality assessment methods are divided into two classes: Full-Reference and No-Reference methods. The Full-Reference method assumes the presence of

an initial reference image and a set of test images that differ from the reference due to the impact of certain distorting factors on the reference. In this case, the task of quality assessment consists of comparing the test and reference images using a pre-selected criterion.

No-reference methods do not assume the presence of a standard and the quality of the tested image assessing using only the internal properties of the image. The literature devoted to methods for assessing image quality is quite extensive. Of particular interest are methods that use the properties of the human visual system (HVS), since the "final judge" of quality assessment is a person. These methods often include Mean Opinion Score (MOS) values obtained by experts for images pre-distorted by different methods, which allows for checking the ability of the tested method to assess image quality. For this purpose, researchers have created extensive image databases accompanied by MOS assessments. Brief descriptions and links to dozens of such databases are given in [1].

Previously, we proposed a method for assessing image quality based on statistical analysis of the gradient field of an image [2]-[3]. In this case, the Weibull distribution model was adopted to describe the set of gradient magnitudes. It is shown that this model allows for solving many relevant applied problems. Thus, in [4], a Full-Reference algorithm for assessing image quality is proposed using the TID2013 database of distorted samples [5], for which MOS values are also given. The latter circumstance allows for assessing the quality of both the tested image and the applied testing algorithm.

This paper attempted to supplement the proposed approach using other gradient field models. The proposed method is based on the Rice distribution, which, unlike the Weibull distribution, converges to a normal distribution with appropriate parameter values, thus creating additional opportunities for adequate analysis and assessment of image quality.

The paper considers the following tasks:

- Modeling Weibull and Rice distributions with the ability to estimate parameters using various methods.
- Calculating the similarity of the original test image with distorted samples based on the proximity of the parameter values of the original and distorted samples. Comparison and analysis of the results obtained for both distribution models.
- Comparison of similarity values with the corresponding MOS values, comparing and analyzing the existing discrepancies, and developing appropriate recommendations.

2. Research Methodology

The methodology involves modeling the Weibull and Rice distributions, calculating the magnitudes of the gradients of the tested images, and estimating the parameters of both distributions based on these data. In this case, the gradients are estimated using the Sobel operator. The parameters of the Weibull distribution are estimated using the method of moments [3], and the maximum likelihood method is used to estimate the parameters of the Rice distribution [6]. The experiments were conducted on images from the TID2013 database, which also contains other auxiliary information. The MOS values, PSNR and W^2 image similarity measures were used to compare the results.

The probability density function of the two-parameter Weibull distribution is defined by the formula

$$f(x; \lambda, \eta) = \frac{\eta}{\lambda} \left(\frac{x}{\lambda}\right)^{\eta-1} \exp\left[-\left(\frac{x}{\lambda}\right)^\eta\right], x \geq 0,$$

where $\eta > 0$ - Shape parameter, and $\lambda > 0$ - Scale parameter.

The Rice distribution density is

$$f(x|\nu, \sigma) = \frac{x}{\sigma^2} \exp\left(-\frac{x^2 + \nu^2}{2\sigma^2}\right) I_0\left(\frac{x\nu}{\sigma^2}\right),$$

where $I_0(z)$ - modified Bessel function of the first kind of zero order.

Unlike the Weibull distribution, in the literature, it is customary to define the shape and scale parameters in the Rice case as the following functions of the initial parameters ν and σ : *Shape parameter* $K = \frac{\nu^2}{2\sigma^2}$, and *Scale parameter* $\Omega = \nu^2 + 2\sigma^2$. With the values of these quantities, we can estimate the initial parameters of the Rice distribution using the formulas

$$\nu = \sqrt{\frac{K\Omega}{K+1}}, \quad \sigma = \sqrt{\frac{\Omega}{2(K+1)}}.$$

It should be noted that in the field of signal processing theory and technology [7], an important characteristic is the signal-to-noise ratio, which is determined by the expression $\xi = \nu/\sigma$. It is known that $\xi \rightarrow \infty$ the Rice distribution tends to a normal distribution with parameters ν and σ . Moreover, for $\xi \geq 3$, this approximation is quite acceptable. This means that under this condition, we have $K \geq 4.5$, and the estimation of the parameters of the Rice distribution can be performed by traditional statistical methods.

The similarity (closeness) of two images can be estimated by the degree of closeness of the corresponding empirical Weibull or Rice distributions constructed from the set of magnitudes of the gradients of the compared images. However, instead of nonparametric statistical criteria of goodness of fit, we use a less accurate but simple measure [2], based on the closeness of the parameter estimates of the of the distributions under study themselves according to the formula

$$W^2 = \frac{\min(\eta_1, \eta_2) \min(\lambda_1, \lambda_2)}{\max(\eta_1, \eta_2) \max(\lambda_1, \lambda_2)} \quad 0 < W^2 \leq 1.$$

The resulting image similarity scores were then compared with the MOS scores using the Spearman correlation coefficient. This measure is often conveniently assessed by visual analysis, classifying their absolute values as equal to or less than one.

We have repeatedly and successfully applied the described method to various problems [3]. In particular, in [4], by analyzing the database data, the types of distortions for which the estimates of the Weibull distribution parameters belonged to one or another class from those described above were identified. In the present work, a similar analysis was carried out concerning the Rice distribution data.

3. Results of Modeling

Modeling was performed on all 3000 images of the database [5] simultaneously using both models. By analyzing the modeling results, the types of distortion identified for which the Weibull model leads to high or low values of the W^2 correlation with MOS. The corresponding values obtained using the Rician model are also recorded. It turned out those types of distortions, and chaotic behaviour of W^2 estimates were observed using the Weibull model, while the situation is much better using the Rician model. Of course, there may also be types of distortions for which the behaviour of these estimates completely coincides. Examples of this kind are given below.

Example 1. Matching indicators. Let us consider the images I01_01 and I01_04 of the base. Table 1 shows the calculation results.

Table 1. Comparative results for images I01 and I04

I01_01	PSNR	W ² Weibull	W ² Rician	MOS	i01_04	PSNR	W ² Weibull	W ² Rician	MOS
i01_01_1	36.50	0.92	0.92	5.51429	i01_04_1	30.14	0.69	0.69	5.76190
i01_01_2	33.56	0.87	0.87	5.56757	i01_04_2	29.26	0.55	0.55	5.47619
i01_01_3	30.48	0.79	0.78	4.94444	i01_04_3	27.85	0.40	0.38	4.92857
i01_01_4	27.51	0.68	0.66	4.37838	i01_04_4	25.95	0.27	0.23	4.26829
i01_01_5	24.50	0.56	0.51	3.86486	i01_04_5	23.61	0.18	0.13	4.00000

Visual analysis of the data in Table 1 shows that the nature of the change in the values of the considered indicators for these images is generally the same. First, we note the monotonic decrease in PSNR with an increase in the degree of applied distortion, which is a serious argument for using this indicator in the absence of MOS-type data. In this case, PSNR can also be used to assess the quality of the experiment to create MOS data. We also note the practical coincidence of the W² values for the considered images and the Weibull and Rice distributions, despite some deviations in the MOS series. However, as shown in [4], these patterns are not always observed, so several similar examples with appropriate comments are given below.

Table 2 compares the calculation results for images i05 and i07, subjected to the same type of distortion (Contrast change). As can be seen, PSNR decreases monotonically in both cases, and W² with the Rice distribution also decreases monotonically in the case of image i05_17. However, deviations from monotony are observed for i0_17.

Table 2. Comparison of similarity scores with MOS scores

I05_17	PSNR	W ² Weibull	W ² Rician	MOS	i07_17	PSNR	W ² Weibull	W ² Rician	MOS
1	33.51	0.9	0.79	5.3	1	35.97	0.9	0.8	5.54545
2	28.92	0.85	0.74	6.82927	2	30.28	0.84	0.77	6.4
3	25.53	0.75	0.55	4.025	3	28.06	0.75	0.55	4.40476
4	22.81	0.77	0.53	6.56098	4	23.60	0.72	0.6	6.72727
5	19.47	0.5	0.24	2.8	5	22.00	0.5	0.25	3.34091

The MOS values do not decrease monotonically, as expected by the meaning of the experiments, but the nature of the changes is similar for both images. This effect can be explained by the peculiarities of the human visual system (HVS) that inadequately react to changes in image contrast in one direction or another.

Thus, the results of Table 2 indicate some advantages of using the Rice distribution when assessing image quality.

It is interesting to compare the calculation results for the same image with different types of distortion. Table 3 shows the data for the i04 image with changes in brightness (Mean shift (intensity shift)) and contrast (Contrast change). In this case, deviations from the monotony of the similarity indices W² with the Weibull model and MOS were observed, while W² with the Rician model decreased monotonically, corresponding to the meaning of the experiment on creating the TID2013 database.

Table 3. Comparison of ratings for different types of image distortion

I04_16	PSNR	W ² Weibull	W ² Rician	MOS	i04_17	PSNR	W ² Weibull	W ² Rician	MOS
1	33.33	0.99	0.84	6.28571	1	30.51	0.9	0.84	6
2	24.63	1	0.68	6.64286	2	28.79	0.81	0.68	6.66667
3	24.52	0.98	0.59	6.09524	3	27.62	0.75	0.59	4.78049
4	17.57	0.99	0.50	5.66667	4	24.47	0.69	0.50	7.21429
5	17.94	0.79	0.26	5.15385	5	23.13	0.50	0.26	3.925

Similar results were obtained for images i21, i24 and several others from the same database with the same types of distortions.

4. Conclusions

The problem of Full-Reference image quality assessment is considered based on applying the mathematical model of the Rice distribution. The previously proposed technique is based on the application of the Weibull distribution model and the measures of mean square and structural similarity of images. In this paper, the properties of images from the TID2013 database are experimentally investigated, evaluating and comparing their similarity indices according to the Weibull and Rice models, as well as the MOS index. This shows that the applied measure of structural similarity is also applicable to the case of the Rice gradient field model. It is also shown that for types of distortion, these indices are in complete agreement, while for some other types; the Rice distribution model shows better results.

□□

References

- [1] □G. Zhai and X. Min, “Perceptual image quality assessment: a survey”, *Sci. China Inf. Sci.*, vol. 63, no.11, 211301, 2020. doi:10.1007/s11432-019-2757-1
- [2] □D. Asatryan and K. Egiazarian, “Quality assessment measure based on image structural properties”, *2009 International Workshop on Local and Non-Local Approximation in Image Processing*, Tuusula, Finland, pp. 70-73, 2009. doi:10.1109/lnla.2009.5278400
- [3] □D. Asatryan, “Gradient-based technique for image structural analysis and applications”, *Computer Optics*, vol.43, no. 2,pp.245-250, 2019. doi: 10.18287/2412-6179-2019-43-2-245-250.
- [4] □D. Asatryan, M. Haroutunian, G. Sazhumyan and G. Hakobyan, “Procedure for analyzing the quality, structure and subjective rating of distorted images by the Full-Reference technique”, *Intern. Scientific Journal Mathematical Modeling*, 2022, vol. 6, no.4, pp. 100-102, 2022.
- [5] □N. Ponomarenko, L. Jin, O. Ieremeiev, V. Lukin, K. Egiazarian, J. Astola, B. Vozel, K. Chehdi, M. Carli, F. Battisti and C.-C. Jay Kuo, “Image database TID2013: Peculiarities, results and perspectives”, *Signal Processing: Image Communication*, vol. 30, pp. 57-77, 2015.

- [6] T. Yakovleva, “Peculiarities of the rice statistical distribution: mathematical substantiation”, *Applied and Computational Mathematics*, Science Publishing Group, vol.7, no. 4, pp. 188-196, 2018. doi: 10.11648/j.acm.20180704.12.
- [7] Б. Левин, “Теоретические основы статистической радиотехники”, М.: Радио и связь, 656 с., 1989.

Ռայսի բաշխման մոդելի հիման վրա ստուգանմուշի հետ համեմատման մեթոդով պատկերի որակի գնահատման ընթացակարգ

Դավիթ Գ. Ասատրյան^{1,2}, Լիանա Կ. Անդրեասյան³ և Գրիգոր Ս. Սաժումյան²

¹ՀՀ ԳԱԱ Ինֆորմատիկայի և ավտոմոտացման պրոբլեմների ինստիտուտ, Երևան, Հայաստան

²Հայ-Ռուսական համալսարան, Երևան, Հայաստան

³Հայաստանի ազգային պոլիտեխնիկական համալսարան, Երևան, Հայաստան

e-mail: dasat@iiap.sci.am, landreasyan@yahoo.com, grigorsazhumyan@gmail.com

Ամփոփում

Դիտարկվում է ստուգանմուշի հետ համեմատման մեթոդով պատկերի որակի գնահատման խնդիրը Ռայսի բաշխման մաթեմատիկական մոդելի կիրառման հիման վրա: Հայտնի է, որ պատկերի գրադիենտային դաշտը համարժեքորեն նկարագրվում է Վեյբուլի բաշխմամբ, ինչը թույլ է տալիս արդյունավետորեն վերլուծել պատկերների հատկությունները, գնահատել դրանց նմանությունը, դասակարգել դրանք ըստ որակի և այլն: Այս հոդվածում փորձ է արվել լուծել նմանատիպ խնդիրներ՝ օգտագործելով վերը նշված մոդելը՝ հենվելով, մասնավորապես, Ռայսի բաշխման լրացուցիչ հատկությունների վրա՝ կապված վերջինիս նորմալ մոտարկման հետ: Ցույց է տրվել, որ տարբեր խնդիրներում օգտագործվող կառուցվածքային նմանության չափանիշը կիրառելի է նաև Ռայսի մոդելի դեպքում: Մասնավորապես, փորձնականորեն ուսումնասիրվել են TID2013 տվյալների բազայի պատկերները: Վեյբուլի և Ռայսի բաշխման մոդելների միջոցով ստացված մոդելավորման արդյունքները համեմատվել են՝ օգտագործելով միջին քառակուսային և կառուցվածքային նմանության չափանիշները, ինչպես նաև՝ փորձագիտական կարծիքի միջին գնահատականի արժեքները (MOS): Ցույց է տրված, որ աղավաղումների տեսակների այս ցուցանիշները լիովին համընկնում են, մինչդեռ որոշ այլ տեսակների համար Ռայսի բաշխման մոդելը ցույց է տալիս ավելի լավ արդյունքներ:

Բանալի բառեր՝ գրադիենտային մագնիտուտ, Վեյբուլի բաշխում, Ռայսի բաշխում, պարամետրերի գնահատում, պատկերների նմանություն, կարծիքի միջին գնահատական (MOS):

Процедура оценивания качества изображения методом сравнения с эталоном на основе модели распределения Райса

Давид Г. Асатрян^{1,2}, Лиана К. Андреасян³ и Григор С. Сажумян²

¹Институт проблем информатики и автоматизации НАН РА, Ереван, Армения

²Российско-Армянский университет, Ереван, Армения

³Национальный политехнический университет Армении, Ереван, Армения
e-mail: dasat@iiap.sci.am, landreasyan@yahoo.com, grigorsazhumyan@gmail.com

Аннотация

Рассматривается задача оценивания качества изображения методом сравнения с эталоном, основанная на применении математической модели распределения Райса. Известно, что градиентное поле изображения достаточно адекватно описывается распределением Вейбулла, что позволяет эффективно анализировать свойства изображений, оценивать их сходство, классифицировать по качеству и др. В данной работе сделана попытка решать аналогичные задачи по упомянутой модели, рассчитывая, в частности, на дополнительные свойства распределения Райса, связанные с нормальным приближением последнего. Показано, что применяемая в разных задачах мера структурного сходства применима и в случае райсовской модели градиентного поля. В частности, экспериментально исследованы изображения из базы данных TID2013. Сопоставлены результаты моделирования, полученные по моделям распределений Вейбулла и Райса, используя меры среднеквадратического и структурного сходства, а также значения экспертных оценок (MOS). Показано, что для определённых типов искажений эти показатели находятся в полном согласии, в то время как для некоторых других типов модель распределения Райса показывает лучшие результаты.

Ключевые слова: магнитуа градиента, распределение Вейбулла, распределение Райса, оценивание параметров, сходство изображений, MOS.

UDC 519.72

Reliability Criteria in Source Coding Problem with Secret Component

Mariam E. Haroutunian¹, Jemma S. Santosyan² and Parandzem M. Hakobyan¹

¹Institute for Informatics and Automation Problems of NAS RA, Yerevan, Armenia

²Vanadzor State University, Vanadzor, Armenia

e-mail: armar@sci.am, j.santosian@gmail.com, par_h@iiap.sci.am

Abstract

This work addresses a source coding problem for one-way sources with correlated outputs. In this scenario, one source output must be transmitted to the receiver within a specified distortion level, similar to conventional source coding. Simultaneously, the other source output must be kept as confidential as possible from the receiver or a potential wiretapper. For this model, the rate-reliability-distortion-equivocation function and the equivocation-reliability-distortion function are defined and analyzed.

Keywords: Rate-reliability-distortion-equivocation function, Source coding.

Article info: Received 27 March 2025; sent for review 1 April 2025; accepted 2 May 2025.

1. Introduction

The source coding problem in information theory focuses on the efficient encoding of information generated by a source so it can be transmitted or stored with minimal redundancy. The main goal is to represent the information as compactly as possible while still enabling perfect or near-perfect reconstruction of the original message.

In lossy coding, some information is sacrificed to achieve greater compression. The reconstructed data is an approximation of the original, acceptable when perfect fidelity isn't necessary. JPEG for images and MP3 for audio are examples of lossy coding methods. In general, source coding is fundamental to efficient data transmission and storage in various fields, including:

- Digital communications (e.g., reducing bandwidth in cellular networks),
- Data compression (e.g., ZIP files, media codecs),
- Machine learning and statistics (e.g., feature selection and data encoding),
- Distributed storage systems (e.g., minimizing storage costs by reducing redundancy).

Shannon **rate-distortion function** (RD) [1] shows the dependence of the asymptotically minimal coding rate on a required average fidelity (distortion) threshold for source noiseless transmission.

The source coding problem for a one-way communication system with correlated source outputs was considered by Yamamoto in [2], where one of the outputs must be transmitted to the receiver within a given distortion level as in ordinary source coding, while the other source output has to be kept as secret as possible from the wiretapper (Fig. 1). The **rate-distortion-equivocation function** (RDE) was defined and evaluated, which is the minimum rate necessary to attain both the equivocation tolerance for the wiretapper and the distortion tolerance for the receiver.

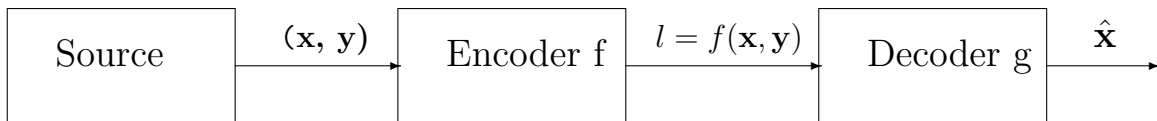


Fig.1. One-way communication system with correlated source outputs.

Previously, Yamamoto [3] studied the source coding problem for cascade and branching communication systems. Later in [4], he considered the RD problem for a communication system with a secondary decoder to be hindered, where security is evaluated by the distortion measure instead of the equivocation function used in [2]. RD problem related to security setting is considered also in [5].

Another characteristic in source coding subject to a distortion criterion can be considered, namely **rate-reliability-distortion function** (RRD) as the minimal rate at which the message of a source can be encoded and then reconstructed by the receiver with an error probability that decreases exponentially with the codeword length. The coding rate as a function of the given distortion level and error exponent E has been studied for various source models. We refer to [6], which in turn refers to the list of main results. In addition to that list, it is worth mentioning [7], where the RRD region with partial secrecy under the distortion criterion is considered, which is the generalization of the encoding problem studied in [3].

Here we introduce and investigate the **rate-reliability-distortion-equivocation function** (RRDE) for the model from [2]. This function combines all aspects, including error control and security. This framework is useful in scenarios involving secure and reliable data transmission, where the goal is to balance the trade-offs among rate, reliability, distortion, and secrecy. Balancing these four elements in a single framework is challenging because improving one aspect often comes at the expense of another.

This setting of source coding with a secret component has many applications, including:

- *sensor networks* in distributed systems like IoT, to ensure that data is compressed, securely transmitted, and reliably received,
- *video and audio streaming* to ensure high-quality, low-latency streaming with some degree of security against unauthorized access,
- *cryptographic communication systems* need guidelines for encoding methods that balance data rate, fidelity, error protection, and secrecy.

Particularly, in [8], the *utility-privacy tradeoff* problem is modeled as source coding and solved using the tool of RRD theory.

In this paper, we introduce and study the set of E -achievable (R, Δ_d, Δ_e) triples. As a consequence, we obtain the equivocation-reliability-distortion function and the rate-reliability-distortion function.

The paper is organized as follows. In the next section, the main notations and definitions are given. The main results are formulated in Section 3. The proof of the main theorem is given in the Appendix. The paper is summarized in Section 5.

2. Notations and Definitions

The Discrete Memoryless Source (DMS) is defined as a sequence $\{(X_i, Y_i)\}_{i=1}^{\infty}$ of discrete independent identically distributed (i. i. d.) random variables X and Y , taking values in finite sets \mathcal{X} and \mathcal{Y} , which are the alphabets of messages of the source, respectively. Let

$$P^* = \{P^*(x, y), x \in \mathcal{X}, y \in \mathcal{Y}\}$$

be the generating probability distribution of the source outputs (X, Y) . The source is memoryless, which means that for N -length vector pairs $\mathbf{x} = (x_1, x_2, \dots, x_N) \in \mathcal{X}^N$ and $\mathbf{y} = (y_1, y_2, \dots, y_N) \in \mathcal{Y}^N$

$$P^{*N}(\mathbf{x}, \mathbf{y}) = \prod_{n=1}^N P^*(x_n, y_n).$$

The finite set $\hat{\mathcal{X}}$, different in general from \mathcal{X} , is the reproduction alphabet at the receiver.

A code (f_N, g_N) is defined by a pair of mappings: a coding

$$f_N : \mathcal{X}^N \times \mathcal{Y}^N \rightarrow \{1, 2, \dots, L(N)\},$$

and decoding

$$g_N : \{1, 2, \dots, L(N)\} \rightarrow \hat{\mathcal{X}},$$

where $L(N)$ is the code volume. Code rate is

$$R(f_N, g_N) = \frac{1}{N} \log L(N).$$

Throughout this paper, all log-s and exp-s are of base 2.

We consider the distortion measure

$$d : \mathcal{X} \times \hat{\mathcal{X}} \rightarrow [0; \infty)$$

between source and reconstruction messages. The distortion measure for N -length sequences is the average of the components' distortions

$$d(\mathbf{x}, \hat{\mathbf{x}}) = \frac{1}{N} \sum_{n=1}^N d(x_n, \hat{x}_n).$$

The task of this system is to ensure restoration of one of the components of source messages, i.e. X , at the receiver within a given distortion level Δ_d and with a small error probability. At the same time, the other source output Y has to be kept as secret as possible from the receiver or wiretapper. This protection level is measured by the **equivocation rate**, defined as

$$R_e = \frac{1}{N} H(\mathbf{Y} | L(N)),$$

where $H(\mathbf{Y}|L(N))$ is the conditional entropy [9]. In other words, the equivocation rate indicates the receiver's uncertainty about \mathbf{y} given l .

We define the **error probability** of the code (f_N, g_N) as

$$e(f_N, g_N, P^*, \Delta_d) = 1 - P^{*N}(\mathcal{A}),$$

where \mathcal{A} is the set of satisfactorily transmitted vectors:

$$\mathcal{A} = \{(\mathbf{x}, \mathbf{y}) : g_N(f_N(\mathbf{x}, \mathbf{y})) = \hat{\mathbf{x}}, d(\mathbf{x}, \hat{\mathbf{x}}) \leq \Delta_d\}.$$

Definition 1. The triple (R, Δ_d, Δ_e) is called E -achievable for given $P^*, E > 0, \Delta_d \geq 0, \Delta_e \geq 0$, if for every $\epsilon > 0, \delta > 0$, there exists a code (f_N, g_N) such that

$$\frac{1}{N} \log L(N) \leq R + \epsilon,$$

the error probability is exponentially small

$$e(f_N, g_N, P^*, \Delta_d) \leq \exp\{-N(E - \delta)\}$$

and the equivocation rate

$$R_e \geq \Delta_e - \epsilon.$$

We denote by $\mathcal{R}^*(E)$ the set of all E -achievable triples. We will consider the **distortion-equivocation E -achievable region**:

$$\mathcal{R}_{\Delta_d, \Delta_e}^*(E) = \{(\Delta_d, \Delta_e) : (R, \Delta_d, \Delta_e) \in \mathcal{R}^*(E) \text{ for some } R \geq 0\}.$$

Then the **RRDE function** is defined as

$$R^*(E, \Delta_d, \Delta_e) = \min_{(R, \Delta_d, \Delta_e) \in \mathcal{R}^*(E)} R.$$

At last, the **equivocation-reliability-distortion function (ERD)** is:

$$\Gamma^*(E, \Delta_d) = \max_{(\Delta_d, \Delta_e) \in \mathcal{R}_{\Delta_d, \Delta_e}^*(E)} \Delta_e.$$

3. Formulation of the Results

Let

$$Q = \{Q(\hat{x}|x, y), x \in \mathcal{X}, y \in \mathcal{Y}, \hat{x} \in \hat{\mathcal{X}}\}$$

be a conditional PD on $\hat{\mathcal{X}}$ for given x, y .

Consider the following set of distributions P :

$$\alpha(E, P^*) = \{P : D(P||P^*) \leq E\},$$

where $D(P||P^*)$ is the KL-divergence [9].

Let $\mathcal{Q}(P, \Delta_d, \Delta_e)$ be the set of all conditional PDs $Q_P(\hat{x}|x, y) = Q_P$, corresponding to the PD P , for which the following conditions hold:

$$\begin{aligned} \mathbf{E}d(X, \hat{X}) &= \sum_{x, y, \hat{x}} P(x, y) Q_P(\hat{x}|x, y) d(x, \hat{x}) \leq \Delta_d, \\ H_{P, Q_P}(Y|\hat{X}) &\geq \Delta_e. \end{aligned} \tag{1}$$

Then

$$\mathcal{Q}(P, \Delta_d) = \bigcup_{H_{P, Q_P}(Y|X) \leq \Delta_e \leq H_{P, Q_P}(Y)} \mathcal{Q}(P, \Delta_d, \Delta_e).$$

The main result of this paper is presented in the following theorem.

Theorem 1. *For given P^* , every $E > 0$,*

$$\mathcal{R}^*(E) = \left\{ \begin{array}{l} (R, \Delta_d, \Delta_e) : \Delta_d \geq 0, \Delta_e \geq 0, \\ 0 \leq R_e \leq \min_{P \in \alpha(E, P^*)} \max_{Q_P \in \mathcal{Q}(P, \Delta_d)} H_{P, Q_P}(Y|\hat{X}), \\ R \geq \max_{P \in \alpha(E, P^*)} \min_{Q_P \in \mathcal{Q}(P, \Delta_d, \Delta_e)} I_{P, Q_P}(X, Y; \hat{X}) \end{array} \right\}.$$

Corollary 2. *The ERD function equals*

$$\Gamma^*(E, \Delta_d) = \min_{P \in \alpha(E, P^*)} \max_{Q_P \in \mathcal{Q}(P, \Delta_d)} H_{P, Q_P}(Y|\hat{X}).$$

Corollary 3.

$$\mathcal{R}_{\Delta_d, \Delta_e}^*(E) = \left\{ \begin{array}{l} R(E, \Delta_d, \Delta_e) : \Delta_d \geq 0, \\ 0 \leq \Delta_e \leq \Gamma^*(E, \Delta_d) \end{array} \right\}.$$

Corollary 4. *The RRDE function equals*

$$R^*(E, \Delta_d, \Delta_e) = \max_{P \in \alpha(E, P^*)} \min_{Q_P \in \mathcal{Q}(P, \Delta_d, \Delta_e)} I_{P, Q_P}(X, Y; \hat{X}).$$

Corollary 5. *The limits of the RRDE and ERD functions when E tends to 0, coincide with the RDR and ED functions stated in [2]:*

$$\lim_{E \rightarrow 0} R^*(E, \Delta_d, \Delta_e) = R^*(\Delta_d, \Delta_e) = \min_{Q_P^* \in \mathcal{Q}(P^*, \Delta_d, \Delta_e)} I_{P^*, Q_P^*}(X, Y; \hat{X}).$$

$$\lim_{E \rightarrow 0} \Gamma^*(E, \Delta_d) = \Gamma^*(\Delta_d) = \max_{Q_{P^*} \in \mathcal{Q}(P^*, \Delta_d)} H_{P^*, Q_{P^*}}(Y|\hat{X}).$$

The proofs are given in the Appendix and are based on the method of types [10].

4. Conclusion

In this paper, we introduced and examined the set of E -achievable (R, Δ_d, Δ_e) triples. Additionally, we defined and analyzed the ERD function and the RRDE. The limits of these functions, when E tends to 0, coincide with the results from [2].

Appendix

For the proof of Theorem 1, we will use the following modification of the Covering Lemma [11], [6].

Lemma 1. *Let for $\epsilon > 0$*

$$J(P, Q) = \exp\{N(I_{P,Q}(X, Y; \hat{X}) + \epsilon)\}.$$

Then, for every type P and conditional type Q , there exists a collection of vectors

$$\{\hat{\mathbf{x}}_j \in \mathcal{T}_{P,Q}^N(\hat{X}), j = 1, \dots, J(P, Q)\},$$

such that the set

$$\{\mathcal{T}_{P,Q}^N(X, Y|\hat{\mathbf{x}}_j), j = 1, \dots, J(P, Q)\},$$

covers $\mathcal{T}_P^N(X, Y)$ for N large enough, that is

$$\mathcal{T}_P^N(X, Y) \subset \bigcup_{j=1}^{J(P,Q)} \mathcal{T}_{P,Q}^N(X, Y|\hat{\mathbf{x}}_j).$$

We omit the proof of Lemma 1, since it is similar to the proof of Lemma 5.5. from [6].

Proof of the Theorem 1: First we shall show that

$$\mathcal{R}^*(E) \supseteq \left\{ \begin{array}{l} (R, \Delta_d, \Delta_e) : \Delta_d \geq 0, \Delta_e \geq 0, \\ 0 \leq R_e \leq \min_{P \in \alpha(E, P^*)} \max_{Q_P \in \mathcal{Q}(P, \Delta_d)} H_{P, Q_P}(Y|\hat{X}), \\ R \geq \max_{P \in \alpha(E, P^*)} \min_{Q_P \in \mathcal{Q}(P, \Delta_d, \Delta_e)} I_{P, Q_P}(X, Y; \hat{X}) \end{array} \right\}.$$

Let us represent the set of all source messages of length N as follows:

$$\mathcal{X}^N \times \mathcal{Y}^N = \bigcup_{P \in \mathcal{P}_N(X \times Y)} \mathcal{T}_P^N(X, Y),$$

where $\mathcal{P}_N(X \times Y)$ is the set of possible types of pairs $(\mathbf{x}, \mathbf{y}) \in \mathcal{X}^N \times \mathcal{Y}^N$.

Using the properties of types and the definition of the set $\alpha(E, P^*)$ for each $\delta > 0$, we can find the estimation of the probability of appearance of the source of types beyond $\alpha(E + \delta, P^*)$ as follows:

$$\begin{aligned} P^{*N} \left(\bigcup_{P \notin \alpha(E+\delta, P^*)} \mathcal{T}_P^N(X, Y) \right) &= \sum_{P \notin \alpha(E+\delta, P^*)} P^{*N} \left(\mathcal{T}_P^N(X, Y) \right) \\ &\leq (N+1)^{|\mathcal{X}||\mathcal{Y}|} \exp \left\{ -N \min_{P \notin \alpha(E+\delta, P^*)} D(P||P^*) \right\} \quad (2) \\ &\leq \exp \{-NE - N\delta + |\mathcal{X}||\mathcal{Y}| \log(N+1)\} \\ &\leq \exp \{-N(E + \delta/2)\}. \end{aligned}$$

For each $\Delta_d \geq 0$, let us pick some types $P \in \alpha(E + \delta, P^*)$ and some $Q_P \in \mathcal{Q}(P, \Delta_d, \Delta_e)$.
Let

$$C(P, Q_P, j) = \mathcal{T}_{P, Q_P}^N(X, Y | \hat{\mathbf{x}}_j) - \bigcup_{j' < j} \mathcal{T}_{P, Q_P}^N(X, Y | \hat{\mathbf{x}}_{j'}), \quad j = \overline{1, J(P, Q_P)}.$$

We define a code (f_N, g_N) for vector pairs of type P with the encoding:

$$f_N(\mathbf{x}, \mathbf{y}) = \begin{cases} j, & \text{when } (\mathbf{x}, \mathbf{y}) \in C(P, Q_P, j), P \in \alpha(E + \delta, P^*), \\ j_0, & \text{when } (\mathbf{x}, \mathbf{y}) \in \mathcal{T}_P^N(X, Y), P \notin \alpha(E + \delta, P^*), \end{cases}$$

and the decoding

$$g_N(j) = \hat{\mathbf{x}}_j, \quad g_N(j_0) = \hat{\mathbf{x}}_0,$$

where the number j_0 and the reconstruction vector $\hat{\mathbf{x}}_0$ are fixed. Obviously, with such code, an error occurs only when the number j_0 is sent.

According to the definition of the code and the inequality (1), for $P \in \alpha(E + \delta, P^*)$ and $Q_P \in \mathcal{Q}(P, \Delta_d, \Delta_e)$ we have:

$$\begin{aligned} d(\mathbf{x}, \hat{\mathbf{x}}_j) &= \frac{1}{N} \sum_{x, \hat{x}} n(x, \hat{x} | \mathbf{x}, \hat{\mathbf{x}}_j) d(x, \hat{x}) \\ &= \sum_{x, y, \hat{x}} P(x, y) Q_P(\hat{x} | x, y) d(x, \hat{x}) \\ &= \mathbf{E}_{P, Q_P} d(X, \hat{X}) \leq \Delta_d, \quad j = \overline{1, J(P, Q_P)}. \end{aligned}$$

According to Lemma 1, the number of vectors $\hat{\mathbf{x}}$ for a fixed type P and corresponding conditional type $Q_P \in \mathcal{Q}(P, \Delta_d, \Delta_e)$ is:

$$L_{P, Q_P}(N) = \exp \left\{ N(I_{P, Q_P}(X, Y; \hat{X}) + \epsilon) \right\}.$$

Then, taking into account that the number of types has a polynomial estimate [10]

$$\begin{aligned} L(N) &\leq \sum_{P \in \alpha(E + \delta, P^*)} \min_{Q_P \in \mathcal{Q}(P, \Delta_d, \Delta_e)} L_{P, Q_P}(N) \\ &\leq (N + 1)^{|\mathcal{X}||\mathcal{Y}|} \max_{P \in \alpha(E + \delta, P^*)} \min_{Q_P \in \mathcal{Q}(P, \Delta_d, \Delta_e)} \exp \left\{ N(I_{P, Q_P}(X, Y; \hat{X}) + \epsilon) \right\}. \end{aligned}$$

Hence, the corresponding limit for the transmission rate is:

$$\begin{aligned} \frac{1}{N} \log L_{P, Q_P}(N) - \epsilon - \frac{1}{N} |\mathcal{X}| |\mathcal{Y}| \log(N + 1) &\leq \\ &\leq \max_{P \in \alpha(E + \delta, P^*)} \min_{Q_P \in \mathcal{Q}(P, \Delta_d, \Delta_e)} I_{P, Q_P}(X, Y; \hat{X}). \end{aligned} \quad (3)$$

Taking into account the arbitrariness of ϵ and δ and the continuity of the information expression (3), we get:

$$R^*(E, \Delta_d, \Delta_e) \leq \max_{P \in \alpha(E, P^*)} \min_{Q_P \in \mathcal{Q}(P, \Delta_d, \Delta_e)} I_{P, Q_P}(X, Y; \hat{X}). \quad (4)$$

For this code, the equivocation rate can be evaluated as follows:

$$\begin{aligned} \frac{1}{N}H(\mathbf{Y}|L(N)) &\geq \frac{1}{N} \sum_{j=1}^{L(N)} H_{P^*,Q_{P^*}}(Y|\mathbf{x}, \mathbf{y} \in C(P, Q_P, j)) P^*\{\mathbf{x}, \mathbf{y} \in C(P, Q_P, j)\} \\ &= \frac{1}{N} \sum_{j=1}^{L(N)} \left[- \sum_{\mathbf{y}:\mathbf{x},\mathbf{y} \in C(P, Q_P, j)} P^*\{\mathbf{y}|\mathbf{x}, \mathbf{y} \in C(P, Q_P, j)\} \log P^*\{\mathbf{y}|\mathbf{x}, \mathbf{y} \in C(P, Q_P, j)\} \right] \\ &\quad \times P^*\{\mathbf{x}, \mathbf{y} \in C(P, Q_P, j)\}. \end{aligned} \quad (5)$$

For any \mathbf{y} such that $\mathbf{x}, \mathbf{y} \in C(P, Q_P, j)$ for some \mathbf{x}

$$\begin{aligned} P^*\{\mathbf{y}|\mathbf{x}, \mathbf{y} \in C(P, Q_P, j)\} &= \frac{P^*\{\mathbf{x}, \mathbf{y} \in C(P, Q_P, j)|\mathbf{y}\} P^*\{\mathbf{y}\}}{P^*\{\mathbf{x}, \mathbf{y} \in C(P, Q_P, j)\}} \\ &= \frac{\sum_{\mathbf{x}, \mathbf{y} \in C(P, Q_P, j)} P^*\{\mathbf{x}, \mathbf{y}|\mathbf{y}\} P^*\{\mathbf{y}\}}{\sum_{\mathbf{x}, \mathbf{y} \in C(P, Q_P, j)} P^*\{\mathbf{x}, \mathbf{y}\}} \leq \frac{\sum_{\mathbf{x} \in \mathcal{T}_{P, Q_P}^N(X|\mathbf{y}, \hat{\mathbf{x}}_j)} P^*\{\mathbf{x}|\mathbf{y}\} P^*\{\mathbf{y}\}}{\sum_{\mathbf{x}, \mathbf{y} \in C(P, Q_P, j)} P^*\{\mathbf{x}, \mathbf{y}\}}. \end{aligned} \quad (6)$$

As the probability of the pair (\mathbf{x}, \mathbf{y}) is constant within the same type, from (6) we obtain that

$$\begin{aligned} P^*\{\mathbf{y}|\mathbf{x}, \mathbf{y} \in C(P, Q_P, j)\} &\leq \frac{|\mathcal{T}_{P, Q_P}^N(X|\mathbf{y}, \hat{\mathbf{x}}_j)|}{|C(P, Q_P, j)|} \\ &\leq \frac{\exp[N(H_{P, Q_P}(X|Y\hat{X}))]}{(N+1)^{|\mathcal{X}||\mathcal{Y}|} \exp[N(H_{P, Q_P}(XY|\hat{X}))]} \leq \exp[-N(H_{P, Q_P}(Y|\hat{X}) - \epsilon)]. \end{aligned} \quad (7)$$

Then, from (5), (7) and (2) we obtain that

$$\begin{aligned} \frac{1}{N}H(\mathbf{Y}|L(N)) &\geq \\ &\frac{1}{N} \sum_{j=1}^{L(N)} \left[N \sum_{\mathbf{y}:\mathbf{x},\mathbf{y} \in C(P, Q_P, j)} P^*\{\mathbf{y}|\mathbf{x}, \mathbf{y} \in C(P, Q_P, j)\} (H_{P, Q_P}(Y|\hat{X}) - \epsilon) \right] \\ &\quad \times P^*\{\mathbf{x}, \mathbf{y} \in C(P, Q_P, j)\} \\ &= P^*\{\mathbf{x}, \mathbf{y} \in \bigcup_{j=1}^{L(N)} C(P, Q_P, j)\} (H_{P, Q_P}(Y|\hat{X}) - \epsilon) \\ &\geq (1 - \exp\{-N(E + \delta/2)\}) (H_{P, Q_P}(Y|\hat{X}) - \epsilon). \end{aligned}$$

For N large enough, we obtain that

$$R_e \geq H_{P, Q_P}(Y|\hat{X}) - \epsilon \geq \Delta_e - \epsilon. \quad (8)$$

According to (2), (4) and (8), we state that the triple (R, Δ_d, Δ_e) is E -achievable.

Now we pass to the inverse part, let us prove that:

$$\mathcal{R}^*(E) \subseteq \left\{ \begin{array}{l} (R, \Delta_d, \Delta_e) : \Delta_d \geq 0, \Delta_e \geq 0, \\ 0 \leq R_e \leq \min_{P \in \alpha(E, P^*)} \max_{Q_P \in \mathcal{Q}(P, \Delta_d)} H_{P, Q_P}(Y|\hat{X}), \\ R \geq \max_{P \in \alpha(E, P^*)} \min_{Q_P \in \mathcal{Q}(P, \Delta_d, \Delta_e)} I_{P, Q_P}(X, Y; \hat{X}) \end{array} \right\}.$$

Let $\epsilon > 0$ be fixed. Consider a code (f_N, g_N) for each blocklength N with (R, Δ_d, Δ_e) E -achievable triple. We must show that for some $Q_P \in \mathcal{Q}(P, \Delta_d, \Delta_e)$ the following inequalities hold for N large enough:

$$\frac{1}{N} \log L(N) + \epsilon \geq \max_{P \in \alpha(E, P^*)} I_{P, Q_P}(X, Y; \hat{X}), \quad (9)$$

$$\frac{1}{N} H(\mathbf{Y}|L(N)) - \epsilon \leq \min_{P \in \alpha(E, P^*)} H_{P, Q_P}(Y|\hat{X}). \quad (10)$$

Let \mathcal{A}' be the complement of the set \mathcal{A} . The following statement is true:

$$|\mathcal{A} \cap \mathcal{T}_P^N(X, Y)| = |\mathcal{T}_P^N(X, Y)| - |\mathcal{A}' \cap \mathcal{T}_P^N(X, Y)|.$$

For $P \in \alpha(E - \epsilon, P^*)$

$$\begin{aligned} |\mathcal{A}' \cap \mathcal{T}_P^N(X, Y)| &= \frac{P^{*N}(\mathcal{A}' \cap \mathcal{T}_P^N(X, Y))}{P^{*N}(\mathbf{x}, \mathbf{y})} \\ &\leq \exp\{N(H_P(X, Y) + D(P||P^*))\} \exp\{-N(E - \epsilon)\} \\ &\leq \exp\{N(H_P(X, Y) - \epsilon)\}. \end{aligned}$$

Hence,

$$\begin{aligned} |\mathcal{A} \cap \mathcal{T}_P^N(X, Y)| &\geq (N + 1)^{-|\mathcal{X}||\mathcal{Y}|} \exp\{NH_P(X, Y)\} - \exp\{N(H_P(X, Y) - \epsilon)\} \\ &= \exp\{N(H_P(X, Y) - \epsilon)\} \left(\frac{\exp\{N\epsilon\}}{(N + 1)^{|\mathcal{X}||\mathcal{Y}|}} - 1 \right) \\ &\geq \exp\{N(H_P(X, Y) - \epsilon)\}. \end{aligned} \quad (11)$$

For each $\mathbf{x}, \mathbf{y} \in \mathcal{A} \cap \mathcal{T}_P^N(X, Y)$ corresponds a unique vector $\hat{\mathbf{x}}$ such that

$$\hat{\mathbf{x}} = g_N(f_N(\mathbf{x}, \mathbf{y})) \quad \text{and} \quad \hat{\mathbf{x}} \in \mathcal{T}_{P, Q}^N(\hat{X}|\mathbf{x}, \mathbf{y}).$$

Let us divide the set of all vectors $|\mathcal{A} \cap \mathcal{T}_P^N(X, Y)|$ into subsets by conditional types Q_P . The class having maximum cardinality for given P , we denote by

$$\left(|\mathcal{A} \cap \mathcal{T}_P^N(X, Y)| \right)_{Q_P}.$$

According to the number of conditional types Q , for sufficiently large N , we have:

$$\begin{aligned} |\mathcal{A} \cap \mathcal{T}_P^N(X, Y)| &\leq (N + 1)^{|\mathcal{X}||\mathcal{Y}|} \left(|\mathcal{A} \cap \mathcal{T}_P^N(X, Y)| \right)_{Q_P} \\ &\leq \exp\{N\epsilon/2\} \left(|\mathcal{A} \cap \mathcal{T}_P^N(X, Y)| \right)_{Q_P}. \end{aligned} \quad (12)$$

Let

$$\mathcal{D} = \left\{ \hat{\mathbf{x}} : g_N(f_N(\mathbf{x}, \mathbf{y})) = \hat{\mathbf{x}}, \text{ for some } (\mathbf{x}, \mathbf{y}) \in \mathcal{A} \cap \mathcal{T}_P^N(X, Y) \cap \mathcal{T}_{P, Q_P}^N(X, Y|\hat{\mathbf{x}}) \right\}.$$

From definition of the code $|\mathcal{D}| \leq L(N)$, then

$$\begin{aligned} \left| (\mathcal{A} \cap \mathcal{T}_P^N(X, Y)) \right|_{Q_P} &\leq \sum_{\hat{\mathbf{x}} \in \mathcal{D}} \left| \mathcal{T}_{P, Q}^N(X, Y | \hat{\mathbf{x}}) \right| \\ &\leq L(N) \exp\{NH_{P, Q_P}(X, Y | \hat{X})\}. \end{aligned} \quad (13)$$

From (11-13) follows

$$L(N) \geq \exp\{N(I_{P, Q_P}(X, Y; \hat{X}) - \epsilon)\}$$

for each $P \in \alpha(E - \epsilon, P^*)$ and some Q_P for which $\mathbf{E}_{P, Q_P} d(X, \hat{X}) \leq \Delta_d$, because $\mathbf{x}, \mathbf{y} \in \mathcal{A}$. From achievability follows that

$$\Delta_e - \epsilon \leq \frac{1}{N} H(\mathbf{Y} | L(N)) \leq H_{P, Q_P}(Y | \hat{X}).$$

So $Q_P \in \mathcal{Q}(P, \Delta_d, \Delta_e)$ and inequalities (9) and (10) are valid. Theorem 1 is proved.

References

- [1] C. E. Shannon, "Coding theorems for a discrete source with a fidelity criterion", *IRE National Convention Record*, vol. 7, pp.142–163, 1959.
- [2] H. Yamamoto, "A source coding problem for sources with additional outputs to keep secret from the receiver or wiretappers", *IEEE Transactions on Information Theory*, vol. 29, no. 6, pp. 918–923, 1983.
- [3] H. Yamamoto, "Source coding theory for cascade and branching communication systems", *IEEE Transactions on Information Theory*, vol. 27, no. 3, pp. 299–308, 1981.
- [4] H. Yamamoto, "A rate-distortion problem for a communication system with a secondary decoder to be hindered", *IEEE Transactions on Information Theory*, vol. 34, no. 4, pp. 835–842, 1988.
- [5] H. Yamamoto, "Rate-distortion theory for the Shannon cipher system", *IEEE Transactions on Information Theory*, vol. 43, no. 3, pp. 827–835, 1997.
- [6] E. Haroutunian, M. Haroutunian and A. Harutyunyan, "Reliability Criteria in Information Theory and in Statistical Hypothesis Testing", *Foundations and Trends in Communications and Information Theory*, vol. 4, nos 2-3, pp. 97–263, 2007. doi: 10.1561/01000000008
- [7] E. Haroutunian, A. Harutyunyan, A. Ghazaryan and E. van der Meulen, "On branching communication system rates-reliability-distortions region with partial secrecy under distortion criterion", *Mathematical Problems of Computer Science*, vol. 21, pp. 61–76, 2000.
- [8] L. Sankar, S. R. Rajagopalan and H. V. Poor, "Utility-privacy tradeoffs in databases: an information-theoretic approach", *IEEE Transactions on Information Theory*, vol. 8, no. 6, pp. 838–852, 2013.
- [9] T. M. Cover and J. A. Thomas, *Elements of Information Theory*, Second Edition. Wiley, New York, 2006.
- [10] I. Csiszár, "Method of types", *IEEE Transactions on Information Theory*, vol. 44, no. 6, pp. 2505–2523, 1998.
- [11] I. Csiszár and J. Körner, *Information Theory: Coding Theorems for Discrete Memoryless Systems*, Academic Press, New York, 1981.

Հուսալիության չափանիշները գաղտնի բաղադրիչով աղբյուրի կոդավորման խնդրում

Մարիամ Ե. Հարությունյան¹, Ջեմմա Ս. Սանթրոսյան² և Փառանձեմ Մ. Հակոբյան¹

¹ՀՀ ԳԱԱ Ինֆորմատիկայի և ավտոմատացման պրոբլեմների ինստիտուտ, Երևան, Հայաստան

²Վանաձորի պետական համալսարան, Վանաձոր, Հայաստան

e-mail: armar@sci.am, j.santrosian@gmail.com, par_h@iiap.sci.am

Անփոփում

Այս աշխատանքում ուսումնասիրվում է կոռելացված ելքերով միակողմանի աղբյուրների կոդավորման խնդիրը: Այս մոդելի համար, ինչպես ավանդական աղբյուրի կոդավորման դեպքում, աղբյուրի մի ելքը փոխանցում է հասցեատիրոջը հաղորդագրությունը որոշակի շեղման մակարդակով: Միևնույն ժամանակ, աղբյուրի մյուս ելքը պետք է հնարավորինս գաղտնի պահվի ստացողից կամ հնարավոր գաղտնալսողից: Այս մոդելի համար սահմանվել և վերլուծվել են արագություն-հուսալիություն-շեղում-անորոշություն և անորոշություն-հուսալիություն-շեղում ֆունկցիաները:

Բանալի բառեր՝ արագություն-հուսալիություն-շեղում-անորոշություն ֆունկցիա, աղբյուրի կոդավորում:

Критерии надёжности в задаче кодирования источника с секретным компонентом

Мариам Е. Арутюнян¹, Джемма С. Сантросян² и Парандзем М. Акопян¹

¹Институт проблем информатики и автоматизации НАН РА, Ереван, Армения

²Ванадзорский государственный университет, Ванадзор, Армения

e-mail: armar@sci.am, j.santrosian@gmail.com, par_h@iiap.sci.am

Аннотация

В данной работе рассматривается задача кодирования источника для односторонних источников с коррелированными выходами. В этой модели один из выходов источника должен быть передан получателю с заданным уровнем искажения, аналогично традиционному кодированию источника. Одновременно с этим, другой выход источника должен быть максимально засекречен от получателя или потенциального перехватчика. Для данной модели определяются и анализируются функции скорость-надёжность-искажение-неопределённость и неопределённость-надёжность-искажение.

Ключевые слова: функция скорость-надёжность-искажение-неопределённость, кодирование источника.

UDC 519.72

Information Theory Tools and Techniques to Overcome Machine Learning Challenges

Mariam E. Haroutunian and Gor A. Gharagyozyan

Institute for Informatics and Automation Problems of NAS RA, Yerevan, Armenia
e-mail: armar@sci.am, gor.gharagyozyan@edu.isec.am

Abstract

In this survey, we explore the broad applications of Information Theory in Machine Learning, highlighting how core concepts like *entropy*, *Mutual Information*, and *KL-divergence* are used to enhance learning algorithms. Since its inception by Claude Shannon, Information Theory has provided mathematical tools to quantify uncertainty, optimize decision-making, and manage the trade-off between model flexibility and generalization. These principles have been integrated across various subfields of Machine Learning, including *neural networks*, where the *Information Bottleneck* offers insights into data representation, and *reinforcement learning*, where entropy-based methods improve exploration strategies. Additionally, measures like *Mutual Information* are critical in *feature selection* and *unsupervised learning*. This survey bridges foundational theory with its practical implementations in modern Machine Learning by providing both historical context and a review of contemporary research. We also discuss open challenges and future directions, such as scalability and interpretability, highlighting the growing importance of these techniques in next-generation models.

Keywords: Information Bottleneck, Neural networks, Entropy-Based regularization, Mutual information, Feature selection, KL-Divergence.

Article info: Received 30 September 2024; sent for review 15 October 2024; received in revised form 1 April 2025, accepted 7 April 2025.

1. Introduction

The intersection of *Information Theory (IT)* and *Machine Learning (ML)* has become increasingly pivotal in advancing the state of the art across a wide range of subfields. *IT*, formalized by Claude

Shannon in his seminal 1948 work [1], introduced foundational concepts like entropy, which measures the uncertainty or disorder of a system, and Mutual Information (MI), which quantifies the amount of information one variable contains about another. These principles have profound implications in ML, particularly in optimizing algorithms, managing uncertainty, and improving decision-making processes.

In the context of ML, models often grapple with the *bias-variance trade-off*, striving to balance flexibility with generalization. Information-theoretic techniques such as *minimum description length* [2] provide an elegant way of navigating this trade-off by minimizing the complexity of models while maintaining accuracy. Similarly, *maximum entropy* models [3] leverage entropy to derive distributions that reflect uncertainty in the absence of prior knowledge, making them useful in many predictive models.

The impact of IT on ML is far-reaching:

- In *neural networks*, the *Information Bottleneck (IB)* method offers a theoretical framework for understanding how deep networks compress and transmit information through their layers [4].
- *Reinforcement learning* employs *entropy-based regularization* to enhance exploration strategies, helping agents avoid local optima and discover better policies [5].
- *Feature selection* relies on *MI* to identify the most relevant variables while discarding redundant or irrelevant data, which is crucial for high-dimensional datasets [6].
- *Unsupervised learning* techniques such as *autoencoders* and *variational autoencoders* rely on information-theoretic measures like *KL-divergence* to ensure that latent representations capture the essential structure of data [7].

As the field of ML continues to evolve, information-theoretic methods remain central to the development of robust and efficient models. Recent advancements have brought renewed attention to these techniques, particularly in addressing the challenges of scalability, interpretability, and privacy in deep learning systems. The *IB* theory, for example, provides insights into how models generalize and perform in real-world tasks by analyzing the flow of information between inputs and outputs [8]. Moreover, information-theoretic approaches have been increasingly employed in cutting-edge fields such as *quantum ML*, where *quantum IT* principles are applied to create more powerful algorithms [9].

This survey aims to provide a comprehensive overview of the recent developments, current applications, and future directions of IT in ML. This investigation will provide future good basis for bridging the gap between foundational theory [10] and cutting-edge research.

The paper is organized as follows: in the next section main concepts of IT are described. Main IT tools applied in ML are discussed in Section 3. Particular emphasis is placed on the IB framework in Section 4. Section 5 discusses the challenges and limitations of IT in ML. The paper is summarized in Section 6.

2. Useful IT Concepts

Entropy: Measuring Uncertainty

Entropy is the cornerstone of IT, introduced by Claude Shannon in 1948 [1], and is a measure of the uncertainty or randomness inherent in a random variable or a probability distribution [11]. In ML, entropy plays critical role in quantifying the amount of unpredictability in data, making it a crucial tool for optimizing algorithms and decision-making processes.

For a discrete random variable X with a probability distribution $P(X)$, where X can take values $\{x_1, x_2, \dots, x_n\}$ with probabilities $\{p(x_1), p(x_2), \dots, p(x_n)\}$, the *entropy* $H(X)$ is defined as:

$$H(X) = -\sum_{i=1}^n p(x_i) \log p(x_i),$$

where:

- $p(x_i)$ is the probability of occurrence of the outcome x_i ,
- \log is the logarithm base 2, as entropy is typically measured in *bits*.

The formula represents the *expected number of bits* required to encode the outcomes of X given their probabilities. Entropy achieves its maximum value when all outcomes are equally probable (maximum uncertainty) and its minimum value when one outcome is certain (no uncertainty).

Conditional Entropy and *Joint Entropy* are extensions of this concept. *Conditional Entropy* $H(X | Y)$ quantifies the uncertainty of X given that Y is known, while *Joint Entropy* $H(X, Y)$ captures the combined uncertainty of two random variables.

$$H(X | Y) = -\sum_{y \in Y} p(y) \sum_{x \in X} p(x|y) \log p(x|y),$$

$$H(X, Y) = -\sum_{y \in Y} \sum_{x \in X} p(x, y) \log p(x, y).$$

Mutual Information: Quantifying Shared Information

MI measures the amount of information shared between two random variables, quantifying how much knowing the value of one variable reduces uncertainty about the other. Formally, the *MI* between two random variables X and Y is defined as:

$$I(X; Y) = H(X) - H(X | Y) = \sum_{y \in Y} \sum_{x \in X} \frac{p(x, y)}{p(x)p(y)}.$$

MI can be thought of as the reduction in uncertainty about X when Y is known. Unlike *correlation*, which captures linear relationships, MI detects any kind of dependency between the variables, making it more robust for applications like *feature selection* [6]. In ML, MI is used to rank features based on their relevance to the target variable, allowing models to focus on the most informative inputs. For example, in *feature selection*, MI helps to identify and remove irrelevant or redundant features, significantly improving model performance by reducing overfitting in high-dimensional spaces.

KL-Divergence: Measuring the Difference Between Distributions

Kullback-Leibler Divergence (KL-Divergence), also known as *relative entropy*, is a measure of

how one probability distribution differs from a second, reference distribution. For two probability distributions P and Q , the KL-Divergence from Q to P is defined as:

$$D_{KL}(P||Q) = \sum_{x \in X} p(x) \log \frac{p(x)}{q(x)}.$$

KL-Divergence is non-negative and equals zero when the distributions are identical. Unlike traditional distance metrics, it is *asymmetric*, meaning $D_{KL}(P||Q) \neq D_{KL}(Q||P)$.

KL-Divergence is particularly useful in tasks where we approximate a complex distribution P with a simpler distribution Q , such as in *variational inference* [7].

In *variational autoencoders*, KL-Divergence is used to measure how close the learned latent variable distribution is to a prior distribution, such as a standard normal distribution. This ensures that the learned representations are regularized and maintain structure during training.

Cross-Entropy: Optimizing Classification Models

Cross-Entropy is closely related to KL-Divergence, but is more commonly used in *classification problems*. While KL-Divergence measures the divergence between two probability distributions, cross-entropy quantifies the total number of bits needed to encode a distribution P using another distribution Q , cross-entropy is given by:

$$H(P, Q) = -\sum_{x \in X} p(x) \log q(x).$$

In ML, cross-entropy loss is widely used as a *loss function* for classification tasks, particularly for models that output probability distributions, like *softmax classifiers*. It measures how well the predicted probabilities (from model Q) align with the true distribution (actual labels, P). Minimizing cross-entropy encourages the model to assign high probabilities to the correct classes.

For binary classification problem, the cross-entropy loss can be written as:

$$L = -[y \log p + (1 - y) \log(1 - p)],$$

where y is the true label (0 or 1), and p is the predicted probability of the label being 1.

Maximum Entropy Principle

The *Maximum Entropy* principle suggests that, when faced with uncertainty, the best distribution to choose is the one that maximizes entropy, subject to any known constraints. This principle underprints *maximum entropy models*, often used in areas like *natural language processing* [12]. These models choose the distribution that remains as uncertain as possible (i.e., has the highest entropy) while still satisfying the constraints imposed by the available data.

The principle encourages generality and reduces assumptions, making it useful for creating unbiased models when prior knowledge is limited.

3. Overview of IT Tools for ML

The application of IT concepts, such as entropy, MI, KL-divergence, and cross-entropy, has significantly advanced ML methodologies. These tools enable effective feature selection, model optimization, regularization, and performance evaluation. Below, we explore how these principles are utilized in practical ML tasks.

Feature Selection and Dimensionality Reduction

One of the most prominent applications of *MI* is in *feature selection*. In high-dimensional datasets, identifying the most relevant features for the model is crucial to improve performance and reduce overfitting. MI helps in selecting features that share maximum information with the target variable while avoiding redundant or irrelevant features. The *Max-Relevance and Min-Redundancy* algorithm is a widely used feature selection technique, that maximizes MI between features and the target variable while minimizing redundancy among the selected features [6]. This ensures that the selected features are both informative and diverse. In [6], MI was applied to gene selection for cancer detection. This approach identified the genes most relevant for distinguishing between cancerous and non-cancerous cells, reducing the dataset's dimensionality while retaining the most predictive features. This process significantly improved the performance of classification algorithms, such as Support Vector Machines, by focusing on the genes that contained the most meaningful information about the cancer type. Here, MI $I(X; Y)$ is used to quantify the relationship between the input features X and the target label Y , ensuring that the selected features contribute significantly to the predictive power of the model.

Building upon MI-driven feature selection, [13] proposed a fast binary feature selection method using Conditional MI. This approach refines MI-based selection by conditioning on already-selected features, ensuring that each additional feature contributes new, independent information to the model. The efficiency of this method enables rapid selection from datasets with tens of thousands of features, making it highly suitable for large-scale applications in computer vision and pattern recognition. Additionally, [14] explored MI-based feature selection techniques tailored for non-Gaussian data distributions. Their work introduced new feature selection and visualization algorithms that address challenges posed by high-dimensional, non-Gaussian datasets. By leveraging information-theoretic measures, their method improves both interpretability and feature selection performance in complex data environments, making it particularly useful in scientific and industrial applications, where data distributions deviate from Gaussian assumptions. Another approach leveraging MI for feature selection is presented in [15]. The method selects *class-specific informative features*, maximizing MI with the target class to enhance classification performance. This allows even a simple linear classifier to be effective, reducing reliance on complex models. While applied to object recognition, its principles extend to high-dimensional classification tasks, where efficient feature selection is essential.

Decision Trees and Information Gain

Entropy plays a central role in the construction of *decision trees*, where it is used to calculate *information gain*. Information gain measures the reduction in uncertainty (or entropy) when a dataset is split based on a particular feature. A decision tree algorithm selects features with the highest information gain to create branches, effectively reducing the overall entropy of the system [16]. In the popular *ID3* and *C4.5* decision tree algorithms, the feature that results in the greatest reduction in entropy after splitting is chosen to create nodes in the tree. This process continues recursively, ensuring that each split reduces uncertainty and leads to the most informative partitions of the data.

$$\text{Information Gain} = H(Y) - H(Y|X).$$

By minimizing entropy at each step, decision trees efficiently organize data and create models that are easy to interpret. However, their usage extends beyond traditional datasets into fields like high-energy physics, where rapid detection of rare phenomena is critical. A recent study [17] demonstrates the application of decision trees in detecting anomalies in proton-proton collision data at nanosecond timescales. This work specifically focuses on identifying rare *Higgs boson decays* in real-time. The decision trees in this application rely on fast, efficient calculations of information gain to classify particle collision data, reducing entropy by isolating potential anomalies that deviate from expected particle behaviors.

Another interesting work is [18]. This study tackles the challenge of securely training and evaluating decision trees in cloud environments without exposing sensitive data. The authors introduce a method based on additive secret sharing and the Paillier cryptosystem to protect both user queries and the cloud-hosted model. Their approach ensures secure computation while supporting offline users, making it suitable for resource-constrained applications like Internet of Thinking. Experimental results confirm its efficiency, particularly for deep but sparse trees, demonstrating reduced computational and communication overhead.

Clustering and Similarity Measurement

In unsupervised learning tasks like clustering, MI is used to measure the similarity between data points or clusters. The goal of clustering is to group similar data points together, and MI can help to determine how much information is shared between the clustering results and the true labels, when available.

One notable application of ML in clustering is *Normalized MI*, which measures the similarity between two clusterings. *Normalized MI* is particularly valuable when evaluating the quality of clustering results, as it quantifies the shared information between the true class labels and the predicted clusters, normalized by the entropy of both distributions. This ensures that the score is independent of the number of clusters and the size of the dataset. *Normalized MI* is widely used in applications such as document clustering, image segmentation and analyzing [19], where it is crucial to assess the quality of unsupervised learning methods.

Fuzzy clustering (a form of clustering in which each data point can belong to more than one cluster) plays a critical role in ML applications. Traditional clustering algorithms, such as k-means, assume hard partitioning of the data, meaning each data point belongs exclusively to one cluster. However, in many real-world scenarios, data points may naturally belong to multiple clusters with varying degrees of membership. Fuzzy clustering, specifically Probabilistic Fuzzy Clustering, allows for such flexibility by assigning each data point a degree of membership across different clusters.

The *Robust Possibilistic Fuzzy Additive Partition Clustering* method, as introduced in a recent study [20], builds upon these principles by incorporating deep local information to optimize the clustering process. This method leverages local data structures to improve clustering accuracy, particularly in noisy and uncertain environments. The algorithm dynamically adjusts the partitioning of data, thus reducing the impact of noise and outliers - a common issue in clustering. A significant extension of MI-based clustering techniques comes from the *Information-Theoretic Co-Clustering* approach introduced in [21]. This method simultaneously clusters both rows and columns of a data matrix, optimizing an MI loss function to uncover latent structures within

datasets. This framework has been particularly influential in *text mining and bioinformatics*, where data is inherently organized in two dimensions, such as documents and words, or genes and experimental conditions. By minimizing information loss in the clustering process, this method provides a more interpretable and structured representation of high-dimensional data.

Further advancing the theoretical foundations of MI in clustering, [22] proposed *Information-Theoretical Clustering via Semidefinite Programming*. Unlike conventional clustering approaches, which often rely on heuristic optimization, this method employs *semidefinite programming* to ensure a *globally optimal partitioning* of data based on MI principles. The approach has shown effectiveness in areas such as *image segmentation and social network analysis*, where precise and stable clustering is crucial.

In the domain of *collaborative filtering*, [23] introduced an *Information-Theoretic Co-Clustering approach* to improve recommendation systems. Traditional collaborative filtering often suffers from sparsity issues, where users have rated only a small fraction of available items. By leveraging MI to extract shared patterns from user-item matrices, this method enhances recommendation accuracy by capturing both cluster-based preferences and rating similarities. This improvement makes it particularly valuable for applications in e-commerce and content recommendation platforms. A more recent contribution by [24] introduces *Co-Clustering via Information-Theoretic Markov Aggregation*. This method constructs a *random walk on a bipartite graph*, optimizing an MI-based cost function to extract meaningful co-clusters. By reducing information loss during clustering, this technique closely aligns with *the IB framework*, demonstrating superior performance in structured datasets like *Newsgroup20* and *MovieLens100k*. Its effectiveness in real-world applications highlights the growing importance of MI-based clustering in data-driven decision-making and knowledge discovery. A new information-theoretical distance measure for evaluating community detection algorithms was introduced in [25].

These contributions collectively reinforce the role of MI in clustering, from optimizing objective functions to handling complex, structured datasets. As research continues, integrating MI-based clustering with deep learning and representation learning frameworks remains a promising direction for uncovering intricate patterns in high-dimensional data.

Regularization and Neural Networks

KL-Divergence plays a central role in *generative models* such as *Variational Autoencoders*, which are used to generate new data samples by learning the latent structure of the data. In this context, KL-divergence is used to regularize the latent space by ensuring that the learned distribution (the approximate posterior) is close to the prior distribution. The KL-divergence regularization term encourages the latent variable distribution to resemble a standard Gaussian distribution, promoting generalization and preventing overfitting [7]. By minimizing KL-divergence, the model ensures that the learned latent representations are smooth and continuous, allowing for better generation of new data samples and improved model robustness. Beyond generative models, MI and IB principles have also been explored as regularization techniques for deep learning. [8] introduced an information-theoretic analysis of Deep Neural Networks, showing that training consists of two key phases: an initial *empirical risk minimization* phase, followed by a *compression phase*, where MI between the input and the hidden layers is gradually reduced. This

compression process aligns with the (IB) principle, acting as a form of implicit regularization. Their findings provide theoretical support for why deep networks generalize well despite overparameterization, suggesting that MI-based constraints naturally shape the learning dynamics. Expanding on this, [26] proposed a framework for *learning deep representations by maximizing MI* between input data and learned representations. Their method, *Deep InfoMax (DMI)*, uses contrastive learning objectives to estimate MI and enforce high-information content in learned representations. Unlike traditional supervised learning, which relies on external labels, DMI ensures that learned features are task-relevant while filtering out noise. This MI maximization strategy has proven effectiveness in improving self-supervised learning, domain adaptation, and robust feature extraction, reinforcing the growing role of *information-theoretic constraints in deep learning regularization*. Cross-entropy remains the standard loss function for optimizing classification tasks, ensuring that models align their predicted probability distributions with true labels to achieve accurate predictions [27]. Together, these information-theoretic measures (KL-Divergence, MI and Cross-Entropy) serve as fundamental tools in deep learning regularization, helping models generalize, reduce overfitting, and learn meaningful representations.

The applications of IT in ML are both diverse and fundamental. Core concepts, such as entropy, MI, KL-divergence and Cross-Entropy, underpin a variety of crucial tasks in ML, from feature selection and decision-making to unsupervised learning and generative modeling.

Metric and Deep Learning

MI and other information-theoretic measures play a fundamental role in *Metric Learning and Deep Learning*, guiding how models learn structured and generalizable representations. By leveraging entropy, divergence measures, and the IB principle, researchers have developed techniques, that enhance similarity learning, privacy-aware learning, and transfer learning.

A foundational contribution in *metric learning* comes from [28], where *Information-Theoretic Metric Learning (ITML)* was introduced. Their method optimizes a Mahalanobis distance metric by minimizing *differential entropy*, ensuring that similar points are pulled closer while maintaining constraints on dissimilarity. Unlike traditional distance-learning approaches, ITML leverages relative entropy constraints, making it more robust in high-dimensional feature spaces. This approach has influenced a range of applications, from face verification to text similarity measurement. Privacy concerns in deep learning have led to the development of information-theoretic frameworks that balance data utility and confidentiality.

[29] proposed a privacy-aware time-series data-sharing framework using *Deep Reinforcement Learning*. Their approach formulates data sharing as an optimization problem, where the agent learns an optimal information disclosure policy under privacy constraints. By integrating MI constraints, the model selectively reveals useful data while minimizing privacy risks, demonstrating its effectiveness in financial and healthcare applications.

The theoretical foundations of *Information-Theoretic Learning (ITL)* were established in [30], introducing a framework for learning based on entropy and divergence measures rather than traditional statistical learning methods. ITL provides a more general approach to feature selection, clustering, and kernel methods, making it a precursor to modern information-based deep learning models. The use of *Renyi entropy* and *Cauchy-Schwarz divergence* in ITL offers an alternative to classical probability-based learning techniques, leading to more flexible and adaptive models.

Beyond individual learning paradigms, information-theoretic generalization bounds provide insights into the transferability of learned representations. [31] explored the role of MI in Transfer Learning, analyzing how information retained from the source domain affects generalization in the target domain. Results of this work highlight the importance of controlling information flow between layers in deep networks to prevent overfitting while maximizing knowledge transfer. This work establishes upper bounds on transfer learning generalization errors, making it highly relevant for domain adaptation and self-supervised learning.

Together, these studies illustrate the growing intersection between *IT* and *Deep Learning*, demonstrating how MI, entropy, and divergence measures drive advancements in metric learning, privacy-aware learning, and transfer learning. As deep learning models continue to evolve, information-theoretic regularization techniques are expected to play an even greater role in improving model robustness and interpretability.

4. IB Framework Applications in ML

The IB framework, first introduced in [32], has become a fundamental tool in ML by providing a principled approach to optimizing information flow in learning systems. IB offers a way to balance compression and relevance, formalizing the principle as an information-theoretic tradeoff between MI with the input and relevance to the target, ensuring that models retain the most essential information while discarding irrelevant noise. Over the years, IB has been applied across various ML domains, including representation learning, clustering, deep learning, privacy-aware learning, and image processing. The follow-up work [33] further refined the mathematical foundations of IB, emphasizing how different *distortion measures* impact information retention in learning systems. [34] expanded IB's role in representation learning, showcasing IB's effectiveness in enhancing generalization for multi-agent systems. In the context of *deep learning*, in [35], the authors introduced *Deep Variational Information Bottleneck*, which extends IB by incorporating variational inference. This approach has been widely adopted in training robust and generalizable neural networks by enforcing a structured latent space that reduces overfitting and improves generalization. Similarly, in [36] information flow in Deep Neural Networks is explored, demonstrating how IB principles guide the learning process by distinguishing between representation compression and task-relevant information. In [37], IB is further analyzed for application in Convolutional Neural Networks, optimizing feature extraction and regularization. In [38], the authors explored IB for splitting composite neural networks, improving model modularity and efficiency.

The IB framework has also found extensive applications in *image processing*. In [39], IB is applied to *image segmentation*, optimizing feature selection for improved segmentation accuracy. In [40], the authors introduced the *Residual Bottleneck Dense Network* for image super-resolution, demonstrating how IB-based architectures enhance high-resolution image synthesis. In [41], IB is explored for compressed sensing image reconstruction, leveraging IB principles to enhance the quality of reconstructed images in resource-constrained environments. IB's role in *5G-LDPC decoding with coarse quantization* is examined in [42], improving information retention in error-correcting code applications. Additionally, in [43], Exponential IB Theory is applied to pedestrian attribute recognition, optimizing robustness against intra-attribute variations.

Beyond vision-related tasks, the IB principle has been successfully applied to a range of other domains, including *clustering and feature selection* [44],[45],[46],[47], *geospatial learning* [48], and *multimodal natural language processing* [49]. The IB framework has also been utilized in *speech and audio processing* [50],[51],[52], as well as in *environmental monitoring and time-series analysis* [53], while continuing to play a central role in self-supervised visual representation learning [54].

In privacy-aware ML, IB has been utilized to balance data utility and confidentiality. A *Privacy-Aware Joint Source-Channel Coding* method based on *Disentangled IB* is introduced in [55], optimizing secure data transmission. Similarly, in [56], the authors proposed *FIBNet*, demonstrating how IB can prevent leakage of sensitive attributes while retaining necessary identification information. In [57], *Robust IB feature extraction* is explored, enhancing adversarial robustness in ML models.

Several additional contributions have extended the application of the IB framework across diverse ML domains. In *reinforcement learning* and *decision-making*, *Collaborative* [58] and *Two-Way Cooperative* [59] IB frameworks were introduced to optimize multi-agent systems under information-theoretic constraints. In the context of *scheduling* and *optimization*, an IB-based heuristic for job-shop scheduling is proposed in [60], demonstrating IB's utility in large-scale combinatorial problems. In [61], the authors applied *tunable IB with Rényi measures* to improve fairness and interpretability in classification tasks.

As IB research continues to evolve, its applications across deep learning, clustering, privacy, and reinforcement learning highlight its broad impact in ML. Future directions include integrating IB with large-scale self-supervised learning and enhancing IB-based optimization techniques for more efficient model training. The increasing adoption of IB principles underscores its importance as a fundamental tool for structured and efficient learning in ML. For more details on this topic, we refer to a comprehensive survey [62].

5. Challenges and Limitations of IT in ML

While IT has significantly contributed to the advancement of ML, its practical application is not without challenges. Techniques using entropy, MI, and KL-divergence offer powerful tools for managing uncertainty, optimizing models, and guiding decision-making. However, as ML models scale to handle ever-increasing amounts of data and complexity, several challenges emerge.

One key limitation is the *scalability* of information-theoretic measures, particularly when applied to high-dimensional datasets. Computing metrics like MI or entropy often becomes computationally expensive as the dimensionality of the data increases. For example, in [63] authors introduced *MINE (Mutual Information Neural Estimation)*, a scalable method for estimating MI by using gradient descent over neural networks. While *MINE* improves scalability, it still faces computational challenges when applied to extremely large datasets or high-dimensional input spaces, requiring efficient optimization techniques to ensure the model doesn't become prohibitively slow.

Another challenge is *Approximation errors*, as noted in [64], estimating MI accurately is difficult in practice, especially for continuous variables. MI is sensitive to the quality of the

probability distribution estimates, and small errors in density estimation can lead to significant misestimation of MI values.

Despite these challenges, efforts to address the limitations of IT in ML are ongoing. Researchers are continuously exploring ways to improve the scalability and accuracy of information-theoretic measures, particularly in high-dimensional spaces. For instance, advancements in approximation techniques, such as neural estimation methods like *MINE*, provide a promising foundation for mitigating computational constraints. Additionally, adaptive models that can handle noisy and imbalanced data more effectively, such as the *IB* framework, continue to evolve.

Moving forward, future work will likely focus on refining these methods to better suit real-world datasets, particularly those characterized by non-stationarity and high dimensionality. By developing more robust estimation techniques and improving the adaptability of models in dynamic environments, researchers can further harness the power of IT to unlock its full potential in ML.

6. Conclusion

This survey has highlighted the critical role that IT plays in ML, providing a framework for managing uncertainty, optimizing models, and improving decision-making. Through the use of concepts like entropy, MI, and KL-divergence, information-theoretic approaches have enhanced various ML tasks. However, challenges such as scalability, approximation errors, and dependency on accurate data modeling remain key obstacles.

Addressing these issues through ongoing research and improved techniques will help unlock the full potential of IT in ML, driving future innovations and making models more robust and adaptable to complex, real-world problems.

References

- [1] C. E. Shannon, "A Mathematical Theory of Communication", *Bell System Technical Journal*, vol. 27, no 3, pp. 379-423, 1948.
- [2] J. Rissanen, "Modeling by shortest data description", *Automatica*, vol. 14, no. 5, pp. 465-471, 1978.
- [3] E. T. Jaynes, "IT and statistical mechanics", *Physical Review*, vol. 106, no. 4, pp. 620-630, 1957.
- [4] N. Tishby and N. Zaslavsky, "Deep learning and the information bottleneck principle", *IEEE IT Workshop*, Jeju Island, Korea, pp. 1-5, 2015.
- [5] V. Mnih, K. Kavukcuoglu and D. Silver, "Human-level control through deep reinforcement learning", *Nature*, vol. 518, pp. 529-533, 2015.
- [6] H. Peng, F. Long and C. Ding, "Feature selection based on MI: Criteria of max-dependency, max-relevance, and min-redundancy", *IEEE Transactions on Pattern Analysis and Machine Intelligence*, vol. 27, no. 8, pp. 1226-1238, 2005.

- [7] D. P. Kingma and M. Welling, “Auto-Encoding Variational Bayes”, *International Conference on Learning Representations*, vol. 1, 2013.
- [8] R. Shwartz-Ziv and N. Tishby, “Opening the black box of Deep Neural Networks via Information”, *arXiv abs/1703.00810*, 2017.
- [9] J. Biamonte, “Quantum Machine Learning”, *Nature*, vol. 549, pp. 195-202, 2017.
- [10] E. Haroutunian, M. Haroutunian and A. Harutyunyan, “Reliability criteria in information theory and in statistical hypothesis testing”. *Foundations and Trends in Communications and Information Theory*, vol 4(2-3), pp. 97-263, 2007.
- [11] T. M. Cover and J. A. Thomas, *Elements of information theory*, Second Edition, Wiley, New York, 2006.
- [12] A. L. Berger, V. J. D. Pietra and S. A. D. Pietra, “A maximum entropy approach to natural language processing”, *Computational Linguistics*, vol. 22, no. 1, pp. 39-71, 1996.
- [13] F. Fleuret, “Fast binary feature selection with conditional mutual information”, *Journal of Machine Learning Research*, vol. 5, pp. 1531-1555, 2004.
- [14] H. H. Yang and J. Moody, “Data visualization and feature selection: new algorithms for nongaussian data”, *Advances in Neural Information Processing Systems*, vol. 12, 2000.
- [15] M. V. Naquet and S. Ullman, “Object recognition with informative features and linear classification”, *Ninth IEEE International Conference on Computer Vision (ICCV)*, pp 281-288, 2003.
- [16] J. R. Quinlan, “Induction of decision trees”, *Machine Learning*, vol. 1, no. 1, pp. 81-106, 1986.
- [17] T. M. Hong, S. T. Roche and B. Carlson, “Nanosecond anomaly detection with decision trees and real-time application to exotic Higgs decays”, *Nature Communications*, vol. 15, 2024.
- [18] L. Liu, R. Chen, X. Liu, J. Su and L. Qiao, “Towards practical privacy-preserving decision tree training and evaluation in the cloud”, *IEEE Transactions on information forensics and security*, vol. 15, pp. 2914-2929, 2020.
- [19] M. Haroutunian, D. Asatryan and K. Mastoyan, “Analyzing the quality of distorted images by the normalized mutual information measure”, *Mathematical Problems of Computer Science*, vol. 61, pp. 7-14, 2024.
- [20] R. G. Congalton, et al., “Robust possibilistic fuzzy additive partition clustering motivated by deep local information”, *Circuits, Systems, and Signal Processing*, 2024.
- [21] I. S. Dhillon, S. Mallela and D. S. Modha “Information-theoretic co-clustering”, *Proceedings of the ninth ACM SIGKDD International Conference on Knowledge Discovery and Data Mining*, pp. 89-98, 2003.
- [22] M. Wang and F. Sha, “Information theoretical clustering via semidefinite programming”, *Proceedings of the Fourteenth International Conference on Artificial Intelligence and Statistics*, pp. 761-769, 2011.
- [23] C. Liang and Y. Leng, “Collaborative filtering based on information-theoretic co-clustering”, *International Journal of Systems Science*, vol. 45, no. 3, pp. 589-597, 2012.
- [24] C. Bloechl, R. A. Amjad and B. C. Geiger, “Co-clustering via information-theoretic Markov aggregation”, *arXiv:1801.00584*, 2018.

- [25] M. Haroutunian, K. Mkhitarian and J. Mothe, “A new information-theoretical distance measure for evaluating community detection algorithms”, *Journal of Universal computer science*, vol. 25, no. 8, pp. 887-903, 2019.
- [26] R. D. Hjelm, A. Fedorov, S. Lavoie-Marchildon, K. Grewal, P. Bachman, A. Trischler and Y. Bengio, “Learning deep representations by mutual information estimation and maximization”, *Proceedings of the International Conference on Learning Representations (ICLR)*, 2019.
- [27] I. Goodfellow, Y. Bengio, and A. Courville, *Deep Learning*, MIT Press, Massachusetts, USA, 2016.
- [28] J. V. Davis, B. Kulis, P. Jain, S. Sra and I. S. Dhillon, “Information-theoretic metric learning”, *Proceedings of the 24th International Conference on Machine Learning (ICML)*, pp. 209–216, 2007.
- [29] E. Erdemir, P. L. Dragotti, D Gunduz, “Privacy-aware time-series data sharing with deep reinforcement learning”, *IEEE Transactions on Information Forensics and Security*, vol. 16, pp. 389-401, 2021.
- [30] J. C. Principe and D. Xu, “An introduction to information theoretic learning”, *Proceedings of the IJCNN'99 International Joint Conference on Neural Networks*, vol. 3, pp. 1783-1787, 1999.
- [31] X. Wu, J. H. Manton, U. Aickelin and J. Zhu, “On the generalization for transfer learning: an information-theoretic analysis”, arXiv:2207.05377, 2022.
- [32] N. Tishby, F. C. Pereira and W. Bialek, “The information bottleneck method”, *arXiv:physics/0004057*, 1999.
- [33] P. Harremoës and N. Tishby, “The information bottleneck revisited or how to choose a good distortion measure”, *2007 IEEE International Symposium on Information Theory*, Nice, France, pp. 566-570, 2007.
- [34] M. Vera, P. Piantanida and L. R. Vega, “The role of the information bottleneck in representation learning”, *IEEE International Symposium on Information Theory (ISIT)*, Vail, CO, USA, pp. 1580-1584, 2018.
- [35] A. A. Alemi, I. Fischer, J. V. Dillon and K. Murphy, “Deep variational information bottleneck”, *arXiv:1612.00410*, 2019.
- [36] R. Shwartz-Ziv, “Information flow in deep neural networks”, *arXiv:2202.06749*, 2022.
- [37] J. Li and D. Liu, “Information bottleneck theory on convolutional neural networks”, *Neural Processing Letters*, vol. 53, no. 2, pp. 1385-1400, 2021.
- [38] S. Han, K. Nakamura and B. Hong, “Splitting of composite neural networks via proximal operator with information bottleneck”, *IEEE Access*, vol. 12, pp. 157-167, 2024.
- [39] A. Bardera, J. Rigau, I. Boada, M. Feixas and M. Sbert, “Image segmentation using information bottleneck method”, *IEEE Transactions on Image Processing*, vol. 18, no. 7, pp. 1601-1612, 2009.
- [40] Z. An, J. Zhang, Z. Sheng, X. Er and J. Lv, “RBDN: Residual bottleneck dense network for image super-resolution”, *IEEE Access*, vol. 9, pp. 103440-103451, 2021.

- [41]□B. Lee, K. Ko, J. Hong, B. Ku and H. Ko, “Information bottleneck measurement for compressed sensing image reconstruction”, *IEEE Signal Processing Letters*, vol. 29, pp. 1943-1947, 2022.
- [42]□M. Stark, L. Wang, G. Bauch and R. D. Wesel, “Decoding rate-compatible 5G-LDPC codes with coarse quantization using the information bottleneck method”, *IEEE Open Journal of the Communications Society*, vol. 1, pp. 646-660, 2020.
- [43]□J. Wu, Y. Huang, M. Gao, Z. Gao, J. Zhao, J. Shi and A. Zhang, “Exponential information bottleneck theory against intra-attribute variations for pedestrian attribute recognition”, *IEEE Transactions on Information Forensics and Security*, vol. 1, pp. 5623-5635, 2023.
- [44]□S. Wang, C. Li, Y. Li, Y. Yuan and G. Wang, “Self-supervised information bottleneck for deep multi-view subspace clustering”, *IEEE Transactions on Image Processing*, vol. 32, pp. 1555-1567, 2023.
- [45]□X. Yan, Y. Ye, Y. Mao and H. Yu, “Shared-private information bottleneck method for cross-modal clustering”, *IEEE Access*, vol. 7, pp. 36045-36056, 2019.
- [46]□Z. Liu, X. Wang, X. Huang, G. Li, K. Sun and Z. Chen, “Incomplete multi-view representation learning through anchor graph-based GCN and information bottleneck”, *Proceedings of the IEEE International Conference on Acoustics, Speech, and Signal Processing, ICASSP*, pp. 71130-71134, 2024.
- [47]□X. Yan, Y. Mao, Y. Ye and H. Yu, “Cross-modal clustering with deep correlated information bottleneck method”, *IEEE Transactions on Neural Networks and Learning Systems*, vol. 35, no. 10, pp. 13508-13522, 2024.
- [48]□K. Yang, W. Tai, Z. Li, T. Zhong, G. Yin, Y. Wang and F. Zhou, “Exploring self-explainable street-level IP geolocation with graph information bottleneck”, *2024 IEEE International Conference on Acoustics, Speech and Signal Processing (ICASSP)*, Seoul, Korea, pp. 7270-7274, 2024.
- [49]□S. Cui, J. Cao, X. Cong, J. Sheng, Q. Li, T. Liu and J. Shi, “Enhancing multimodal entity and relation extraction with variational information bottleneck”, *IEEE/ACM Transactions on Audio, Speech, and Language Processing*, vol. 32, pp. 1274-1285, 2024.
- [50]□T. Gu, G. Xu and J. Luo, “Sentiment analysis via deep multichannel neural networks with variational information bottleneck”, *IEEE Access*, vol. 8, pp. 121014-121021, 2020.
- [51]□Z. Wu and S. King, “Improving trajectory modelling for DNN-based speech synthesis by using stacked bottleneck features and minimum generation error training”, *IEEE/ACM Transactions on Audio Speech and Language Processing*, vol. 24, 2016.
- [52]□S. H. Lee, H. R. Noh, W. J. Nam and S. -W. Lee, “Duration controllable voice conversion via phoneme-based information bottleneck”, *IEEE/ACM Transactions on Audio, Speech, and Language Processing*, vol. 30, pp. 1173-1183, 2022.
- [53]□C. Wang, S. Du, W. Sun and D. Fan, “Self-supervised learning for high-resolution remote sensing images change detection with variational information bottleneck”, *IEEE Journal of Selected Topics in Applied Earth Observations and Remote Sensing*, vol. 16, pp. 5849-5866, 2023.

- [54] X. Liu, Y. I. Li and S. Wang, “Learning generalizable visual representations via self-supervised information bottleneck”, *2024 IEEE International Conference on Acoustics, Speech and Signal Processing (ICASSP)*, Seoul, Korea, pp. 5385-5389, 2024.
- [55] L. Sun, C. Guo, M. Chen and Y. Yang, “Privacy-aware joint source-channel coding for image transmission based on disentangled information bottleneck”, *2024 IEEE International Conference on Acoustics, Speech and Signal Processing (ICASSP)*, Seoul, Korea, pp. 9016-9020, 2024.
- [56] Z. Chen, Z. Yao, B. Jin, M. Lin and J. Ning, “FIBNet: Privacy-enhancing approach for face biometrics based on the information bottleneck principle”, *IEEE Transactions on Information Forensics and Security*, vol. 19, pp. 8786-8801, 2024.
- [57] A. Pensia, V. Jog and P. L. Loh, “Extracting robust and accurate features via a robust information bottleneck”, *IEEE Journal on Selected Areas in Information Theory*, vol. 1, no. 1, pp. 131-144, 2020.
- [58] M. Vera, L. R. Vega and P. Piantanida, “Collaborative information bottleneck”, *IEEE Transactions on Information Theory*, vol. 65, no. 2, pp. 787-815, 2019.
- [59] M. Vera, L. Rey Vega and P. Piantanida, “The two-way cooperative information bottleneck”, *2015 IEEE International Symposium on Information Theory (ISIT)*, Hong Kong, China, pp. 2131-2135, 2015.
- [60] Z. Yan, G. Hanyu and X. Yugeng, “Modified bottleneck-based heuristic for large-scale job-shop scheduling problems with a single bottleneck”, *Journal of Systems Engineering and Electronics*, vol. 18, no. 3, pp. 556-565, 2007.
- [61] A. Gronowski, W. Paul, F. Alajaji, B. Gharesifard and P. Burlina, “Classification utility, fairness, and compactness via tunable information bottleneck and Rényi measures”, *IEEE Transactions on Information Forensics and Security*, vol. 19, pp. 1630-1645, 2024.
- [62] Z. Goldfeld, Y. Polyanskiy, “The information bottleneck problem and its applications in machine learning”, *IEEE Journal On Selected Areas In Information Theory*, vol. 1, no. 1, pp. 19-38, 2020.
- [63] M. I. Belghazi, “Mutual information neural estimation (MINE)”, *Proceedings of the 35th International Conference on Machine Learning*, Stockholm, Sweden, pp. 1391-1400, 2018.
- [64] D. McAllester and K. Stratos, “Formal limitations on the measurement of mutual information”, *The Proceedings of AISTATS 2020*, pp. 875-884, 2020.

Ինֆորմացիայի տեսության գործիքներն ու տեխնիկաները մեքենայական ուսուցման մարտահրավերների հաղթահարման համար

Մարիամ Ե. Հարությունյան և Գոռ Ա. Ղարազյոզյան

ՀՀ ԳԱԱ Ինֆորմատիկայի և ավտոմատացման պրոբլեմների ինստիտուտ, Երևան, Հայաստան
e-mail: armar@sci.am, gor.gharagozyan@edu.isec.am

Ամփոփում

Այս հոդվածում ուսումնասիրվում է Ինֆորմացիայի տեսության լայն կիրառությունները մեքենայական ուսուցման մեջ՝ ընդգծելով, թե ինչպես են հիմնական հասկացությունները օգտագործվում ուսուցման ալգորիթմները բարելավելու համար: Ինֆորմացիայի տեսության գործիքները ինտեգրվել են մեքենայական ուսուցման տարբեր ճյուղերում, այդ թվում՝ ներդրումային ցանցերում: Մասնավորապես, Ինֆորմացիոն խցանի մեթոդը առաջարկում է պատկերացումներ տվյալների ներկայացման և «Ամրապնդող ուսուցման» վերաբերյալ, որտեղ էնտրոպիայի վրա հիմնված մեթոդները բարելավում են հետազոտության ռազմավարությունները: Ավելին, փոխադարձ ինֆորմացիան կենտրոնական դեր է խաղում չկառավարվող ուսուցման և հատկանիշների ընտրության խնդիրներում: Տրամադրելով և՛ վերջին տարիների արդյունքները, և՛ ժամանակակից հետազոտությունների միտումները, այս հոդվածը կապում է հիմնարար տեսությունը ժամանակակից մեքենայական ուսուցման մեջ իր գործնական իրականացման հետ: Քննարկվում են նաև բաց հարցերը և ապագա ուղղությունները, ինչպիսիք են՝ մասշտաբայնությունը, մեկնաբանելիությունը՝ ընդգծելով այս մեթոդների աճող կարևորությունը նոր սերնդի մոդելներում:

Բանալի բառեր՝ ինֆորմացիոն խցան, ներդրումային ցանցեր, էնտրոպիայի հիմքով կարգավորում, փոխադարձ ինֆորմացիա, հատկանիշների ընտրություն, Կուլբակ-Լեյբլերի տարամիտություն:

Инструменты и техники теории информации для преодоления вызовов машинного обучения

Мариам Е. Арутюнян и Гор А. Карагёзьян

Институт проблем информатики и автоматизации НАН РА, Ереван, Армения
e-mail: armar@sci.am, gor.gharagyozyan@edu.isec.am

Аннотация

В данной статье рассматривается широкое применение Теории Информации в Машинном Обучении, подчеркивается, как основные понятия используются для улучшения алгоритмов обучения. Техники Теории информации были интегрированы в различные подполя Машинного Обучения, включая нейронные сети. В частности метод Информационной пробки дает представление о данных, и обучение с подкреплением, где методы, основанные на энтропии, улучшают стратегии поиска. Кроме того, такие величины, как взаимная информация, имеют решающее значение для отбора признаков и обучения без контроля. Предоставляя последние достижения и обзор современных тенденций, эта статья связывает фундаментальную теорию с ее практической реализацией в современном машинном обучении. Мы также обсуждаем открытые проблемы и будущие направления, такие как масштабируемость, интерпретируемость, подчеркивая растущую важность этих методов в моделях нового поколения: масштабируемость, интерпретируемость, подчеркивая растущую важность этих методов в моделях нового поколения.

Ключевые слова: информационная пробка, нейронные сети, регуляризация на основе энтропии, взаимная информация, выбор характеристик, КЛ-дивергенция .

UDC 51-7, 514

Fractal Geometry and Quantitative Evaluation of the Aesthetic Appeal of Ancient Armenian Architecture Monuments

Aren A. Nahapetyan

University La Sapienza, Rome, Italy
e-mail: ar.nahapetyan@gmail.com

Abstract

A fractal analysis of the most important architectural monuments (temples) of medieval Armenia is given. Quantitative (objective) evaluations of their artistic appeal are obtained. These evaluations confirm the generally accepted (subjective) appeal of these temples as masterpieces of Armenian architecture. Based on the fractal data obtained, statistical conclusions are made about the high degree of architectural compatibility of the plans and facades of the monuments under consideration.

Keywords: Fractal, Fractal dimension, Architecture, Psychology.

Article info: Received 24 April 2025; sent for review 25 April 2025; accepted 2 May 2025.

Acknowledgments: The author would like to thank L. Khachatryan for her helpful advice and ongoing support in writing this paper.

1. Introduction

The basic figures of classical (Euclidean) geometry are simple and clear: circle, sphere, cylinder, pyramid, etc. The impressive achievements of this science allowed ancient thinkers to assume that the geometric picture of the world is described by Euclidean geometry based on the five Platonic solids (regular polyhedra).

Over time, it became clear that this position was only partly true, since it was impossible to describe the shapes of objects such as clouds, mountain ranges, coastlines of seas and lakes, etc. within the framework of classical geometry.

The question of the existence of a geometry that can describe and study the forms of such objects has been a topic of interest for scientists for a long time. However, it was only with the development of powerful computing systems (enabling us to visualize such structures) that the construction of such a theory became possible.

Geometry describing non-standard forms was proposed by B. Mandelbrot [1] based on the concept of fractal introduced by him. It was called fractal geometry.

The difference between this geometry and classical Euclidean geometry is as follows. In classical geometry, objects are idealized, meaning their surfaces are assumed to be perfectly smooth, without any irregularities, cracks, or breaks. In contrast, fractal geometry studies the patterns inherent in natural objects, processes, and phenomena with the presence of roughness, brokenness, and other complexities (see, for example, [2, 3]). It offers a variety of ways to describe and measure both natural and man-made objects.

Thanks to the development of fractal geometry, it has recently become possible to objectively (quantitatively) evaluate the aesthetic appeal of architectural compositions for the first time.

There are many monuments of world architecture for which fractal analysis has been carried out. These are remarkable Gothic cathedrals in Europe, beautiful mosques of Islamic architecture, unique Hindu temples (see, for example, [4, 5, 6, 7]). Such an analysis has not been carried out for Armenian temples. This paper attempts to fill this gap. It is devoted to the application of fractal geometry to the quantitative evaluation of the attractiveness of such outstanding architectural monuments of medieval Armenia as the Zvartnots, Hripsime and the Cathedral of the Holy Virgin in Ani.

When conducting fractal analysis, various computing tools are used. In this work, the analysis is carried out on the basis of the FrakOut! package, which is very convenient for calculating the fractal parameters of buildings. When evaluating the architectural compatibility of the plan and facade of the temples under consideration, the STATISTICA software package was used to find statistical estimates based on the available data.

2. Fractals and Fractal Geometry

According to Mandelbrot [1], a fractal is a structure consisting of parts that are in some sense similar to the whole (or to each other).

Fractals can be found almost everywhere in nature. For example, tree crowns, snowflakes, broccoli heads, crystals, etc.

From a mathematical point of view, a fractal is a geometric figure (a set of points in Euclidean space) whose fractal dimension (the Hausdorff–Besicovitch dimension) is either fractional or exceeds its topological dimension.

The Hausdorff-Besicovitch dimension of some finite set G , $G \subset \mathcal{R}^n$, is defined as follows. Consider an n -dimensional cubic lattice in \mathcal{R}^n with the length of the edge of a cube (cell) equal to Δ . Let $N(\Delta)$ be the minimum number of cubes needed to cover the set G . Then the fractal dimension D of this set is defined based on the following requirement:

$$\lim_{\Delta \rightarrow 0} N(\Delta)\Delta^d = \begin{cases} 0, & \text{if } d > D, \\ \infty, & \text{if } d < D. \end{cases}$$

From this it is clear that the dimension D of the set G is essentially the boundary that shows that if $d < D$, then the number of cubes $N(\Delta)$ is insufficient to cover the set G , and if $d > D$, then the number of cubes $N(\Delta)$ is excessive for coverage.

It is generally accepted that the fractal dimension is a characteristic property of fractals, i.e., if the dimension D is not an integer, then the set G is considered a fractal. In practice, approximate numbers are used. For $\Delta \approx 0$, $D \approx -\ln N(\Delta)/\ln \Delta$.

In addition to natural fractals, there are also artificial (non-natural) fractals. The first examples of non-natural fractals were constructed at the end of the nineteenth century in

connection with purely mathematical problems of function theory. From the point of view of classical mathematical analysis, they had extremely unusual properties. For example, this is the Cantor set (Cantor dust), the nowhere differentiable Weierstrass function, the Koch snowflake, the Brownian curve on the plane, etc. For some of them, fractal dimensions have been calculated: the Cantor set has a fractal dimension of $D = \ln 2 / \ln 3$, and for a Brownian curve on a plane, it is equal to 2, that is, exceeds its topological dimension.

It should also be noted that fractal principles are present in the theory of fractional integro-differentiation as well. The fact is that in a fractal environment, the change in physical quantities can slow down to such an extent that it is impossible to describe such a process using an ordinary derivative. This can only be done using integro-differential equations that include a fractional derivative with respect to time. Armenian mathematicians M. Djrbashian and A. Nersessian made a significant contribution to this theory (see [8]).

3. Quantitative Evaluation of Aesthetic Appeal of Fractal Structures

Fractal geometry can be used as a method for analyzing the structure of buildings. It has been noted that if the fractal component of an architectural structure is clearly traced, then this structure has strong architectural aesthetics. Psychologists have developed a quantitative method to assess such aesthetics.

The first systematic studies of the perception of fractal forms were conducted by J. Sprott and his colleagues. These studies analyzed the relationships between objective (fractal dimension) and subjective assessments of the visual attractiveness of various objects (the results of these works are summarized in [9]). It was later shown that subjective assessments of visual attractiveness correlate quite strongly with fractal dimension and are reproduced upon repeated testing [10, 11, 12]. It was also shown that the fractal dimension is the main factor influencing subjective assessments of the attractiveness of objects with fractal properties. Preference is given to objects with an average fractal dimension in the range of 1.3–1.5 (flat images). Subsequently, many studies were devoted to the empirical study of the perception of fractals of natural and artificial origin (see, for example, [13, 10, 14, 15]).

Research by K. Hagerhall and her group [14] has established that emotional states in relation to natural landscapes can be predicted by typical fractal characteristics, i.e., by fractal dimension.

These studies confirmed the relationship between assessments of aesthetic appeal and complexity with fractal dimension.

4. Fractal Analysis of Armenian Temples

In architecture, fractal principles are used in the design of objects using computer modeling. These principles can be used to create unique and very interesting architectural forms (see, for example, [16]). In this case, practical methods for calculating the fractal dimension of the structures under consideration play an important role.

One of the most popular methods is the method of counting cells that have a non-empty intersection with the image being studied (box-counting dimension method). Apparently, W. Lorenz [17] and C. Bovill [18] were the first to study and use this method most fully.

Let us describe in general terms the algorithm for applying this method.

In the first step, a cubic (square) grid with the cell edge length (scale) equal to Δ is superimposed on the image under study. Initially, Δ is taken to be equal to L , where L is

the length of the rectangle containing all the images. Let $N(\Delta)$ be the number of all cubes that have a non-empty intersection with the image under study.

Next, the following ration is considered

$$-\log N(\Delta)/\log \Delta,$$

and its behavior is investigated under stepwise changes in the scale Δ .

The scale is reduced by half at each step. The process can continue indefinitely, but in practical applications, it is stopped depending on the requirements of the task. The slope of the graph of $\log N(\Delta)$ from $-\log \Delta$ gives an approximate value of the fractal dimensions of the image.

Below, we will present a fractal analysis of the temples of Hripsime and Zvartnots, as well as the Ani Cathedral, using the FrakOut! program. In parallel, a statistical analysis of the compatibility of the plan and facade of these buildings is also carried out.

The results obtained show that the temples under consideration have high architectural attractiveness, and their plan and facade are in excellent agreement with each other.

4.1 Hripsime

The temple was built by Catholicos Komitas in 618 to the east of Echmiadzin on the burial site of Saint Hripsime. It is a central-domed structure with an internal cross-shaped base. It is a recognized masterpiece of Armenian architecture.

Appendix 1 contains fragments of the process of calculating the fractal dimension of the facade and plan of the Hripsime temple. The results of the calculations are summarized in Table 1.

Table 1. Fractal dimension of the Hripsime Cathedral facade and plan

Calculation of fractal dimension between:		fractal dimension	
large grid size	small grid size	facade	plan
200	100	1.46	1.74
100	50	1.48	1.58
50	25	1.49	1.49
25	12.5	1.49	1.51
general fractal dimension		1.48	1.58

From the obtained data, it follows that the temple of Hripsime has an average fractal dimension of 1.48. The calculations also show that the standard deviation of these data from the average is 0.014. Regarding the architectural plan, the following estimates were obtained: the average fractal dimension is 1.58 with a standard deviation of 0.113. The correlation between the fractal dimensions of the facade and the plan is -0.997 .

Fig. 1 shows a graph of the dependence of $\log N(\Delta)$ on $-\log \Delta$ for the facade of the temple, which is a linear regression constructed using the obtained values of the fractal dimension.

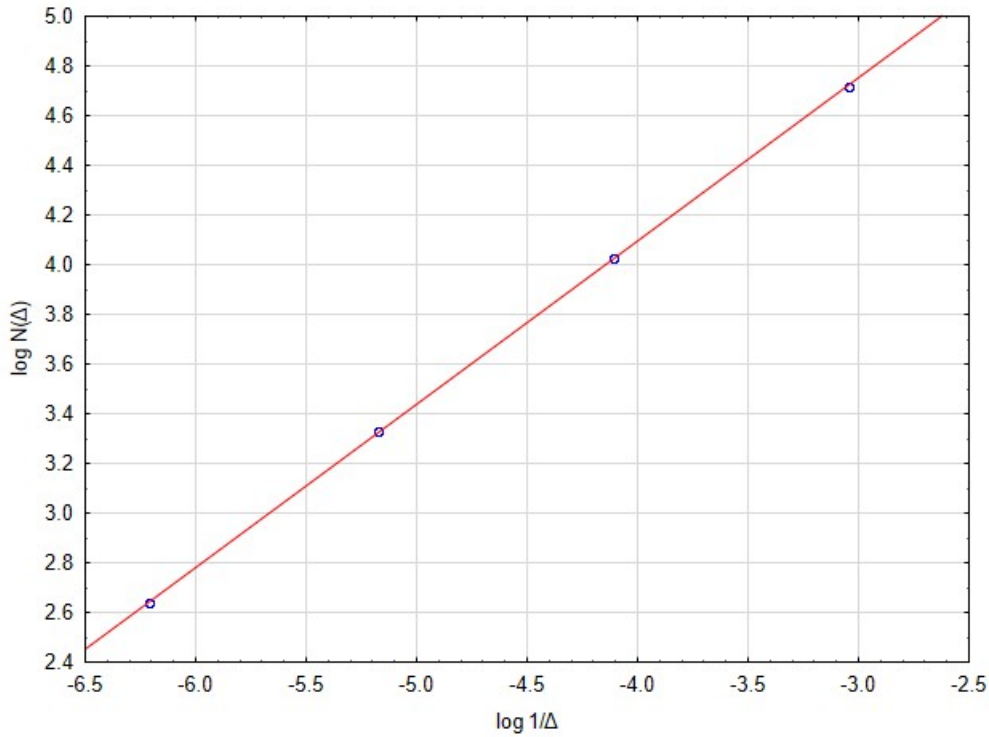


Fig. 1. Hripsime: graph of the dependence of $\log N(\Delta)$ on $\log(1/\Delta)$.

4.2 Zvartnots

The Zvartnots Cathedral was founded by Catholicos Nerses III in the middle of the 7th century, not far from Vagharshapat (Echmiadzin) in the place where, according to legend, Gregory the Illuminator and the king of Armenia Trdat met. This majestic temple is a tetraconch (a central-domed structure with a plan in the form of a cross with rounded ends).

Appendix 2 contains fragments of the process of calculating the fractal dimension of the facade and plan of the Zvartnots temple. The results of the calculations are summarized in Table 2.

Table 2. Fractal dimension of the Zvartnots Cathedral facade and plan.

Calculation of fractal dimension between:		fractal dimension	
large grid size	small grid size	facade	plan
200	100	1.64	1.67
100	50	1.54	1.57
50	25	1.48	1.49
25	12.5	1.47	1.43
general fractal dimension		1.533	1.540

From the obtained data, it follows that the Zvartnots temple has an average fractal dimension of 1.533. The calculations also show that the standard deviation of these data from the average is 0.008. Regarding the architectural plan, the following estimates were

obtained: the average fractal dimension is 1.54 with a standard deviation of 0.104. The correlation between the fractal dimensions of the facade and the plan is 0.974.

Fig. 2 shows a graph of the dependence of $\log N(\Delta)$ on $-\log \Delta$ for the facade of the temple, which is a linear regression constructed using the obtained values of the fractal dimension.

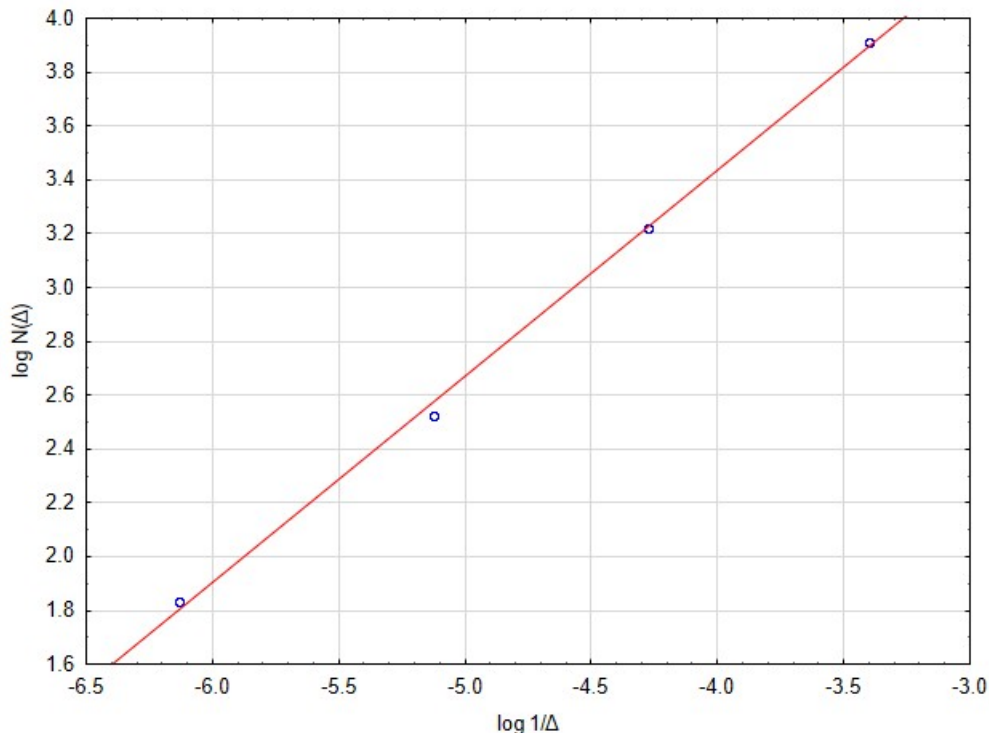


Fig. 2. Zvartnots: graph of the dependence of $\log N(\Delta)$ on $\log(1/\Delta)$.

4.3 Cathedral of the Holy Virgin in Ani

The Ani Cathedral is the pinnacle of Armenian architecture of the 9th-11th centuries. It is a prototype of Gothic architecture. Its architectural forms are similar to European Gothic.

Regarding Gothic, we note that there is a very reasonable assumption that the first object where Gothic principles were applied was not the Cathedral of Saint-Denis (a suburb of Paris), but the Cathedral of the Holy Virgin in Ani. The interior of this temple clearly contains such architectural compositions as elongated pointed arches, bunches of columns with ribbed vaults. These compositions were developed in Gothic architecture, which was widespread in Western Europe.

In his major work [19], Professor of the University of Vienna J. Strzygowski writes: “Consequently, it remains to be recognized that the Armenians built in the Gothic style approximately 150 years earlier than was the case in Europe”.

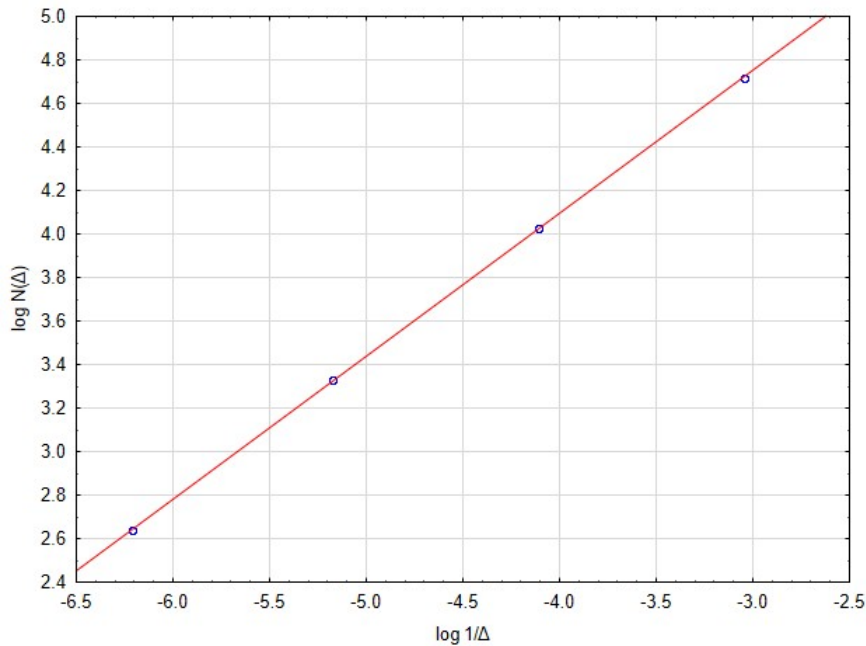
Appendix 3 contains fragments of the process of calculating the fractal dimension of the facade and plan of the Ani Cathedral. The results of the calculations are summarized in Table 3.

Table 3. Fractal dimension of the Ani Cathedral facade and plan.

Calculation of fractal dimension between:		fractal dimension	
large grid size	small grid size	facade	plan
200	100	1.56	1.48
100	50	1.53	1.50
50	25	1.56	1.43
25	12.5	1.5	1.13
general fractal dimension		1.537	1.385

From the obtained data, it follows that the Ani Cathedral has an average fractal dimension of 1.537. The calculations also show that the standard deviation of these data from the average is 0.029. Regarding the architectural plan, the following estimates were obtained: the average fractal dimension is 1.385 with a standard deviation of 0.172. The correlation between the fractal dimensions of the facade and the plan is 0.797.

Fig. 3 shows a graph of the dependence of $\log N(\Delta)$ on $-\log \Delta$ for the facade of the temple, which is a linear regression constructed using the obtained values of the fractal dimension.

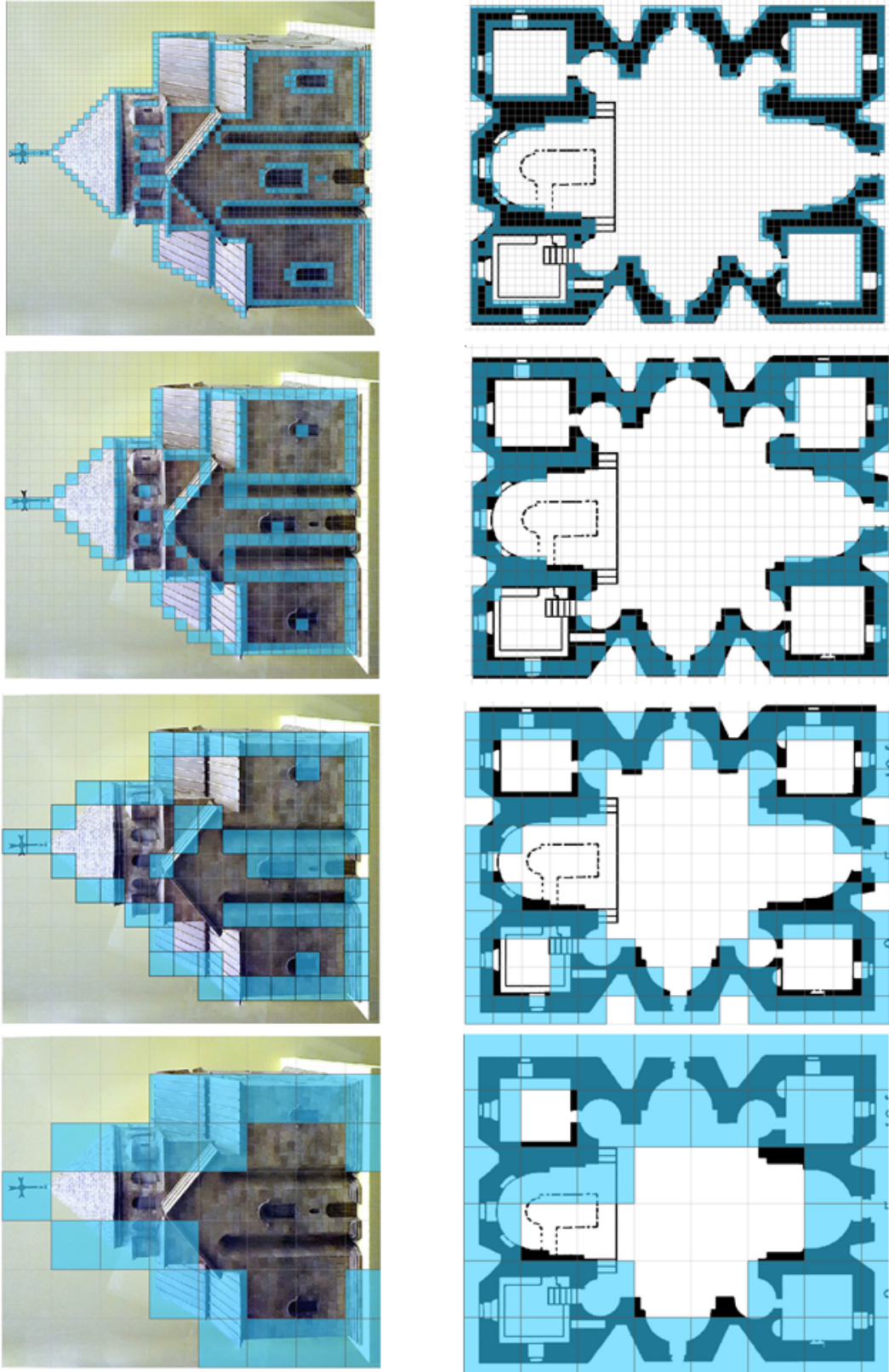
Fig. 3. Cathedral in Ani: graph of the dependence of $\log N(\Delta)$ on $\log(1/\Delta)$.

5. Conclusion

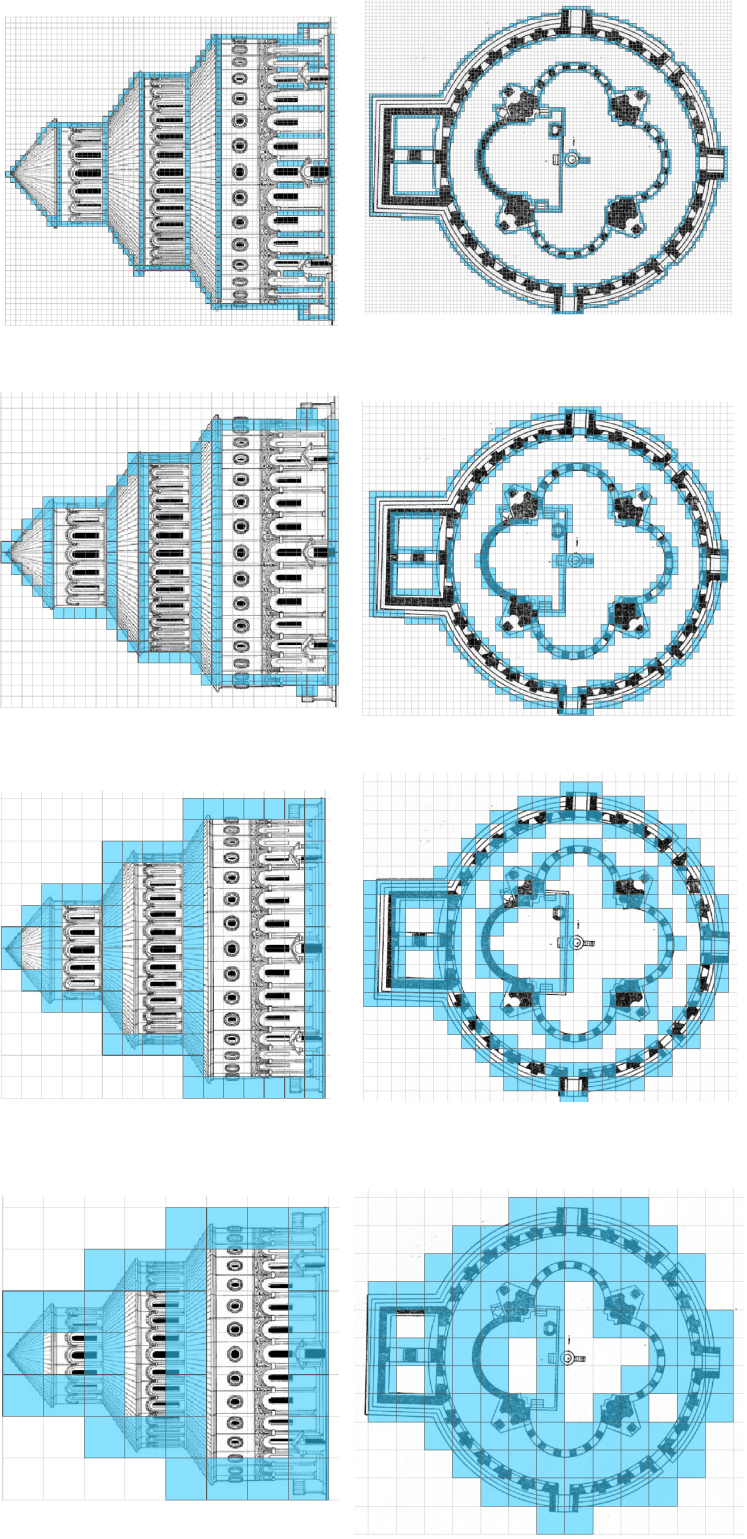
Fractal analysis of the examined Armenian churches showed a high level of consistency between subjective and objective assessments of their aesthetic appeal.

Appendix

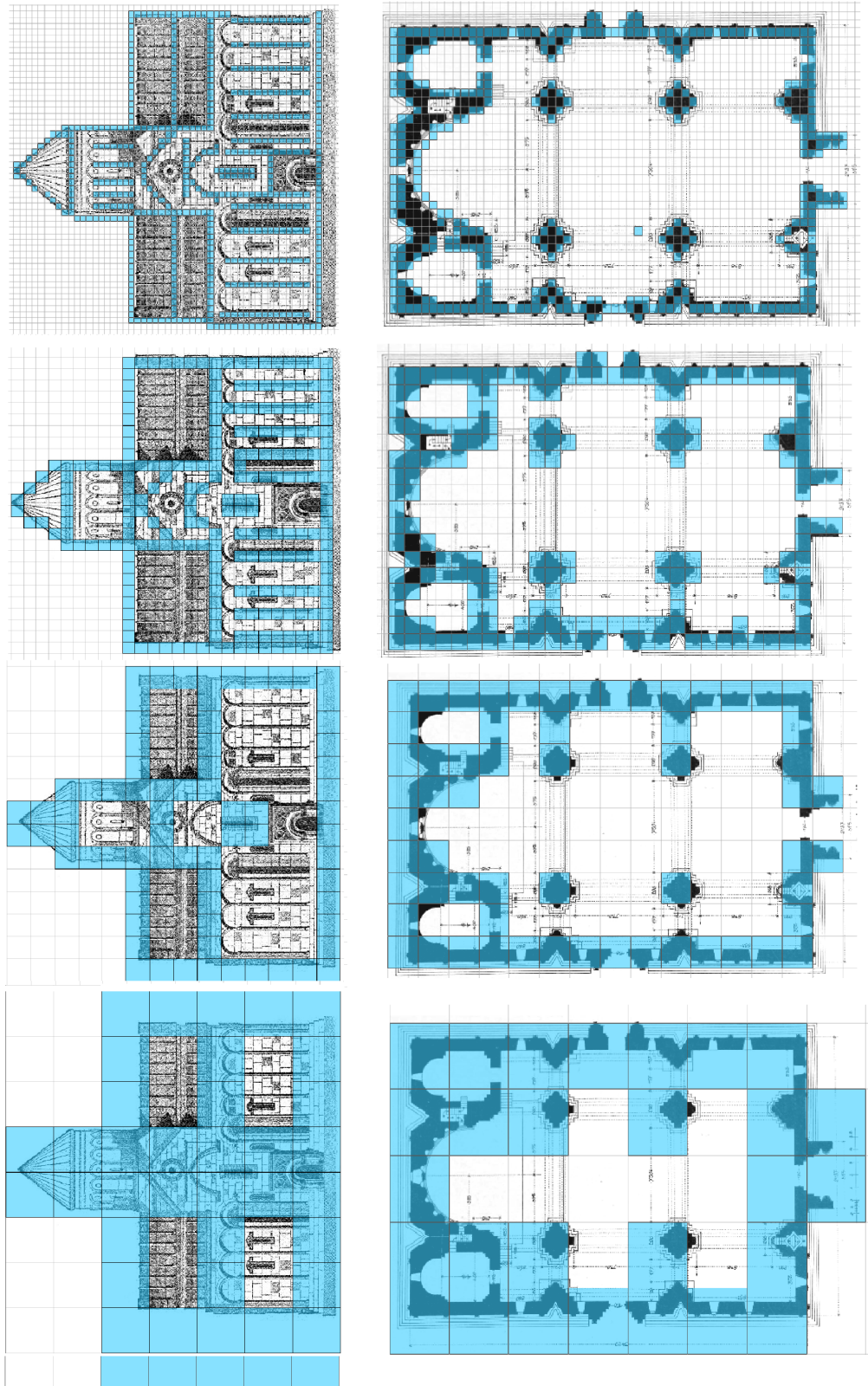
Appendix 1. Calculation of the fractal dimension of the facade and plan of the Hripsime temple.



Appendix 2. Calculation of the fractal dimension of the facade and plan of the Zvartnots temple.



Appendix 3. Calculation of the fractal dimension of the facade and plan of the Ani Cathedral.



References

- [1] B. B. Mandelbrot, *The Fractal Geometry of Nature*, Freeman, San Francisco, 1982.
- [2] R. M. Crownover, *Introduction to Fractals and Chaos*, Jones and Bartlett Publishers, 1995.
- [3] J. Feder, *Fractals*, Publisher New York: Plenum Press, 1988.
- [4] P. K. Acharya, *An encyclopaedia of Hindu architecture*, Oxford University Press, 2010.
- [5] H. D. A. Ismail, “Fractal analysis of masterpieces of Islamic architecture — Ahmad Shah Mosque and Taj Mahal: justification of the method and experience of application”, (in Russian), *Architecture and Modern Information Technologies*, vol. 4, no. 21, 11 pp., 2012.
- [6] H. D. A. Ismail and M. Yu. Shishin, “Application of multi-stage fractal method in the analysis of the masterpiece of Islamic architecture — Ahmad Shah Mosque”, (in Russian), *Art of Eurasia*, vol. 3, no. 10, pp. 37–47, 2018.
- [7] I. A. Mayatskaya, G. I. Fazylzyanova, B. M. Yazyev and S. B. Yazyeva, “Fractality of gothic architecture”, (in Russian), *Engineering Bulletin of the Don*, vol. 4, 15 pp., 2025.
- [8] M. M. Djrbashian and A. B. Nersessian, “Fractional derivatives and the Cauchy problem for differential equations of fractional order”, (in Russian), *Izv. Akad. Nauk Armjan. SSR. Ser. Mat.*, vol. 3, pp. 3–29, 1968.
- [9] J.C. Sprott, *Strange attractors: Creating patterns in chaos*, New York, M&T Books, 1993.
- [10] N. A. Salingaros, “Fractal art and architecture reduce physiological stress”, *Computers and Graphics*, vo. 27, no. 5, pp. 813–820, 2003.
- [11] S. Pyankova, “Fractal analysis in psychology: perception of self-similar objects”, (in Russian), *Psychological Studies*, vol. 9, no. 46, 14 pp., 2016.
- [12] S. Pyankova, “Subjective estimates of visual complexity and aesthetical appeal of fractal images: individual differences and genetic influences”, (in Russian), *Psychological Studies*, vol. 12, no. 63, 16 pp., 2019.
- [13] R. P. Taylor, “Reduction of Physiological Stress Using Fractal Art and Architecture”, *Leonardo*, vol. 39, no. 3, 2006.
- [14] C. M. Hagerhall, T. Purcell and R. Taylor, “Fractal dimension of landscape silhouette outlines as a predictor of landscape preference”, *Journal of Environmental Psychology*, vol. 24, no. 2, pp. 247–255, 2024.
- [15] F. I. Mavrikidi, “Fractal mathematics and the nature of change” (in Russian), *Delphis*, vol. 54, no. 2, 2008.
- [16] N. A. Salingaros, “Architecture, Patterns, and Mathematics”, *Nexus Network Journal*, vol. 1, no. 1, pp. 75–86, 1999.
- [17] W. E. Lorenz, *Fractals and Fractal Architecture*, Department of Computer Sided Planning and Architecture: Site Vienna University of Technology Vienn, 2003, www.fractalatinitest.com
- [18] C. Bovill, “Fractal geometry in architecture and design”, *Birkhäuser*, pp. 73–92, 1996.
- [19] J. Strzygowski, *Die Baukunst der Armenier und Europa: Ergebnisse einer vom Kunsthistorischen Institute der Universitat Wien 1913 durchgeführten Forschungsreise*. Kunstverlag Anton Schroll & Co., 1918.

Ֆրակտալ երկրաչափություն և հին հայկական ճարտարապետական հուշարձանների գեղագիտական գրավչության քանակական գնահատում

Արեն Ա. Նահապետյան

Սապիենցա համալսարան, Հռոմ, Իտալիա
e-mail: ar.nahapetyan@gmail.com

Ամփոփում

Ներկայացվել է միջնադարյան Հայաստանի ամենակարևոր ճարտարապետական հուշարձանների (տաճարների) ֆրակտալ վերլուծություն: Ստացվել են դրանց գեղարվեստական գրավչության քանակական (օբյեկտիվ) գնահատականներ: Այս արդյունքները հաստատում են տվյալ հուշարձանների՝ որպես հայկական ճարտարապետական գլուխգործոցների ընդունված (սուբյեկտիվ) գնահատականը: Ստացված ֆրակտալ տվյալների հիման վրա կատարվել են վիճակագրական եզրակացություններ դիտարկվող հուշարձանների հատակագծերի և ճակատների ճարտարապետական համապատասխանության բարձր աստիճանը:

Բանալի բառեր՝ ֆրակտալ, ֆրակտալ չափականություն, ճարտարապետություն, հոգեբանություն:

Фрактальная геометрия и количественная оценка эстетической привлекательности памятников древнеармянской архитектуры

Арен А. Нахапетян

Римский университет Ла Сапиенца, Рим, Италия
e-mail: ar.nahapetyan@gmail.com

Аннотация

Дан фрактальный анализ важнейших архитектурных памятников (храмов) средневековой Армении. Получены количественные (объективные) оценки их художественной привлекательности. Эти результаты подтверждают общепринятую (субъективную) оценку этих храмов как шедевров армянской архитектуры. На основе полученных фрактальных данных сделаны статистические выводы о высокой степени архитектурной совместимости планов и фасадов рассматриваемых памятников.

Ключевые слова: фрактал, фрактальная размерность, архитектура, психология.

UDC 519.2

Regularly Varying of the Normalizing Constants in the Theorem of Convergence to a Positive Stable Distribution

Robert N. Chitchyan

Institute for Informatics and Automation Problems of NAS RA, Yerevan, Armenia
e-mail: rchitchyan@gmail.com

Abstract

This article examines the behavior of the normalizing constants in V. Feller's theorem on the convergence of distributions for sums of independent, identically distributed random variables with heavy tails at infinity. It is proved that, in this setting, the normalizing constant is regularly varying at infinity.

Keywords: Insurance, random variable, regularly varying function, slowly varying function, stable distribution.

Article info: Received 1 October 2024; sent for review 15 October 2024; received in revised form 1 December 2024; accepted 3 April 2025.

1. Introduction

We consider a sequence of independent, identically distributed random variables with the distribution function $F(x)$. Suppose that for $x \rightarrow +\infty$, an asymptotic relation is executed:

$$1 - F(x) \sim \frac{x^{-\alpha}L(x)}{\Gamma(1 - \alpha)}, \quad (1)$$

where $0 < \alpha < 1$, $\Gamma(\alpha) = \int_0^\infty x^{\alpha-1}e^{-x}dx$, $L(x)$ - slowly varying function at infinity (SVFI), i.e., a positive function defined for $(0, \infty)$ and for each $x > 0$ fulfills the condition

$$\lim_{t \rightarrow +\infty} \frac{L(tx)}{L(t)} = 1.$$

Subsequently, according to Theorem 2 (see [1], XIII.6, p. 448), if F is the probability distribution, concentrated on $(0, \infty)$ and such that upon $n \rightarrow \infty$

$$F^{n*}(a_n x) \rightarrow G(x), \quad (2)$$

(at points of continuity), where $F^{n*}(\cdot)$ - n -fold convolution of distribution F with itself, while G is the proper distribution, not concentrated at one point and if the type of distribution F is (1), a_n variates in standard measure may be selected in a way that

$$\frac{nL(a_n)}{a_n^\alpha} \rightarrow 1. \quad (3)$$

In this case, the asymptotic relation (2) is executed along with the distribution of probabilities $G = G_\gamma$, where G_α is a stable distribution with $0 < \alpha < 1$, parameter focused on $(0, \infty)$ having Laplace-Stieltjes transform $e^{-\lambda^\alpha}$.

2. The Behavior of the Normalizing Constants in V. Feller's Theorem at Infinity

The positive function R is called (accurately) regularly varying at infinity if it is measurable on the $[A, \infty)$, $A > 0$ semiaxis and there exists such a number as $\alpha \in (-\infty, +\infty)$, which for a certain $x > 0$

$$\lim_{t \rightarrow +\infty} ((R(xt)/(R(t)) = x^\alpha.$$

Meanwhile, α is called the order (indicator) of the function R .

Suppose that $a_n = n^{1/\alpha}\varphi(n)$ and find out what features shall possess function $\varphi(n)$ in order to execute asymptotic (3).

By plugging in (3) an equation for a_n , we will deduce an equivalent (3) relation:

$$L(n^{1/\alpha}\varphi(n)) \sim \varphi^\alpha(n),$$

or in a more general form:

$$L(t^{1/\alpha}\varphi(t)) \sim \varphi^\alpha(t). \quad (4)$$

Consider the following relation:

$$R_t(x) = \frac{L((xt)^{1/\alpha}\varphi(tx))}{L(t^{1/\alpha}\varphi(t))}. \quad (5)$$

By virtue of asymptotic relation (4) upon $t \rightarrow +\infty$ out of (5), it follows that

$$R_t(x) \sim \left(\frac{\varphi(tx)}{\varphi(t)} \right)^\alpha. \quad (6)$$

In ([2], p. 10), the following is proved:

Theorem 1. (On the introduction of SVFI). If function L , defined on semiaxis $[A, +\infty)$, $A > 0$ - SVFI, such number $B \geq A$ will be found so that for all $x \geq B$ occurs the following representation:

$$L(x) = \exp \left\{ \eta(x) + \int_B^x \frac{\varepsilon(u)}{u} du \right\}, \quad (7)$$

where η - limited measurable function on $[B, +\infty)$ is such that

- a) $\eta(x) \rightarrow c$ ($|c| < \infty$) and
- b) $\varepsilon(x)$ - continuous function on $[B, +\infty)$ is such that $\varepsilon(x) \rightarrow 0$ in case of $x \rightarrow +\infty$.

Since L is SVFI, therefore using the relation (5), it is not complicated to deduce the following equation for $R_t(x)$:

$$R_t(x) = \exp\{\eta((tx)^{1/\alpha}\varphi(tx)) - \eta((t)^{1/\alpha}\varphi(t))\} \cdot \exp\left\{\int_{t^{1/\alpha}\varphi(t)}^{(tx)^{1/\alpha}\varphi(tx)} \frac{\varepsilon(y)}{y} dy\right\}. \quad (8)$$

By introducing the notation $a_t(x) = \frac{\varphi(tx)}{\varphi(t)}$, the expression (7) will be transformed into the following type:

$$R_t(x) = \exp\{\eta((tx)^{1/\alpha}\varphi(tx)) - \eta((t)^{1/\alpha}\varphi(t))\} \cdot \exp\left\{\int_1^{x^{1/\alpha}a_t(x)} \frac{\varepsilon(\varepsilon(t^{1/\alpha}\varphi(t)z))}{z} dz\right\}. \quad (9)$$

In the case of $t \rightarrow +\infty$, the first factor in the right-hand part of the relation (8) by virtue of condition b) of Theorem 1, tends to unity. Therefore, upon the availability of sufficiently high t

$$R_t(x) \sim \exp\left\{\int_1^{x^{1/\alpha}a_t(x)} \frac{\varepsilon(s(t^{1/\alpha}\varphi(t)y))}{y} dy\right\}. \quad (10)$$

Theorem 2. *In case of any $x > 0$, the following equation is true:*

$$\lim_{t \rightarrow +\infty} x^{1/\alpha}a_t(x) = 1.$$

Proof. It shall firstly be proved that $\overline{\lim}_{t \rightarrow +\infty} a_t(x) \rightarrow +\infty$ for all $x \in (0, +\infty)$. Suppose that the contrary takes place: then for each $x > 0$, there exists a sufficiently high $t_0 = t_0(x)$, that in the case of all $t > t_0$, the following condition is executed:

$$x^{1/\alpha}a_t(x) > 1. \quad (11)$$

Further, condition b) means that for any $\delta > 0$, there exists $y_0 = y_0(\delta)$, such that for all $y > y_0$ occurs the the following inequality:

$$\varepsilon(y) < \delta. \quad (12)$$

Besides, since $t^{1/\alpha}\varphi(t) \rightarrow +\infty$ in case of $t \rightarrow +\infty$, we will select $t_1 \geq t_0$ such that upon $t > t_1$ inequality $t^{1/\alpha}\varphi(t) > y_0$ is executed by virtue of selecting t_0 and condition $z \geq 1$ apparent from (12), uniformly in z follows the inequality $\varepsilon(zt^{1/\alpha}\varphi(t)) < \delta$. Therefore, after uncomplicated transformation, the following inequality is deduced:

$$\exp\left\{\int_1^{x^{1/\alpha}a_t(x)} \frac{s(t^{1/\alpha}\varphi(t)y)}{y} dy\right\} \leq x^{\delta/\alpha}a_t^\delta(x). \quad (13)$$

On the other hand, by virtue of asymptotic relation (4) in the case of $t \rightarrow +\infty$, the following is concluded:

$$R_t(x) = \frac{L((xt)^{1/\alpha}\varphi(tx))}{L(t^{1/\alpha}\varphi(t))} \sim \left(\frac{\varphi(tx)}{\varphi(t)}\right)^\alpha = a_t^\alpha(x). \quad (14)$$

That's the inequality (11) from which we deduce the following:

$$x^{\delta/\alpha}a_t^\delta(x) \geq a_t^\alpha(x).$$

By selecting $\delta < \alpha$ from the previous inequality, we have the following:

$$x^{\delta/\alpha} \geq a_t^{\alpha-\delta(x)}. \quad (15)$$

Upon fixing $x > 0$, the left-hand side of (13) is limited, while the right-hand side by the virtue of limitation $\alpha - \delta > 0$ for $t \rightarrow +\infty$ tends to infinity, resulting in a contradiction. Thus, it can be concluded from (10) that for any $x > 0$, the following inequality holds:

$$\lim_{t \rightarrow +\infty} x^{1/\alpha} a_t(x) \leq 1. \quad (16)$$

Let's demonstrate that $a_t(x) \rightarrow 0$ in the case of $t \rightarrow +\infty$. We'll also conduct the proof by an indirect proof method. Assume that for each $x > 0$ there exists such $t' = t'(x)$, that for all $t > t'$, the following condition is satisfied:

$$x^{1/\alpha} a_t(x) < 1. \quad (17)$$

Simultaneously $t'' > \max(t', t_1)$ may be taken as high that

$$x^{1/\alpha} a_t(x) \cdot t^{1/\alpha} \varphi(t) = (xt)^{1/\alpha} \varphi(xt) > y_0,$$

where y_0 is defined in (11).

Taking into consideration the above, it is not difficult to prove that

$$\begin{aligned} \exp \left\{ \int_1^{x^{1/\alpha} a_t(x)} \frac{\varepsilon(t^{1/\alpha} \varphi(t) y)}{y} dy \right\} &= \exp \left\{ - \int_{x^{1/\alpha} a_t(x)}^1 \frac{\varepsilon(t^{1/\alpha} \varphi(t) y)}{y} dy \right\} \\ &\geq \exp \left\{ -\delta \ln z \Big|_{x^{1/\alpha} a_t(x)}^1 \right\} \\ &= a_t^\delta(x) \cdot x^{\delta/\alpha}. \end{aligned} \quad (18)$$

On the other hand, for all $x > 0$ upon sufficiently high t from (14), we have the following:

$$R_t(x) \sim a_t^\alpha(x) \geq a_t^\delta(x) \cdot x^{\delta/\alpha}.$$

By selecting $\delta < \alpha$, in (12) we will have the following:

$$a_t(x) \geq x^{\frac{\delta}{\alpha-\delta}} > 0,$$

that in the case of $t \rightarrow +\infty$ contradicts our assumption, i.e., the condition (17) is inexecutable. Thus, Theorem 2 is proved. ■

Thereof, it follows that for all $x > 0$ $\lim_{t \rightarrow +\infty} R_t(x) = 1$, while from relation (6) it is concluded that function $\varphi(t)$ is SVFI.

Thus, the following is proven:

Theorem 3. *If conditions (1) – (3) are executed, the norming quantity a_n is a regularly varying function at infinity with the parameter $1/\alpha$.*

3. Conclusion

If F is the distribution of probabilities, concentrated on $(0, \infty)$, for which in case of $x \rightarrow +\infty$ asymptotic relation (1) is executed and G_α is a stable distribution with the parameter $0 < \alpha < 1$ concentrated on $(0, \infty)$, then

$$F^{n*} (n^{1/\alpha} \varphi(n) \cdot x) \rightarrow G_\alpha(x),$$

where $\varphi(\cdot)$ is SVFI connected with SVFI $L(\cdot)$ by the following asymptotic relation

$$L(n^{1/\alpha} \varphi(n)) \sim \varphi^\alpha(n).$$

References

- [1] V. Feller, *An Introduction to Probability Theory and its Applications*, vol. 2, MIR printing house, Moscow, 1984.
- [2] E. Seneta, *Regularly Varying Functions*, Nauka printing house, Moscow, 1985.
- [3] R.L. Dobrushin, “Lemma on the limit of a complex random function”, *UMN*, pp. 157-159, 1955
- [4] J. Magyorodi, “Limit distribution of sequences of random variables with random indices, *Transactions of the Forth Prague Conference on Information Theory, Statistical Decision Functions, Random Processes*, Prague, pp.463-470, 1967.
- [5] L. A. Zolotukhina, “On the asymptotic distribution of sequences with random indices, *Mathematical notes of the Academy of Sciences of the USSR*, vol. 6, pp. 887-891, 1969.
- [6] R.N.Chitchyan, “On the asymptotic behaviour of distributions of random sequences with random induces and regularly varying ”tails””, *Abstracts of Secnd International Conference ”Mathematics in Armenia. Advances and Perspectives”*, Tsaghkadzor, Armenia, pp. 82-83. 2013.

Չուգամիտության թեորեմում նորմալացնող հաստատունների կանոնավոր փոփոխությունը դեպի դրական կայուն բաշխում

Ռոբերտ Ն. Չիտչյան

ՀՀ ԳԱԱ Ինֆորմատիկայի և ավտոմատացման պրոբլեմների ինստիտուտ, Երևան, Հայաստան
e-mail: rchitchyan@gmail.com

Անփոփում

Այս հոդվածն ուսումնասիրում է նորմալացնող հաստատունների վարքագիծը Վ. Ֆելլերի թեորեմում՝ կապված անկախ, նույնականորեն բաշխված պատահական փոփոխականների գումարների համար բաշխումների Չուգամիտության հետ, որոնք ունեն եծանրե պոչեր անվերջության մեջ: Յույց է տրվում, որ այս համատեքստում նորմալացնող հաստատունը կանոնավոր կերպով փոփոխվում է անվերջության մեջ:

Բանալի բառեր՝ ապահովագրություն, պատահական փոփոխական, կանոնավոր կերպով փոփոխվող ֆունկցիա, դանդաղ փոփոխվող ֆունկցիա, կայուն բաշխում:

Регулярное изменение нормализующих констант в теореме сходимости к положительному устойчивому распределению

Роберт Н. Читчян

Институт проблем информатики и автоматизации НАН РА, Ереван, Армения
e-mail: rchitchyan@gmail.com

Аннотация

В данной статье рассматривается поведение нормирующих констант в теореме В. Феллера о сходимости распределений сумм независимых одинаково распределенных случайных величин с "тяжелыми" хвостами на бесконечности. Демонстрируется, что в данном контексте нормирующая константа регулярно меняется на бесконечности.

Ключевые слова: страхование, случайная величина, регулярно меняющаяся функция, медленно меняющаяся функция, устойчивое распределение.

UDC 511

A Quantum Diophantine Equation Solution Finder*

Lara Tatli¹ and Paul Stevenson²

¹ University of Durham, Durham, DH1 3LE, UK

² University of Surrey, Guildford, Surrey, GU2 7XH, UK

e-mail: lara.tatli@durham.ac.uk, p.stevenson@surrey.ac.uk

Abstract

Diophantine equations are multivariate equations, usually polynomial, in which only integer solutions are admitted. A brute force method for finding solutions would be to systematically substitute possible integer values for the unknown variables and check for equality.

Grover's algorithm is a quantum search algorithm which can find marked indices in a list very efficiently. By treating the indices as the integer variables in the Diophantine equation, Grover's algorithm can be used to find solutions in a brute force way more efficiently than classical methods. We present a hand-coded example for the simplest possible Diophantine equation, and results for a more complicated, but still simulable, equation encoded with a high-level quantum language.

Keywords: Quantum computing, Grover's algorithm, Diophantine equations.

Article info: Received 13 November 2024; sent for review 25 November 2024; accepted 3 April 2025.

Acknowledgements: PDS acknowledges support from UK STFC under grant ST/W006472/1. We acknowledge the use of IBM Quantum Lab in the early stages of this work.

1. Introduction

A Diophantine equation is an equation, typically polynomial, with integer coefficients, in more than one integer variable. A famous example occurs as Fermat's Last Theorem, which states that

$$x^n + y^n = z^n \tag{1}$$

has no solutions for $n \geq 3$ where n , x , y , and z are all natural numbers. The simplest Diophantine equation is linear in two variables and is of the form

$$ax + by = n, \tag{2}$$

*Data Availability: Codes for all parts of this work are available at <https://github.com/LaraTatli18/grovers-algorithm>.

where a , b , and n are given constants. While this equation has well-known solutions, in many other cases, solutions to Diophantine equations are not known (see e.g. the regularly-updated paper by Grechuk keeping track of some open and solved problems [1]). Seeking solutions to Diophantine solutions through numerical search is an established method, where searches can prove the existence of solutions where it is posited that none exist [2].

Here, we bring quantum computing to bear upon the search for Diophantine equation solutions, using Grover's algorithm [3] to look for solutions for the simple linear equation of the form (2). We choose $a = b = 1$ and $n = 5$ arbitrarily for definiteness, and also explore a simple quadratic equation to give an indication of scaling. Both examples are deliberately simple so that they can be encoded in a workable number of qubits on an available simulator. While we are not aware of works explicitly solving Diophantine equations with a quantum search algorithm, we note recent work using Grover's algorithm to perform a series of basic arithmetic procedures through search [4]. In our work we use standard classically-inspired quantum circuits for arithmetic (not using search) and use Grover for the search for equality.

2. Grover's Algorithm as Equation Solution Searcher

We give here a brief discussion of the principles of a quantum search algorithm, following the treatment in Nielsen and Chuang's textbook [5]. The search algorithm generally searches through a search space of N elements. It is supposed that one can work at the level of the index of the elements such that if presented with the index, it is easy to check if it is the element sought. This is the case in our example where checking if given numbers x and y are solutions of the given equation is straightforward by direct substitution and evaluation.

The algorithm uses an oracle, \mathcal{O} , which acts as

$$\mathcal{O}|x\rangle|q\rangle \rightarrow |x\rangle|q \oplus f(x)\rangle. \quad (3)$$

Here, $|x\rangle$ is a register of index qubits, and $|q\rangle$ is the oracle qubit. \oplus is addition modulo 2 and $f(x)$ is a function which returns 0 if index x is not a solution to the search problem, and 1 if index x is a solution.

If the oracle qubit is prepared in the state $|-\rangle = (|0\rangle - |1\rangle)/\sqrt{2}$ then the action of the oracle is

$$\mathcal{O}|x\rangle \left(\frac{|0\rangle - |1\rangle}{\sqrt{2}} \right) \rightarrow (-1)^{f(x)}|x\rangle \left(\frac{|0\rangle - |1\rangle}{\sqrt{2}} \right), \quad (4)$$

thus the action of the oracle marks out, with a phase change, components of the register state $|x\rangle$ which are solutions to the problem - i.e. have $f(x) = 1$. The full Grover algorithm then amplifies the states which have been marked, and suppresses the unmarked states, using a "diffuser" circuit. The oracle-diffuser combination together constitute a single Grover iteration. A total of $O(\sqrt{N/M})$ iterations are needed in general to have the solutions selected in the register with high probability, where M is the number of solutions in the N -element space. Note that the standard diffuser requires that valid solutions do not account for the majority of the solution space, but this is the usual condition for an interesting Diophantine equation.

For the case of our linear equation (2), the indexing register works by having $2m$ qubits in which each half encodes one of the numbers x and y . The encoding is made directly in standard binary and we do not consider negative numbers. Clearly the size of m will determine the available integers in the search space, and one must apply ever more qubits

to increase the size of the search space, though one benefits from an exponential increase in search space as the number of qubits increases linearly.

For this exploratory study, to find solutions to the equation $x + y = 5$ we use a $2m = 6$ qubit register $|x\rangle$ to encode two 3-bit numbers to add together. The oracle performs the addition and checks the result against the desired solution. The details of the quantum adder we use is given in the next section.

3. Quantum Adder Circuit

A quantum adder capable of calculating the sum of two 3-qubit binary numbers was produced using Qiskit. The adder was designed in such a way that the registers storing the input numbers were not overwritten during the calculation, as is the case with e.g. ripple-carry adders [6]. Retaining the input numbers is useful for use in further calculation, though not vital in our case.

In this setup, shown in Fig. 1, the first 3 qubits, x_0 , x_1 and x_2 , denote the binary digits representing a natural number x in the format $x_0x_1x_2$, where x_2 is the least significant bit. In the same manner, qubits y_0 , y_1 and y_2 denote the natural number y in the format $y_0y_1y_2$. Qubits a_0 and a_1 represent ancillary qubits used to hold carry bits in the addition. Qubits s_0 , s_1 , s_2 and s_3 denote the solution to $x + y$ in the form $s_0s_1s_2s_3$, where s_3 is the least significant bit. The figure shows all qubits that are needed for the full Grover algorithm. Qubit q_{12} is the oracle qubit $|q\rangle$ as in equation (3).

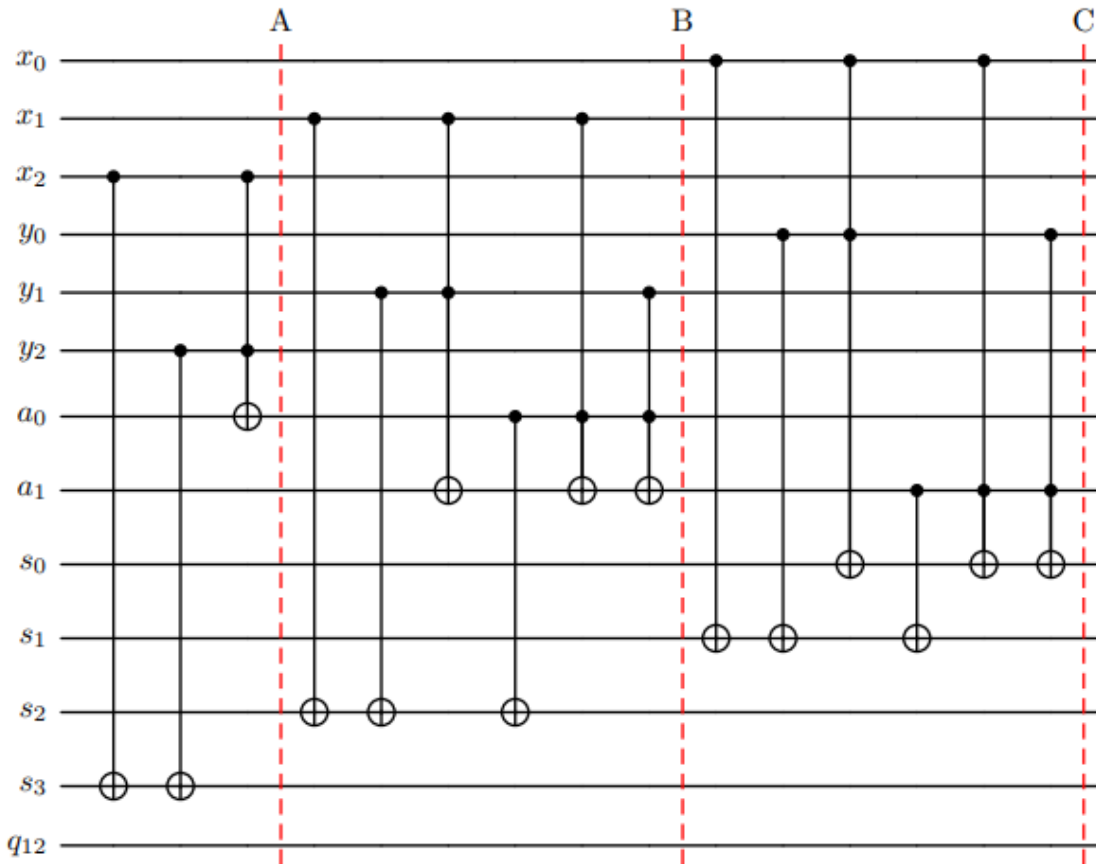


Fig. 1. A diagram of the quantum adder with barriers included to visually indicate each section.

The dividers labelled A, B, and C in the circuit help label different functional parts.

In the section terminated by divider A, an addition operation is performed on the qubits representing the least significant bits x_2 and y_2 using two CNOT gates and one Toffoli gate, with the result stored in the qubit s_3 and the first carry bit stored in a_0 .

In the section between dividers A and B, the qubits representing x_1 , y_1 , and the carry bit a_0 are added using three CNOT gates; the target is set to the sum digit s_2 . Three Toffoli gates are used to compute the second carry bit, stored in a_1 .

In the section between B and C, the sum digit s_1 is calculated using three CNOT gates acting on the qubits representing x_0 , y_0 , and the second carry bit in a_1 . The final sum digit, s_0 , is calculated using three Toffoli gates and takes into consideration the second carry bit.

In total, this adder employs 8 CNOT gates and 7 Toffoli gates collectively acting over 12 qubits. In terms of scaling to larger registers, adding two m -bit numbers requires $4m$ qubits ($2m$ representing the numbers to be added, $m - 1$ ancillary carry bits, and $m + 1$ to represent the sum). The number of gates is $3m - 1$ CNOT gates and $3m - 2$ Toffoli gates.

4. Application of Grover's Algorithm

In order to apply Grover's algorithm to solve a linear Diophantine equation $ax + by = n$ in the case $a = b = 1$ and $n = 5$, it is first necessary to apply a Hadamard gate to each of the qubits $|x_0 \dots x_2, y_0 \dots y_2\rangle$ encoding x and y . This produces the initial superposition state with all possible solution strings present with equal amplitude.

We then construct a quantum oracle capable of "marking" the solutions once queried. This consists of the quantum adder and its inverse circuit with a query circuit in between which applies a phase shift of -1 to the solution qubits of the adder, if and only if, the solution is in the state $|s_0 s_1 s_2 s_3\rangle = |0101\rangle$. All other states are left unchanged. This is achieved using two X-gates and a multi-controlled Toffoli gate targeting q_{12} , configured to be in the $|-\rangle$ state prior to implementing Grover's algorithm. X-gates are re-applied to reverse the computation. The query circuit design used for this example is provided in the left-hand part of Fig. 2.

Each iteration of the oracle is followed by the circuit used for the diffusion operator, which by acting across the six qubits $|x_0 \dots x_2, y_0 \dots y_2\rangle$ amplifies states that sum to give the desired solution only. In this diffuser circuit, shown for our case in the right-hand part of Fig. 2, the combination of Hadamard and X-gates, in conjunction with a multi-controlled Toffoli gate, enable a phase change of -1 to be applied to the initial superposition state. This completes one full iteration of the Grover algorithm. After the desired number of algorithms, one would then perform a measurement on a real quantum computer, identically prepared through many repeated experiments, to build up a histogram of most probable outcomes corresponding to the sought solution(s). The multiple measurements are known as "shots" in the language of quantum computation. In our present example, we simulate our circuit using a full quantum statevector, so present results in the next section by simply reading off the amplitudes of each register state. We show a simulation of a shot-based calculation later, for the case of a quadratic equation.

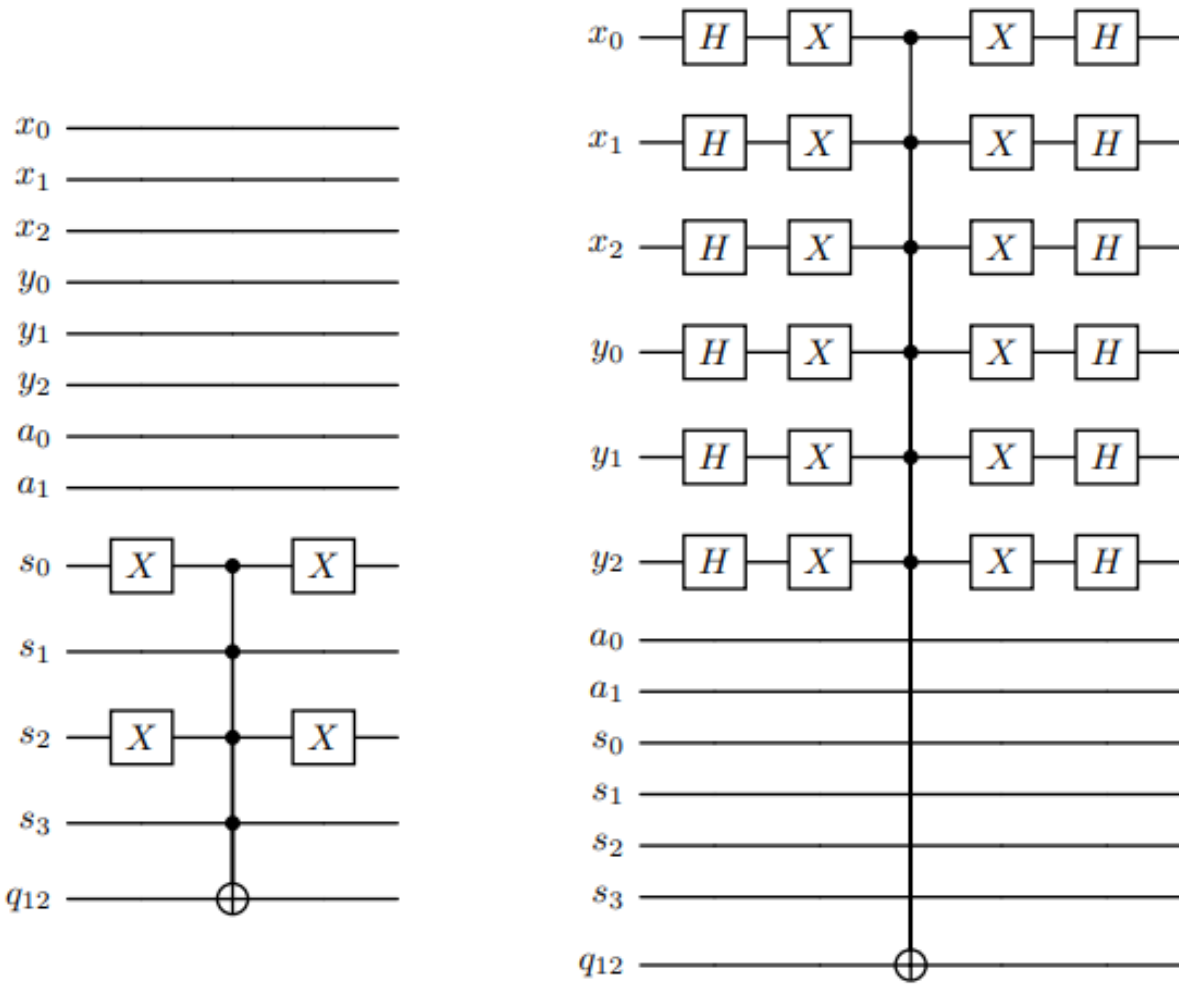


Fig. 2. Left: Diagram of the query circuit and its inverse used for the oracle operation, \mathcal{O} , for the case $|s_0s_1s_2s_3\rangle = |0101\rangle$. This circuit is run after the quantum adder circuit and is followed by the inverse quantum adder, forming a complete oracle. Right: The diffuser circuit used to amplify the solution(s).

5. Implementation and Result

The full quantum circuit, including the Hadamards to initialize the superposition of the x and y register qubits and the $|-\rangle$ initialization of the oracle qubit, is shown for one iteration in Fig 3. By running this full quantum circuit on BlueQubit’s statevector simulator, it is shown that two iterations of Grover’s algorithm are sufficient to generate the full set of solutions to our simple Diophantine equation.

The histogram displayed after one iteration is displayed in Fig. 4; the histogram for two iterations is displayed in Fig. 5. Note that the solution should be read from left to right, with the first three digits representing $x_0x_1x_2$ and the following digits $y_0y_1y_2$.

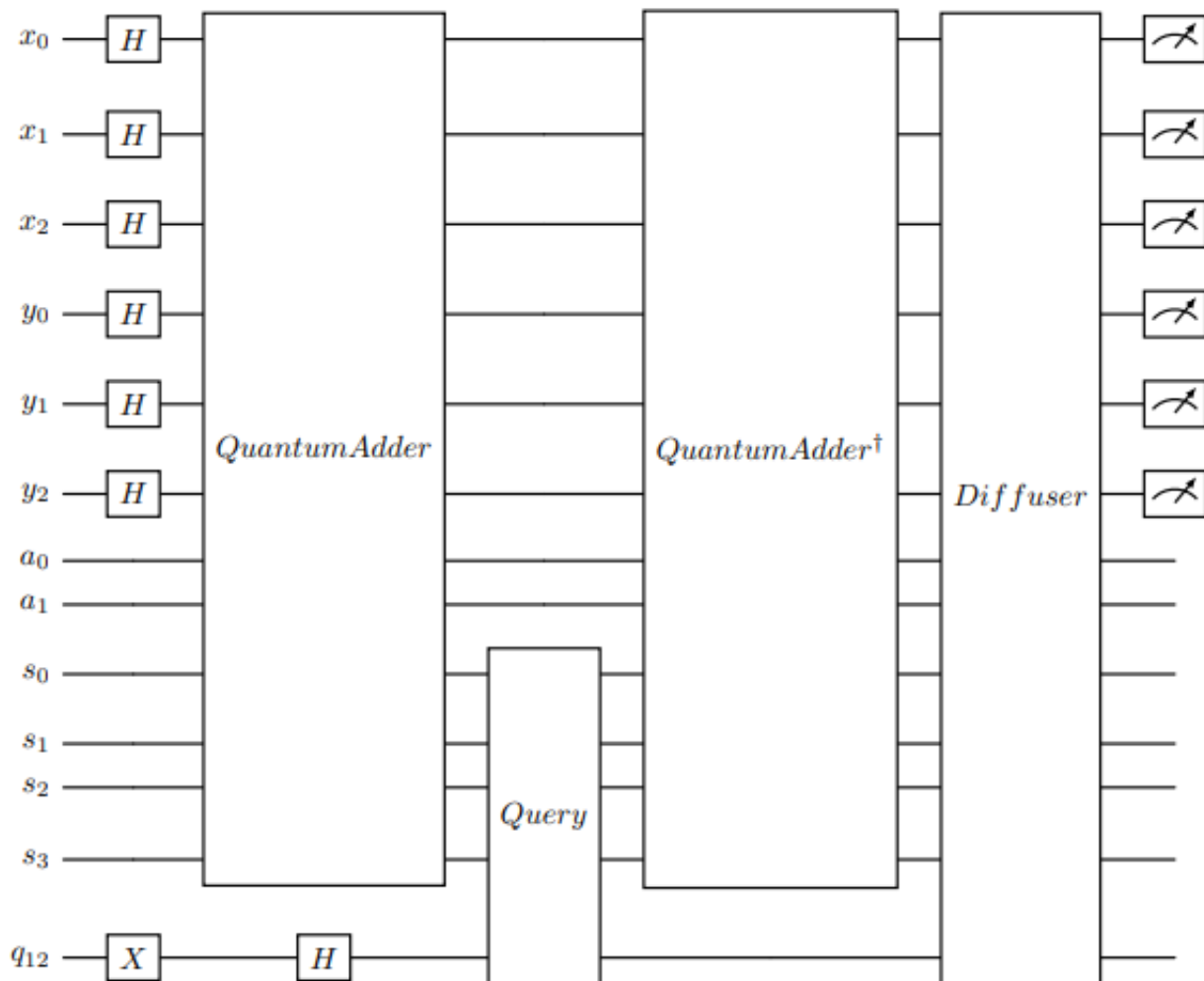


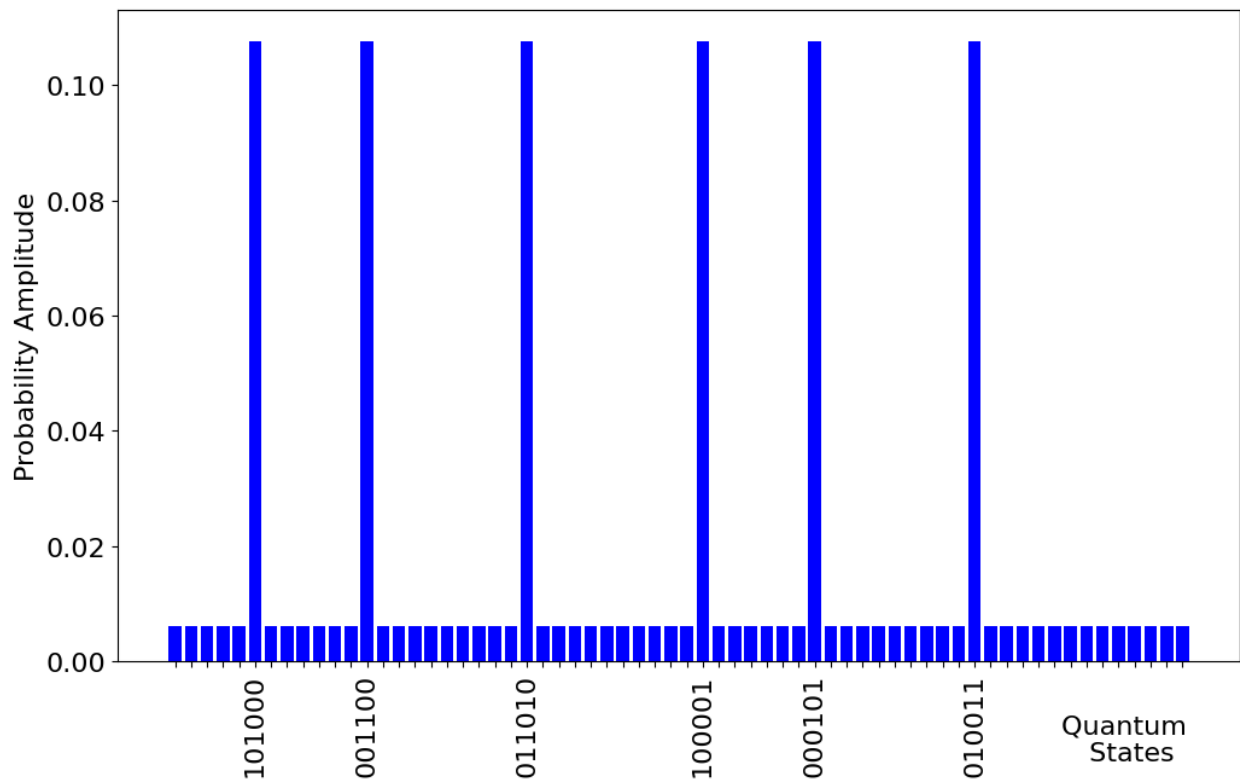
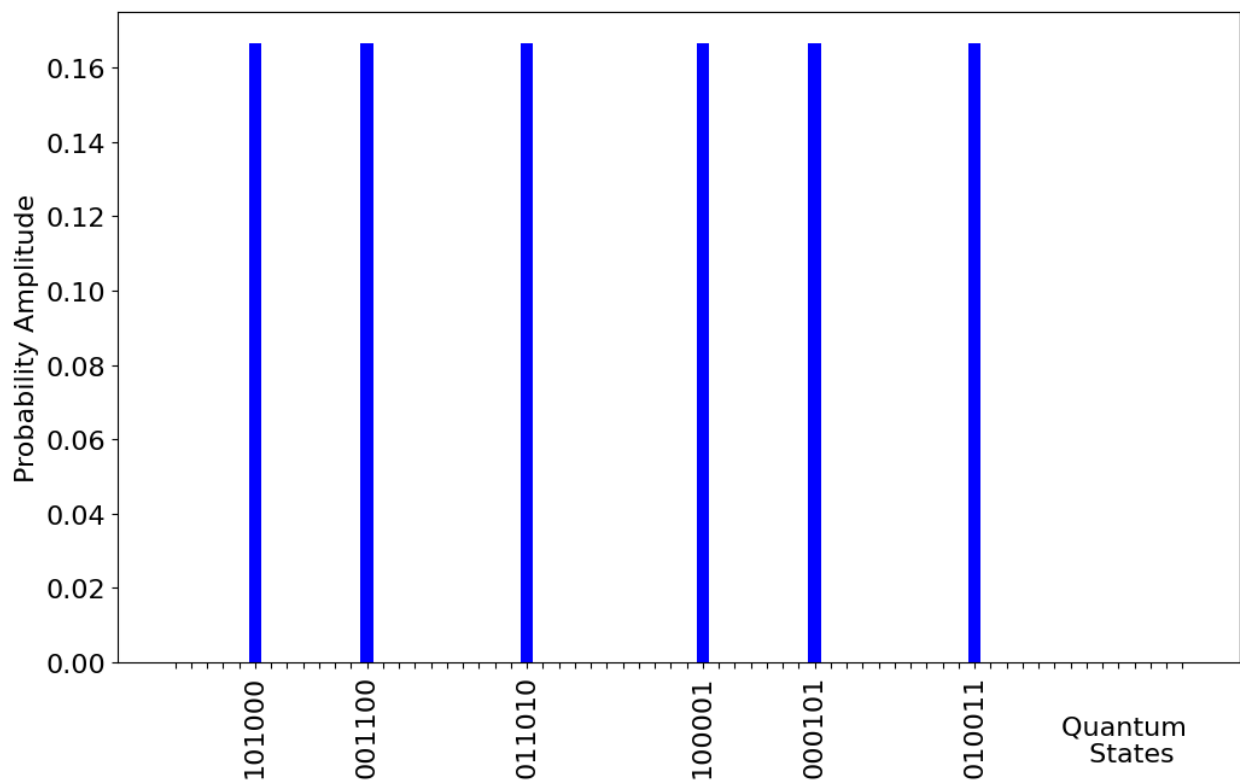
Fig. 3. The complete circuit employing one Grover iteration. The \dagger symbol indicates Hermitian conjugate.

The solutions are seen to be correct solutions of the Diophantine equation $x + y = 5$, and we tabulate them for clarity in Table 1.

Table 1. Solution states picked out by Grover's algorithm in search for solutions to Diophantine equation $x + y = 5$.

quantum state	x (base 2)	y (base 2)	x (base 10)	y (base 10)	$x + y$ (base 10)
101000	101	000	5	0	5
001100	001	100	1	4	5
011010	011	010	3	2	5
100001	100	001	4	1	5
000101	000	101	0	5	5
010011	010	011	2	3	5

We find that six iterations of Grover's algorithm are required to return to the probability distribution shown in Fig. 4.

Fig. 4. Histogram for $n=1$ iterations.Fig. 5. Histogram for $n=2$ iterations - probabilities of incorrect solutions effectively become zero.

6. Example with squaring

As an example of a more complicated equation, we look for solutions of the equation

$$x^2 + y^2 = z. \quad (5)$$

The complication of raising variables to a power brings in an increased overhead in ancillary qubits and in depth of quantum circuit necessary to perform the calculations, meaning a more automated method for circuit generation is necessary, as opposed to the hand-made adder used in our first example.

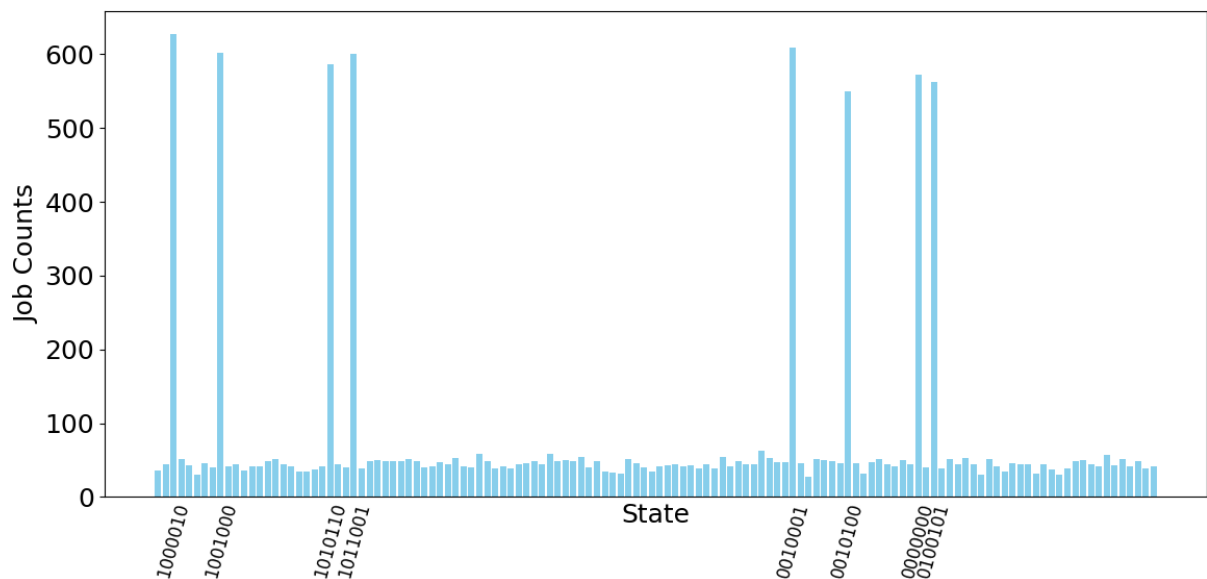


Fig. 6. Grover search for $x^2 + y^2 = z$.

Table 2. Results of simulation of quadratic equation $x^2 + y^2 = z$ using Classiq platform

index	x	y	z
1000010	2	0	4
1001000	0	2	4
1010110	2	1	5
1011001	1	2	5
0010001	1	0	1
0010100	0	1	1
0000000	0	0	0
0100101	1	1	2

We made use of the *Classiq* framework [7], which is able to automate the conversion of quantum algebra into circuit form. The equation (5), when variables x , y , and z are encoded with 2, 2, and 3 qubits respectively, is converted into a 18 qubit circuit with a depth of 502

basis gates. In order to search for Pythagorean triples, the circuit for $x^2 + y^2 = z^2$, with the minimum bit-representation to find the $\{3, 4, 5\}$ triple was designed on the Classiq system, and has a qubit count of 33 and a depth of 981. This latter circuit cannot be simulated on the free Classiq platform and we present results of the simpler equation (5), shown in Fig. 6, using a 10,000 shot simulation, as opposed to the exact statevector calculation for our first example.

The labelled peaks, reading from left to right are shown in Table 2. Note that the encoding used by Classiq is such that the seven bits in the indices encode the variables as $z_0z_1z_2y_0y_1x_0x_1$, with the least significant bit at the right in each variable encoding. Note that the noisy background for the non-amplified non-solutions in Fig. 6 is due to “shot noise” that comes from the statistical analysis of the quantum measurement.

7. Conclusions

Grover’s algorithm can be implemented to search for solutions to simple linear Diophantine equations. We have not attempted implementation on a real quantum computer, and the ability of our circuit to operate on noisy intermediate-scale quantum devices would need to be evaluated. Nevertheless, further work could investigate more complicated Diophantine equations, if access to sufficient real or simulated qubits is available. In that case, more interesting unsolved cases, like those listed in Grechuk’s paper [1] could be tackled.

Furthermore, we have not attempted to refine or optimize the quantum algorithm, rather concentrating on a straightforward implementation. Techniques to improve the Grover convergence [8] could be applied, while inclusion of a quantum counting approach [9] would allow one to gain knowledge of how many Grover iterations should be applied in advance of performing each calculation. For a more general Diophantine equation solver, such enhancements would be desirable. We also comment that we have preformed a naive brute force search, while standard methods for solving Diophantine equations can be invoked to reduce the search space.

References

- [1] B.Grechuk, “Diophantine equations: a systematic approach”, arxiv:2108.08705, 2022. <https://doi.org/10.48550/arXiv.2108.08705>
- [2] R.E. Frye, “Finding $95800^4 + 217519^4 + 414560^4 = 422481^4$ on the connection machine”, *Supercomputing 88:Proceedings of the 1988 ACM/IEEE Conference on Supercomputing, Science and Applications*, vol. 2, pp. 1061162, 1988. DOI: 10.1109/SUPER.1988.74138
- [3] L.K. Grover, “A fast quantum mechanical algorithm for database search”, *Proceedings of the Twenty-Eighth Annual ACM Symposium on Theory of Computing. STOC 96*, Association for Computing Machinery, New York, NY, USA, pp. 212219, 1996. <https://doi.org/10.1145/237814.237866>
- [4] A. Roy, J.L. Pachuau, G. Krishna and A.K. Saha, “Applying Grovers algorithm to implement various numerical and comparison operations”, *Quantum Studies: Mathematics and Foundations*, vol. 11, pp. 291306, 2024. <https://doi.org/10.1007/s40509-024-00323-w>

- [5] M. A. Nielsen and I.L. Chuang, *Quantum Computation and Quantum Information*, 10th Anniversary Edition, Cambridge University Press, Cambridge, UK 2010. <https://doi.org/10.1017/CBO9780511976666>
- [6] F. Orts, G. Ortega, E. F. Combarro and E.M. Garzon, “A review on reversible quantum adders”, *Journal of Network and Computer Applications*, vol. 170, 102810, 2020. <https://doi.org/10.1016/j.jnca.2020.102810>
- [7] Classiq: Classiq Platform. <https://platform.classiq.io/> Accessed 2024-11-13
- [8] I. Abdulrahman, “Enhancing Grover’s search algorithm: a modified approach to increase the probability of good states”, *The Journal of Supercomputing* vol. 80, pp. 1804818061, 2024. <https://doi.org/10.1007/s11227-024-06142-5>
- [9] S. Aaronson and P. Rall, “Quantum approximate counting, simplified”, *Proceedings 2020 Symposium on Simplicity in Algorithms (SOSA)*, Society for Industrial and Applied Mathematics, Philadelphia, PA, pp. 24–32, 2020. <https://doi.org/10.51137/1.9781611976014>.

Քվանտային Դիոֆանտյան հավասարումների լուծումների որոնիչ

Լարա Թաթլի¹ և Փոլ Սթիվենսոն²

¹Ֆիզիկայի ֆակուլտետ, Դարհեմի համալսարան, Դարհեմ, H1 3LE, Մեծ Բրիտանիա

²Մաթեմատիկայի և ֆիզիկայի դպրոց, Սուրեյի համալսարան, Սուրեյ, GU2 7XH, Մեծ Բրիտանիա
e-mail: lara.tatli@durham.ac.uk, p.stevenson@surrey.ac.uk

Անփոփում

Դիոֆանտյան հավասարումները բազմաչափ հավասարումներ են, սովորաբար բազմանդամ, որոնք ընդունում են միայն ամբողջ թվերի լուծումներ: Լուծումներ գտնելու համար կոպիտ ուժի մեթոդը ներառում է անհայտ փոփոխականների համար հնարավոր ամբողջ թվերի համակարգված փոխարինումը և հավասարության ստուգումը:

Գրովերի ալգորիթմը քվանտային որոնման ալգորիթմ է, որը կարող է շատ արդյունավետորեն գտնել նշված ինդեքսները ցանկում: Դիոֆանտյան հավասարման մեջ ինդեքսները որպես ամբողջ թվերի փոփոխականներ դիտարկելով՝ թվերի ալգորիթմը կարող է օգտագործվել կոպիտ ուժի կիրառմամբ լուծումներ գտնելու համար շատ ավելի արդյունավետ, քան դասական մեթոդները: Մենք ներկայացնում ենք Դիոֆանտյան ամենապարզ հնարավոր հավասարման ձեռքով կողավորված օրինակ և ավելի բարդ, բայց դեռևս մոդելավորելի հավասարման արդյունքներ, որոնք կողավորված են բարձր մակարդակի քվանտային լեզվով:

Բանալի բառեր՝ քվանտային հաշվարկներ, թվերի ալգորիթմ, Դիոֆանտյան հավասարումներ:

Поиск решения квантового диофантового уравнения

Лара Татли¹ и Пол Стивенсон²

¹Кафедра физики, Университет Дарема, Дарем, DH1 3LE, Великобритания

²Школа математики и физики, Университет Суррея, Гилфорд,
e-mail: lara.tatli@durham.ac.uk, p.stevenson@surrey.ac.uk

Аннотация

Диофантовы уравнения - это многомерные уравнения, обычно полиномиальные, в которых допускаются только целочисленные решения. Метод грубой силы для поиска решений заключается в систематической подстановке возможных целочисленных значений вместо неизвестных переменных и проверке равенства.

Алгоритм Гровера - это квантовый алгоритм поиска, который может очень эффективно находить отмеченные индексы в списке. Обработывая индексы как целочисленные переменные в Диофантовом уравнении, алгоритм Гровера может быть использован для поиска решений грубой силой гораздо эффективнее, чем классические методы. Мы представляем пример с ручным кодированием для простейшего возможного Диофантова уравнения и результаты для более сложного, но все еще моделируемого уравнения, закодированного с помощью квантового языка высокого уровня.

Ключевые слова: квантовые вычисления, алгоритм Гровера, Диофантовы уравнения.

UDC 519.6

Implementation of an Automata Mechanism for a Self-Organizing Swarm of Drones Platform

Agit F. Atashyan, Artyom A. Lazyan, Davit V. Hayrapetyan and Vahagn S. Poghosyan

Institute for Informatics and Automation Problems of NAS RA, Yerevan, Armenia
e-mail: agitatashyan1@gmail.com, artyomlazyan@gmail.com,
hayrapetyan96@gmail.com, povahagn@gmail.com

Abstract

Drone technology has enabled major advancements in autonomous systems, particularly in swarm robotics. This paper presents a novel automation technique aimed at enhancing the efficiency, adaptability, and robustness of self-organizing drone swarms. The system uses decentralized control algorithms and robust communication protocols to enable real-time adaptive learning and decision-making among drones. Each drone acts as an autonomous agent, adjusting its behavior based on environmental inputs and interactions with other drones. A hybrid communication model blending peer-to-peer and cluster-based protocols ensures effective information sharing and coordination. To build a scalable and resilient architecture, multi-agent systems theory is integrated with advanced self-organizing strategies. Extensive modeling and real-world testing evaluated the systems performance in complex scenarios such as disaster response, environmental monitoring, and surveillance. Results demonstrate significant improvements in swarm efficiency, resilience to failures, and adaptability to dynamic environments. The incorporation of adaptive learning algorithms further optimized task allocation and execution in real time. This work represents a substantial advancement in autonomous aerial robotics, offering a comprehensive framework for deploying intelligent, self-organizing drone swarms and highlighting the transformative potential of automata-based approaches in future autonomous systems.

Keywords: Swarm of drones, Automata, Self-organizing system, Mathematical models.

Article info: Received 3 November 2024; sent for review 25 November 2024; accepted 30 January 2025.

Acknowledgment: The research was supported by the Science Committee of the Republic of Armenia within the frames of the research projects 21AG-1B052 and 24DP-1B016.

1. Introduction

Drone technology has improved dramatically in recent years, including benefits in agriculture, logistics, surveillance, and disaster response. Among these advances, swarm robotics

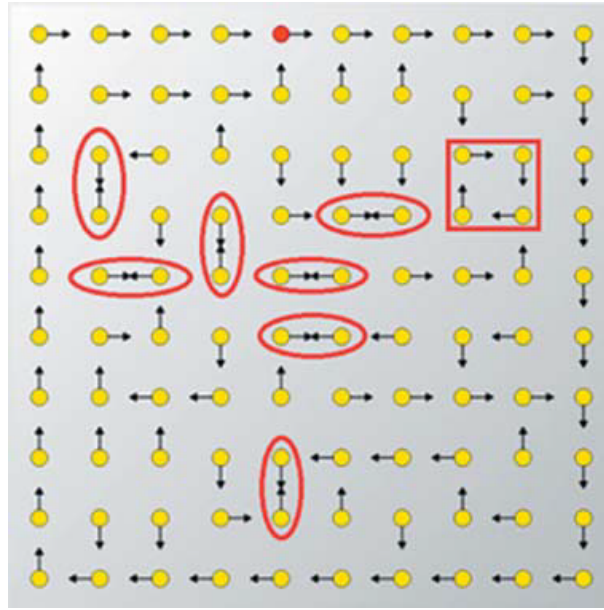
has emerged as a particularly promising field of study and application. Swarm robotics draws inspiration from natural systems such as ant colonies and bird flocks to create decentralized, self-organizing groups of robots capable of performing complicated tasks more effectively than individual units [1, 2]. This technique uses the collective intelligence and collaborative skills of several robots to achieve goals that would be difficult or impossible for a single robot [3]. The application of an automata mechanism to a self-organizing swarm of drones represents a significant leap in the field of autonomous aerial robotics. In the context of drone swarms, an automata mechanism enables individual drones to operate independently while seamlessly coordinating with other drones in the group. This decentralized strategy enhances the swarm's ability to adapt to changing conditions, handle system failures, and optimize work distribution in real-time [4, 5]. This research focuses on the creation and implementation of decentralized control algorithms, resilient communication protocols, and adaptive learning techniques. Decentralized control algorithms enable each drone to make autonomous decisions using local data and interactions with its peers. This method is similar to that of social insects, in which simple individual norms evolve into complex and flexible group behavior. Implementing such algorithms allows the drone swarm to self-organize, distribute duties, and respond to environmental changes without the need for a central controller [6]. Robust communication protocols are required for swarm cohesion and coordination. These protocols ensure that drones can communicate data despite communication delays or breakdowns. Integrating peer-to-peer communication and clustering techniques allows the swarm to strike a compromise between efficiency and endurance. This hybrid communication architecture enables the dynamic formation of subgroups inside the swarm, resulting in more efficient task execution and resource allocation [7]. Adaptive learning techniques broaden the swarm's potential by allowing drones to learn from their experiences and improve their performance over time. Machine learning techniques, such as reinforcement learning and neural networks, can be linked to the automata process, allowing drones to optimize their activities based on environmental feedback. This continual learning process enables the swarm to adapt to new problems while improving its overall efficiency and effectiveness [8]. A self-organizing drone swarm has several potential applications. Drone swarms can be used in disaster response scenarios to quickly assess damage, find survivors, and provide crucial supplies. Swarms can collect data across huge areas for environmental monitoring, providing vital insights into ecosystem health and climate change. In surveillance and security operations, drone swarms may also cover large regions, monitor targets, and provide real-time situational awareness. The goal of this study is to give a thorough framework for implementing an automata mechanism in drone swarms while exhibiting the advantages of decentralized control, robust communication, and adaptive learning. By tackling the problems and opportunities connected with this technology, we hope to pave the way for future developments in autonomous aerial robotics and open up new avenues for a variety of applications.

2. Self-Organized Systems and Gossiping Algorithms

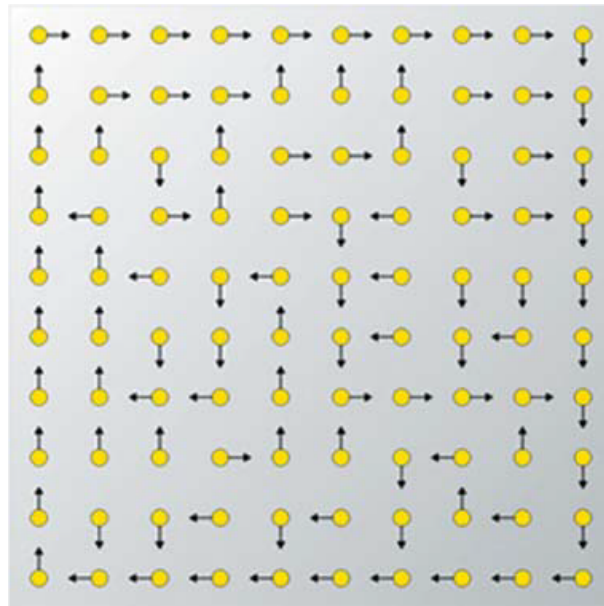
Self-organization, also called spontaneous order in the social sciences, is a process where some form of overall order arises from local interactions between parts of an initially disordered system [9]. The process can be spontaneous when sufficient energy is available without outside control. Self-organization is often triggered by seemingly random fluctuations amplified by positive feedback. Self-organization is wholly decentralized and distributed over all the

components of the entire system. As such, the organization is typically robust and able to survive or to self-repair from substantial perturbations. A narrower, still much closed concept related to self-organization is the phenomenon of self-ordering of systems. Complex dynamic systems are often self-organizing, and depending on the specified leading groups of properties, they are also called self-regulating, self-adjusting, self-learning, or self-algorithmizable systems. The Abelian sandpile model is the simplest and analytically tractable model of self-organized criticality [10]. In [11], a detailed overview of the known results about height probabilities and special correlation functions of the model is presented. In parallel, the research also focuses on the rotor-router model [12], where a one-to-one correspondence between the defined recurrent states and the graph spanning trees is observed. The rotor mechanism, first proposed in the theory of self-organized criticality under the name Eulerian walk, was rediscovered independently as a tool for the de-randomization of the random walk [13]. The dynamics of the rotor-router walk can be modeled over a square lattice with arrows attached to the sites, where arrows are directed toward one of the neighbors. A particle (a chip) performs a walk, jumping from a site to a neighboring site. Arriving at a given site, the particle changes the direction of the arrow at that site in a prescribed order and moves toward the neighbor pointed out by the new position of the arrow. Obviously, given an initial orientation of arrows on the whole lattice, the rotor-router walk is deterministic. The walk starting from uniformly distributed random initial configurations is called a uniform rotor walk. If the lattice is finite, the walk starting from an arbitrary site settles into an Eulerian circuit where each edge of the lattice is visited exactly once in every direction. When the walker is on the Eulerian circuit, the configurations of rotors associated with each site are recurrent. Graphically, the recurrent configuration representation is a unicycle. This is a specific state where the arrows form a spanning set of directed edges containing a unique directed cycle to which the particle belongs. Correlation between the Abelian sandpiles, Euler circuits and the rotor-router model is a subject to a rigorous mathematical survey [14]. The essential idea highlighted in the survey is the consideration of the rotor-routing action of the sandpile group on spanning trees in parallel with rotor-routing on unicycles. The rotor-router walk started from an arbitrary rotor configuration on a finite sink-free directed graph G , enters into an Euler circuit (Euler tour) and remains there forever (Fig. 1) after a finite number of steps.

In [13], the following property is proved: if at some moment, the rotors form a closed clockwise contour on the planar graph, then the clockwise rotations of rotors generate a walk which enters into the contour at some vertex, performs a number of steps inside the contour so that the contour formed by rotors becomes anti-clockwise, and then leaves the contour at the same vertex. This property generalizes the previously proved theorem for the case when the rotor configuration inside the contour forms a cycle-rooted spanning tree, and all rotors inside the contour perform a full rotation. We use this proven property for an analysis of the sub-diffusive behavior of the rotor-router walk. The suggested swarm algorithms and models have been designed based on the obtained results of the authors given below. The distinguishing characteristic of our approach against the existing solutions is that it meets all the classical requirements imposed on self-organizing systems, whereas the existing implementations each addresses the swarm construction and management specifically. Based on the analysis of available solutions and to best meet the requirements for UAV swarms construction, an optimally distributed software-hardware cloud system is suggested to manage self-organizing UAV swarms with the below mentioned capabilities. UAVs are loaded with basic schemes for information exchange. The development of decentralized and self-



(a) with cycle



(b) without cycle

Fig. 1. Cycle erasing illustration

organizing swarms of logically linked UAVs involved the design of optimal and fault-tolerant schemes (gossip/broadcast models). This enabled performing dynamic snapshotting and full exchange of captured images of the surveyed areas during the swarm quasi-random walk (rotor-router model). Essential definitions, concepts, and mathematical models of the construction are given below [15]. The gossip problem is formulated as follows: each of the

participants within the group possesses distinct information. The goal is to distribute all the messages among all participants via phone calls. The minimum number of required calls is well-known: $\tau = 2n - 4$, $n > 4$. This problem can be modeled as a weighted graph, with vertices representing participants and edges representing the times at which peer communications occur. Unlike the existing methods, our approach enables communication between any two vertices (peers) to happen instantaneously, requiring only a single time tick. The utilization of k -fault-tolerant gossip graphs allows for the extension of the gossip problem to accommodate up to k arbitrary call failures. It is noteworthy that in the event of a call failure, no information exchange takes place. Subsequently, the subsequent objective was to determine the minimum number of calls required to achieve k -fault tolerance among n participants, denoted as $\tau(n, k)$, which remains an unresolved challenge. Presently, there exist only upper or lower bounds for

$$\tau(n, k) \leq \frac{n}{2} \log_2 n + \frac{nk}{2} \quad (1)$$

for n being a power of 2, and

$$\tau(n, k) \leq 2n \lfloor \log_2 n \rfloor + n \lceil \frac{k-1}{2} \rceil, \quad (2)$$

otherwise [16].

Definition 1. A Knödel graph with $n \geq 2$ the vertices (n is even) and $1 \leq \Delta \leq \lfloor \log_2 n \rfloor$ degrees is denoted by $W_{\Delta, n}$, where vertices are pairs of type (i, j) , $i = 1, 2; 0 \leq j \leq \frac{n}{2} - 1$. For each of j and l , $0 \leq j \leq \frac{n}{2} - 1, l = 1, \dots, \Delta$, there exists an edge weighted l between $(1, j)$ and $(2, j + 2l - 1 - 1 \bmod \frac{n}{2})$ nodes.

3. Implementation of an Automata System Using Cloud Infrastructure and Physical Drones

This section discusses the automata environment provided by the platform, including dynamic scenarios and environmental variables (see Fig. 2).

3.1 Generate requests from QT

The Applications collection is produced utilizing the C++/QT library and Flask APIs. So, everything manages the toolset utilizing the QT environment. This section explains how to create requests from the QT environment to power the platform's functionality. An active server is required to start the preparation platform, and programs must automatically establish connections. Users upload location images to the server, which displays an input window displaying a map based on the image's coordinates. While users enter the appropriate coordinates, the system computes the real-world coordinates for each pixel, ensuring accuracy while configuring the simulation environment. The QT service layer protects against attacks by utilizing strong encryption while sending data to virtual servers in the cloud architecture over secure Internet TCP protocol communication channels. The drone map/automata graph module allows users to construct and manage maps for drone swarm navigation and task management. The JSON structure of all queries ensures that the platform and the QT environment communicate effectively and transparently. Users design a flight operation

network for the drone swarm using the computed absolute coordinates of the pixels in the landscape image. The classification of vertices into Corner, Side Border, and Inner types facilitate precise drone operations planning. After that, users enter the drone's IP port to commence communication and select specific side vertices for drone installation. When the return router method completes any network cycles, the system generates coordinates and navigation data, which are then sent to the drone ground station. With the correct coordinates, the drones can travel the network without assistance from a person. Users can indicate target locations for drone strikes on a terrain image using internal geographic coordinates. Users can adjust the default network topology as needed. All changes are logged in a detailed log, which immediately alerts the cloud server and ensures that all users' graphical interfaces are consistent.

3.2 Cloud Infrastructure

The development of a cloud-based platform for mission preparation for self-organizing drone swarms using multi-agent systems, such as sandpile models, rotor-router models, and optimal gossip broadcast schemes, represents a significant innovation in the domain of logically interconnected and decentralized intelligent networks (see Fig 2.).

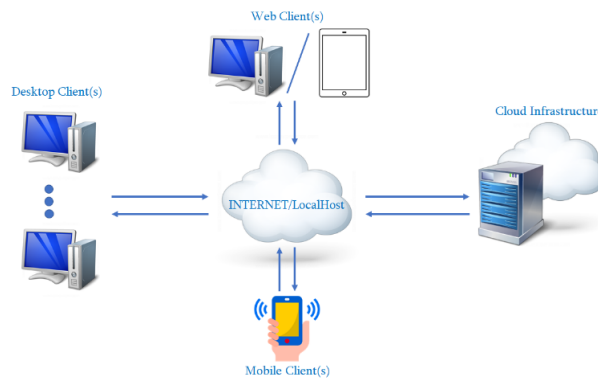


Fig. 2. Cloud infrastructure

The development of software toolsets for managing self-organizing drone swarms is both difficult and costly. As a result, combining virtual environments, cloud technologies, and computational resources into a single platform provides realistic solutions to these issues. The proposed platform seeks to enable autonomous mission execution across a wide range of activities and scenarios while lowering the time and cost associated with drone swarm missions. Our proposed and validated solutions for building high-performance computing infrastructures serve as the foundation for the design and implementation of this cloud platform, which adheres to modern standards and includes AI-powered collection, categorization, and processing of massive data, improved electronic infrastructure energy usage and cloud computing settings, efficient use of HPC resources for linear algebra computations, and cloud service disposal. Cloud computing has substantially improved the efficiency of image-processing for drones by leveraging scalable computer resources and large amounts of storage. Our proposed and validated solutions for building high-performance computing infrastructures serve as the foundation for the design and implementation of this cloud

platform, which adheres to modern standards and includes AI-powered collection, categorization, and processing of massive data, improved electronic infrastructure energy usage and cloud computing settings, efficient use of HPC resources for linear algebra computations, and cloud service disposal. Cloud computing has substantially improved the efficiency of UAV image-processing processes by leveraging scalable computer resources and large amounts of storage. Our strategy makes use of a serverless cloud platform for high-performance computing (HPC), which has been precisely engineered to properly handle the drone swarm's HPC workloads, guaranteeing that swarm operations are completed on time. A server execution environment is created within the cloud architecture, with one server dedicated to swarm or single-drone flying operations. This server's IP address is documented in a functional log file that users can access via a graphical user interface. Each server is assigned a specific task, which involves initiating data processing and ensuring that results are visible and synced. This architecture facilitates the dispersed and efficient execution of drone flying operations and data processing.

4. Conclusion

This study effectively demonstrated the use of an automata mechanism to improve a drone swarm's self-organizing capabilities. The swarm functions efficiently and adapts to changing situations without central control by utilizing decentralized control algorithms, strong communication protocols, and adaptive learning processes. The use of cloud services enhances these capabilities by providing scalable computer resources and real-time data processing. Cloud-based infrastructure improves swarm communication and coordination, enabling more efficient information sharing and dynamic work allocation. The experimental results indicate considerable gains in task performance, resource utilization, and adaptability, demonstrating the system's usefulness in a variety of applications such as disaster response, environmental monitoring, and surveillance. Finally, the synergy between automata mechanisms and cloud services provides a solid foundation for future advances in autonomous drone swarms, paving the way for novel solutions in complex and dynamic circumstances.

References

- [1] V. Subbarayalu and M. A. Vensuslaus, "An intrusion detection system for drone swarming utilizing timed probabilistic automata", *Drones*, vol. 7, no.4, 248, 2023. <https://doi.org/10.3390/drones7040248>
- [2] W. Jung, C. Park, S. Lee and H. Kim, *Enhancing UAV Swarm Tactics with Edge AI: Adaptive Decision Making in Changing Environments*, *Drones*, vol. 8, no. 10, 582, 2024. <https://doi.org/10.3390/drones8100582>
- [3] J. Kusyik, M.U.Uyar, K. Ma et al., "Artificial intelligence and game theory controlled autonomous UAV swarms", *Evol. Intel.* vol. 14, pp. 17751792, 2021. <https://doi.org/10.1007/s12065-020-00456-y>
- [4] M. Abdelkader, S. Gler, H. Jaleel and J. S. Shamma "Aerial swarms: Recent applications and challenges", *Current robotics reports*, vol.2, no. 3, pp. 309-320, 2021.
- [5] W. Y. H. Adoni, J. S. Fareedh, S. Lorenz, R. Gloaguen, Y. Madriz, A. Singh and T. D. Khne Intelligent Swarm: Concept, Design and Validation of Self-Organized UAVs

- Based on LeaderFollowers Paradigm for Autonomous Mission Planning, *Drones*, vol. 8, no. 10, 575, 2024. <https://doi.org/10.3390/drones8100575>
- [6] V. Poghosyan, S. Poghosyan, A. Lazyan, A. Atashyan, D. Hayrapetyan, Y. Alaverdyan and H. Astsatryan, “Self-organizing multi-user UAV swarm simulation platform”, *Programming and Computer Software*, vol. 49, Suppl 1, pp. S7-S15, 2023.
- [7] Y. Ding, Z. Yang, Q. V. Pham, Y. Hu, Z. Zhang and M. Shikh-Bahaei, “Distributed machine learning for uav swarms: Computing, Sensing, and Semantics”, *IEEE Internet of Things Journal*, vol. 11, no. 5, pp. 7447-7473, 2024.
- [8] U.S. Government Accountability Office, Science and Tech Spotlight, Drone Swarm Technologies, 2023. <https://www.gao.gov/assets/gao-23-106930.pdf>
- [9] P. Bak, C. Tang and K. Wiesenfeld, “Self-organized criticality: an explanation of the $1/f$ noise”, *Phys. Rev. Lett.*, vol. 59, no. 4, pp. 381384, 1987. <https://doi.org/10.1103/PhysRevLett.59.381>
- [10] D. Dhar, “Self-organized critical state of sandpile automaton models”, *Phys. Rev. Lett.*, vol. 64, no. 14, pp. 16131616, 1990. <https://doi.org/10.1103/PhysRevLett.64.1613>
- [11] P. Ruelle, “Sandpile models in the large, Front”, *Phys.*, vol. 9, p. 641966, 2021. <https://doi.org/10.3389/fphy.2021.641966>
- [12] V.B. Priezzhev, D. Dhar, A. Dhar and S. Krishnamurthy, “Eulerian walkers as a model of self-organized criticality”, *Phys. Rev. Lett.*, vol. 77, no. 25, pp. 50795082, 1996. <https://doi.org/10.1103/PhysRevLett.77.5079>
- [13] V.V. Papoyan, V.S. Poghosyan and V.B. Priezzhev, “A loop reversibility and subdiffusion of the rotor-router walk”, *J. Phys. A: Math. Theor.*, vol. 48, no. 28, p. 285203, 2015. <https://doi.org/10.1088/1751-8113/48/28/285203>
- [14] A.E. Holroyd, L. Levine, K. Meszaros, Y. Peres, J. Propp and D.B. Wilson, “Chip-firing and rotor-routing on directed graphs”, *In and Out of Equilibrium*, vol. 2, pp. 331364, 2008. https://doi.org/10.1007/978-3-7643-8786-0_17
- [15] S. Poghosyan, Y. Alaverdyan, V. Poghosyan, S. Abrahamyan, A. Atashyan, H. Astsatryan and Y. Shoukourian, “Certain methods for investigating epidemics and preventing the spread of viruses in self-organizing systems”, *AIP Conf. Proc.*, vol. 2757, no. 1., 2023. <https://doi.org/10.1063/5.0135809>
- [16] A. M. G. Gbagir, K. Ek, and A. Colpaert, “Open-DroneMap: multi-platform performance analysis”, *Geographies*, vol. 3, no. 3, pp. 446-458, 2023. <https://doi.org/10.3390/geographies3030023>

Ավտոմատների մեխանիզմի իրականացումը ինքնակազմակերպվող ԱԹՍ-երի երամի հարթակի համար

Ազիթ Ֆ. Աթաշյան, Արտյոմ Ա. Լազյան, Դավիթ Վ. Հայրապետյան
Վահագն Ս. Պողոսյան

ՀՀ ԳԱԱ Ինֆորմատիկայի և ավտոմատացման պրոբլեմների ինստիտուտ, Երևան, Հայաստան
e-mail: agitatashyan1@gmail.com, artyomlazyan@gmail.com
hayrapetyan96@gmail.com, povahagn@gmail.com

Ամփոփում

Անօդաչու թռչող սարքերի տեխնոլոգիան հնարավորություն է տվել զգալի առաջընթացի հասնել ինքնավար համակարգերում, մասնավորապես՝ երամային ռոբոտատեխնիկայի ոլորտում: Այս հոդվածում ներկայացվում է ավտոմատների նոր տեխնոլոգիա, որը նպատակ ունի բարձրացնել ինքնակարգավորվող անօդաչու երամի արդյունավետությունը, հարմարվողականությունը և հուսալիությունը: Համակարգը օգտագործում է կենտրոնացված կառավարման ալգորիթմներ և հուսալի հաղորդակցման պրոտոկոլներ՝ անօդաչու սարքերի միջև իրական ժամանակում հարմարվողական ուսուցման և որոշումների ընդունման ապահովման համար: Յուրաքանչյուր անօդաչու սարք գործում է որպես ինքնավար գործակալ՝ իր վարքը փոփոխելով՝ ելնելով շրջակա միջավայրի ներմուծումներից և մյուս սարքերի հետ փոխազդեցությունից: Հաղորդակցության հիբրիդային մոդելը, որը համատեղում է peer-to-peer և կլաստերային պրոտոկոլները, ապահովում է տեղեկատվության արդյունավետ փոխանակում և համաժամեցում: Մասշտաբային և կայուն ճարտարապետություն ստեղծելու համար բազմագործակալ համակարգերի տեսությունը ինտեգրվել է ինքնակազմակերպման առաջադեմ ռազմավարությունների հետ: Ընդգրկում մոդելավորումը և իրական պայմաններում փորձարկումները գնահատել են համակարգի աշխատանքը բարդ սցենարներում, ինչպիսիք են աղետների արձագանքը, շրջակա միջավայրի մոնիթորինգը և հսկողության առաքելությունները: Արդյունքները ցույց են տվել երամի արդյունավետության, խափանումների նկատմամբ կայունության և դինամիկ միջավայրերին հարմարվելու ունակության զգալի բարելավում: Հարմարվողական ուսուցման ալգորիթմների ներգրավումը հետագա կերպով օպտիմալացրել է առաջադրանքների բաշխումը և կատարումը իրական ժամանակում: Այս աշխատանքը կարևոր առաջընթաց է ինքնավար օդային ռոբոտատեխնիկայում՝ առաջարկելով ինտելեկտուալ, ինքնակարգավորվող ԱԹՍ երամի տեղակայման համապարփակ շրջանակ և ընդգծելով ավտոմատների վրա հիմնված մոտեցումների փոխակերպող ներուժը ապագա ինքնավար համակարգերում:

Բանալի բառեր՝ ԱԹՍ երամ, ավտոմատներ, ինքնակարգավորվող համակարգ, մաքեմատիկական մոդելներ:

Реализация механизма автоматов для самоорганизующейся платформы роя дронов

Агит Ф. Аташян, Артём А. Лазян, Давид В. Айрапетян и Ваагн С. Погосян

Институт проблем информатики и автоматизации НАН РА, Ереван, Армения

e-mail: agitatashyan1@gmail.com, artyomlazyan@gmail.com

hayrapetyan96@gmail.com, povahagn@gmail.com

Аннотация

Технология дронов позволила добиться значительных успехов в автономных системах, в частности в роевой робототехнике. В этой статье представлена новая технология автоматизации, направленная на повышение эффективности, адаптивности и надежности самоорганизующихся роев дронов. Система использует децентрализованные алгоритмы управления и надежные протоколы связи для обеспечения адаптивного обучения и принятия решений в реальном времени среди дронов. Каждый дрон действует как автономный агент, корректируя свое поведение на основе входных данных окружающей среды и взаимодействия с другими дронами. Гибридная модель связи, сочетающая одноранговые и кластерные протоколы, обеспечивает эффективный обмен информацией и координацию. Для создания масштабируемой и устойчивой архитектуры теория многоагентных систем интегрирована с передовыми стратегиями самоорганизации. Обширное моделирование и тестирование в реальных условиях оценивали производительность систем в сложных сценариях, таких как реагирование на стихийные бедствия, мониторинг окружающей среды и наблюдение. Результаты демонстрируют значительные улучшения эффективности роя, устойчивости к сбоям и адаптивности к динамическим средам. Включение адаптивных алгоритмов обучения еще больше оптимизировало распределение и выполнение задач в реальном времени. Эта работа представляет собой существенный прогресс в автономной воздушной робототехнике, предлагая комплексную структуру для развертывания интеллектуальных, самоорганизующихся роев дронов и подчеркивая преобразующий потенциал подходов на основе автоматов в будущих автономных системах.

Ключевые слова: рой дронов, автоматы, самоорганизующаяся система, математические модели.

UDC 544.12, 004.942

FlashRMSD: An Effective Approach for Symmetry-Corrected RMSD Calculation with Extensive Benchmark Analysis

Vahagn N. Altunyan

Yerevan State University, Yerevan, Armenia
e-mail: altunyanv@gmail.com

Abstract

Root-mean-square deviation (RMSD) is a crucial metric for quantifying molecular structure similarity. However, the associated combinatorial challenges complicate the calculation process when dealing with highly symmetric molecules. Although several open-source tools have been developed to perform symmetry-corrected RMSD computations, each has limitations in terms of speed, accuracy, or usability. In this paper, we introduce FlashRMSD, a novel, rapid approach for symmetry-corrected RMSD calculation. In addition, we present an extensive benchmark dataset to evaluate RMSD calculation tools and provide a comparative analysis of existing methods alongside our proposed tool.

Keywords: Symmetry corrected RMSD, FlashRMSD, Molecular docking, Backtracking.

Article info: Received 30 March 2024; sent for review 1 April 2025; accepted 2 May 2025.

1. Introduction

Root Mean Square Deviation (RMSD) is a cornerstone metric in computational chemistry, widely employed to measure the similarity between molecular conformations. It is pivotal in applications such as assessing docking outcomes, guiding lead optimization, and filtering large sets of candidate structures in high-throughput screening. However, RMSD calculations become problematic when molecules exhibit symmetry—such as repeated functional groups or identical substituents—because standard atom-to-atom mappings often ignore these chemical equivalences. This oversight can produce inflated RMSD values and hinder accurate comparisons.

Several open-source tools attempt to address these symmetry-related challenges, but each exhibits notable constraints in terms of computational efficiency. Moreover, the field currently lacks a standardized dataset that captures the full breadth of symmetrical molecular structures. This absence complicates the fair evaluation of different RMSD methods, as it is challenging to determine whether the observed failures originate from the algorithms themselves or from insufficient testing.

Our previous studies [1] demonstrated that while existing RMSD tools can effectively process highly symmetrical structures, they often struggle with certain specific molecular configurations that are overlooked during benchmarking. These structural cases, left unexamined in typical tool evaluations, highlight gaps in current methodologies and the need for more comprehensive benchmarking datasets.

To address these challenges, we make two key contributions in this work:

1. **Comprehensive Dataset** – We curate a dataset designed to challenge RMSD tools by incorporating molecules with diverse and tricky symmetry patterns that can mislead certain tools into unnecessary computations. By spanning a broad range of molecular scaffolds, this dataset provides a rigorous benchmark for evaluating both existing and novel methods.
2. **FlashRMSD: A Symmetry-Corrected RMSD Tool** – We introduce *FlashRMSD*, an efficient approach for symmetry-aware RMSD calculation. Our method leverages an optimized backtracking algorithm with pruning strategies to account for chemical equivalences, ensuring both accuracy and computational efficiency.

The remainder of this paper is structured as follows. First, in Section 2, we describe the construction and scope of our new dataset. Section 3 then introduces the *FlashRMSD* tool, detailing its theoretical background and practical implementation. Next, in Section 4, we outline the benchmark setup used to evaluate *FlashRMSD* alongside other RMSD calculation tools. Finally, Section 5 presents our comparative results, and Section 6 discusses edge cases of molecules that are challenging for some or all RMSD calculation tools.

1.1. Background and Related Work

1.1.1 RMSD and Symmetry Challenges

RMSD quantifies the structural similarity between two molecular conformations by measuring the root mean squared distance between corresponding atoms. While seemingly straightforward, RMSD calculations can be undermined by molecular symmetry. In symmetrical molecules, multiple valid atom mappings exist, and failing to account for all chemically equivalent correspondences can lead to erroneous or inflated RMSD values. These inaccuracies can influence the results of tasks like molecular docking, virtual screening, and structure-based drug design, where having reliable similarity metrics is crucial.

1.1.2 Existing RMSD Tools

Several RMSD tools have been developed, each tackling different aspects of the problem with varying degrees of effectiveness:

- **spyRMSD[2]:**
Designed for flexibility and ease of use, *spyRMSD* integrates with popular libraries such as RDKit and Open Babel, leveraging Python for accessibility. However, its reliance on libraries for graph isomorphism calculations lacks problem-specific optimizations, making it highly inefficient. Additionally, it offers limited support for bond-type variations.
- **DockRMSD[3]:**
Optimized for computational efficiency, *DockRMSD* is implemented in C, allowing for rapid calculations with minimal overhead. However, its functionality is restricted to specific MOL2 file formats, and it may fail silently (e.g., via segmentation faults) when encountering format inconsistencies or complex symmetries. While it does account for bond types, it silently ignores them if no valid mappings are found.
- **obrms:**
As part of the OpenBabel[4] cheminformatics toolkit, *obrms* supports multiple file formats and cross-RMSD calculations. While it is both efficient and versatile, its packaging introduces some overhead, making it slightly less efficient than *DockRMSD*.

Collectively, these tools highlight a common limitation: while each addresses specific user needs, none effectively balances speed, reliability, and robust handling of symmetrical equivalences. Furthermore, the absence of a comprehensive, standardized dataset encompassing diverse symmetrical structures makes it challenging to objectively evaluate their strengths and weaknesses.

1.1.3 Motivating a New Dataset

In the absence of a dedicated dataset that systematically tests RMSD performance on symmetrical structures, evaluations often rely on ad hoc collections of molecules or focus on only a few specific chemotypes. This approach fails to capture the breadth of symmetry types encountered in real-world applications, ranging from simple ring systems to large, multiply substituted scaffolds.

By presenting a new dataset that features a wide range of symmetrical patterns, we aim to provide a benchmark that can reveal subtle performance gaps in existing RMSD tools. This resource will also serve as the testing ground for our proposed *FlashRMSD* tool, enabling transparent comparisons and guiding future improvements in symmetry-corrected RMSD algorithms.

2. Dataset

Our dataset was constructed using molecules from two primary sources: the **Chemical Component Dictionary (CCD)**¹[5] and the **Biologically Interesting Molecule Reference**

¹ <https://www.wwpdb.org/data/ccd>

Dictionary (BIRD)², both obtained from the RCSB Protein Data Bank (PDB). As of February 2024, the CCD dataset contained 45,622 molecules, primarily small organic compounds commonly found in macromolecular crystallography, while the BIRD dataset contained 819 molecules, representing biologically relevant non-polymeric entities. These datasets were selected for their structural diversity and derivation from real protein–ligand systems. They include a number of challenging symmetric or pseudo-symmetric structures, which we analyze in detail through specific case studies in Section 6.

2.1 Data Preprocessing

Since the datasets were originally in different formats, we generated a new conformation for each entry, saved them in the SDF file format for further processing, and subsequently merged both datasets.

Initial conformer generation was primarily performed using the EmbedMolecule function of the RDKit toolkit [6], followed by structural optimization with the MMFF94 force field [7]. RDKit was chosen due to its efficient 3D embedding algorithm, improved handling of torsional strain, and its ability to generate high-quality conformers that are more physically realistic. In cases where RDKit’s conformer generation failed, OpenBabel’s conformer generation was used as a fallback due to its broader support for certain chemical structures and alternative embedding methods. Entries for which both tools failed to generate conformers were excluded from the dataset. Additionally, molecules containing fewer than five heavy atoms were removed to ensure structural relevance and meaningful molecular modeling.

After preprocessing, the final dataset comprised 45,706 molecules. An overview of the dataset is provided in Table 1.

Table 1: Overview of Molecule Sources.

Source	Molecules Retrieved	Molecules Retained	Conformer Generation Tool	
			RDKit	Openbabel
CCD	45622	44901	44630	271
BIRD	819	805	755	50
Total	46441	45706	45385	321

2.2 Conformer Generation

To generate realistic 3D conformations of molecules for downstream analysis (see Section 4), we employed **SMINA**[8], a fork of AutoDock Vina, using structure-based docking against a protein target.

The chosen target was **HIV-1 protease** from PDB entry **1EBY**, selected for the following reasons:

² <https://www ww pdb.org/data/bird>

- □ **Symmetrical Dimeric Structure:** HIV-1 protease functions as a symmetrical homodimer, which mirrors the structural symmetry observed in many small molecules, making it a relevant docking environment.
- □ **Large Binding Pocket:** The active site is spacious and capable of accommodating a wide variety of ligand sizes, supporting the diversity of our dataset.

For the docking simulations, default parameters were used with one exception: the exhaustiveness setting, which determines the thoroughness of the search, was reduced from the default value of 8 to 4 to obtain results within a reasonable computation time.

For each ligand, up to nine docked conformations were generated and saved in a single SDF file. These conformations were subsequently used for downstream analyses, including symmetry evaluation and conformational clustering.

2.3 Final Data Format and Organization

To ensure compatibility with various RMSD calculation tools, including *DockRMSD*, the dataset underwent the following formatting and organization steps:

- □ **Conversion to MOL2 Format:** All SDF files containing multiple conformations per molecule were converted to MOL2 format using the obabel tool from Openbabel toolkit, ensuring broad compatibility with RMSD tools.
- □ **Individual Conformation Files:** In addition to multi-conformer files, separate files for each conformation were generated in both SDF and MOL2 formats to facilitate structure-specific analyses.

The dataset is systematically organized to provide clear accessibility:

- □ **Parent Directories:** Molecules are categorized based on their source repository:
 - □ CCD/[MOLECULE_ID]/
 - □ BIRD/[MOLECULE_ID]/
- □ **Per-Molecule Subdirectories:** Each molecule is stored in a folder named after its unique identifier, which contains the following files:
 - □ `all_poses.sdf` – Multi-conformation file in SDF format.
 - □ `all_poses.mo12` – Multi-conformation file in MOL2 format.
 - □ `pose_X.sdf` – Individual conformation X in SDF format.
 - □ `pose_X.mo12` – Individual conformation X in MOL2 format.

This structured approach ensures efficient data retrieval, compatibility with docking validation tools, and seamless RMSD analysis across different molecular modeling workflows.

2.4 Statistical Analysis of Benchmark Molecules

To better understand the composition and structural diversity of our dataset, we performed a statistical analysis focusing on problem-related molecular properties like heavy atom count

distribution, distinct atom types count distribution, and also combinatorial properties like automorphisms count distribution. The results provide a comprehensive overview of the dataset's characteristics, aiding in molecular modeling and cheminformatics applications.

Heavy Atom Count Distribution: As noted earlier, atom count significantly impacts the computational complexity of molecular comparison tasks. However, hydrogen atoms are typically omitted in RMSD calculations, making heavy atom count a more relevant metric. In our dataset, heavy atom counts range from 5 to 244, reflecting a wide range of molecular sizes. The majority of molecules, however, contain fewer than 50 heavy atoms, indicating a concentration of compact, chemically meaningful structures (Fig. 1).

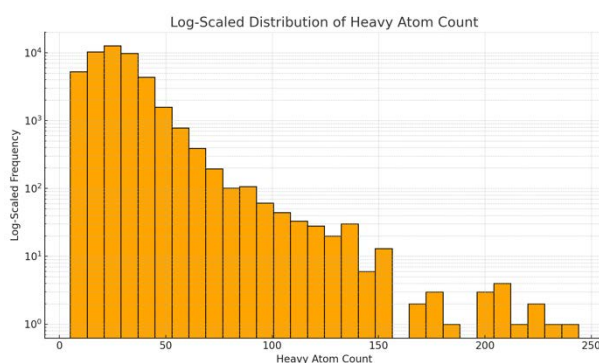


Fig. 1. Log-scaled distribution of heavy atom counts across the dataset.

Distinct Atom Types Count Distribution: While not as directly influential as total or heavy atom counts, the number of distinct atom types in a molecule can affect RMSD calculations by increasing the number of potential matching groups. In our dataset, this value typically ranges from 3 to 6, with a maximum of 8 (Fig. 2), reflecting a moderate yet meaningful degree of elemental diversity. This variation further supports the structural richness and chemical diversity of the dataset.

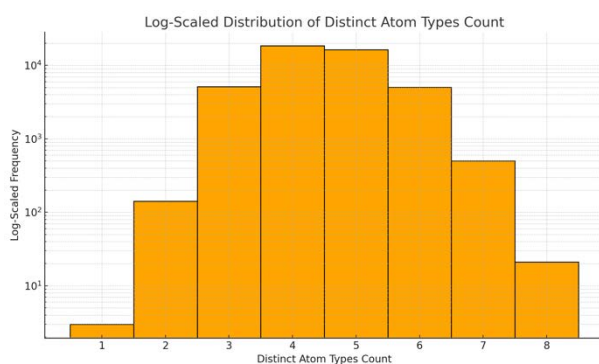


Fig. 2. Log-scaled distribution of distinct atom type counts across the dataset.

Automorphisms Count Distribution: We used the latest version (2.8.9) of the **dreadnaut** tool from nauty&Traces [9] toolset to quantify molecular symmetry. Graph representation files were generated for all molecular structures, which were then processed using **dreadnaut** to compute the number of automorphisms for each molecule. The resulting statistics are summarized in Fig. 3. Notably, a large portion of the dataset falls into the <2, 2–5, and 5–10 bins. Molecules with

moderate symmetry (10–100 automorphisms) form a secondary peak, while highly symmetric structures (over 1000 automorphisms) are rare.

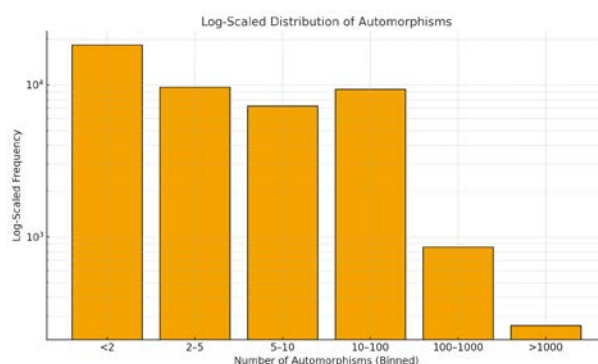


Fig. 3: Log-scaled distribution of the number of automorphisms across the dataset.

3. FlashRMSD Tool

3.1 Overview

The *FlashRMSD* tool is designed for efficient and robust symmetry-corrected RMSD calculations, supporting multiple molecular file formats including SDF, MOL, and MOL2, as well as files containing multiple conformations. It accommodates both standard and advanced use cases through a comprehensive set of configurable options.

The tool provides several key features:

- **Naïve calculation (-n flag):** Runs naïve search, by iterating over all permutations of possible matching atom groups. Can be used for results validation.
- **Hydrogen inclusion (-h flag):** Includes hydrogen atoms in RMSD calculations.
- **Bond order enforcement (-b flag):** Ensures strict bond order matching during atom mapping, preserving chemical integrity. This deterministic feature distinguishes *FlashRMSD* from other tools by enforcing chemically valid matches.
- **Verbose and assignment output (-v, -a flags):** Provides detailed runtime diagnostics and atom-to-atom assignment outputs for in-depth analysis.
- **Cross-RMSD calculation (-x flag):** Computes pairwise RMSD across all conformations within a single file, similar to the functionality of *obrms*.
- **Multi-query input support:** Allows a reference conformation (first structure in a template file) to be compared against all conformations in a query file, enabling batch comparison workflows.

3.2 Algorithm

FlashRMSD utilizes a two-stage approach that combines descriptor-based atom featurization with an optimized backtracking algorithm to achieve symmetry-aware atom mapping.

Stage 1: Atom Descriptor Generation

Each atom is encoded with a descriptor array created via breadth-first traversal of the molecular graph starting from that atom as a root. For each traversed atom, its periodic table number and the distance from the root atom are encoded into a single integer (descriptor) using the formula:

$$\text{DescriptorEncodedValue} = 2^{10} \cdot \text{distance} + \text{PeriodicTableNumber}$$

The resulting descriptor arrays for each atom are sorted and eventually hashed into a single integer. Hashing is used to avoid costly array comparisons; thus, any consistent function can be used. The encoding formula ensures that after sorting a descriptor array, descriptors from the same BFS (Breadth-First Search) layer occupy adjacent positions. This has the same effect as if we kept an array of descriptor arrays per distance from the root atom. In this way, a sorted descriptor array effectively encodes all level neighborhood information, and so does its hash. As these values encode BFS layers' information, we'll refer to them as **Layer Data**.

Although this stage has a complexity of $O(C \times N^2)$ (where C is the number of conformations and N the number of atoms), it lays the groundwork for efficient atom mapping. This approach becomes particularly advantageous during cross-RMSD calculations. In a standard RMSD comparison between two conformers, only two featurizations and one RMSD calculation are required. However, in cross-RMSD mode, the process involves C featurizations followed by $C(C - 1)/2$ RMSD computations. As the number of conformers increases, the computational load shifts from featurization to RMSD calculation, highlighting the importance of optimizing the latter.

Here's an example of how atom descriptors are generated for a single **O** atom of **SO₄** molecule (see Fig. 4).

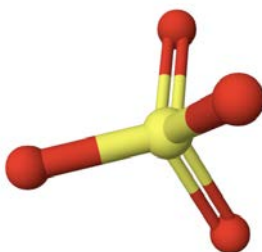


Fig. 4. **SO₄** molecule, with the sulfur atom shown in yellow and oxygen atoms in red.

During BFS traversal, we'll visit **O** atom at distance 0, **S** atom at distance 1, and 3 more **O** atoms at distance 2, thus **O** atoms descriptor will have the following value:

$$\text{hash}([0 + 8, 1024 + 16, 2048 + 8, 2048 + 8, 2048 + 8]) = 1428496640$$

Stage 2: Atom Mapping via Backtracking

The following algorithm is presented for mapping atoms between a pair of conformations, after the atom descriptor generation stage is completed for each:

- Candidate lists are generated for each atom in the first conformation based on descriptor matches.

- □ An optimized backtracking search is performed to determine the best atom-to-atom mapping, with the following optimization levels:
 - □ **Level 1:** Naive backtracking using all candidates.
 - □ **Level 2:** Trivial one-to-one matches are resolved and removed before backtracking to reduce complexity.
 - □ **Level 3 (default):** After excluding trivial matches, atoms are grouped into independent blocks using a Disjoint Set Union (DSU) based on descriptor matches or bonding. Each block is processed independently, and results are combined for the final mapping.

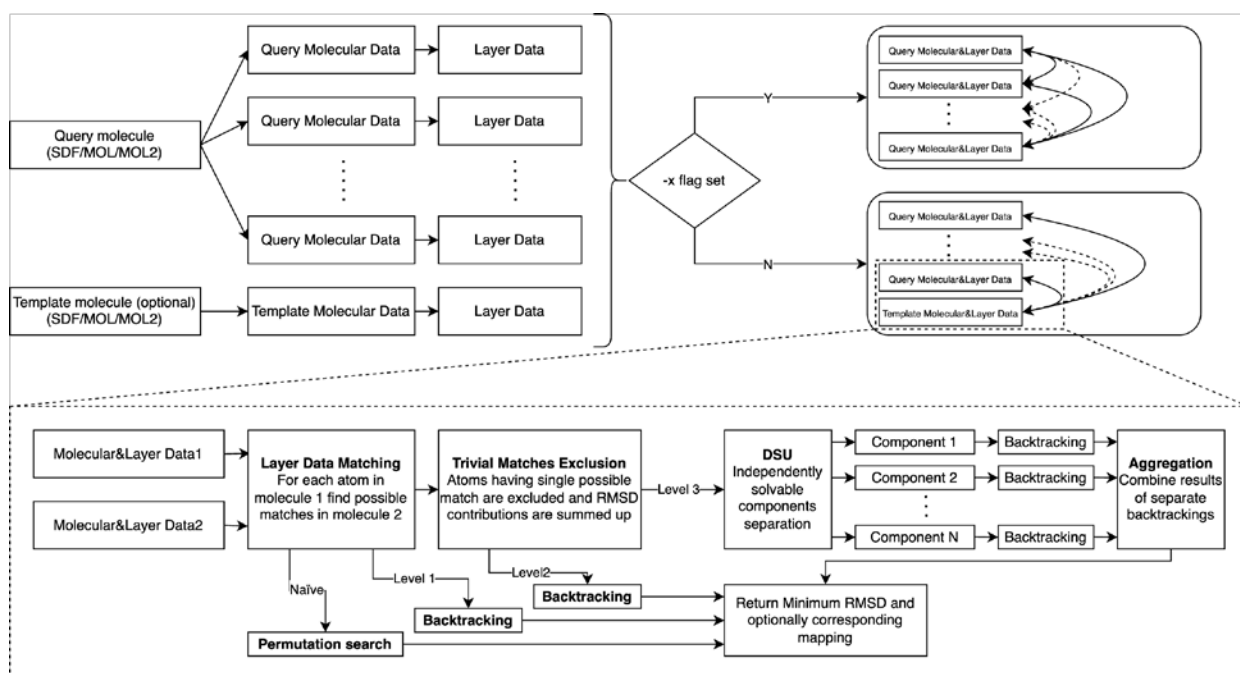


Fig. 5. Flowchart of the FlashRMSD Algorithm.

This flowchart illustrates the two main stages of the *FlashRMSD* algorithm (see Fig. 5). The first stage includes the atom featurization, where each atom's descriptor is generated through a breadth-first traversal and hashed to produce a unique fingerprint, and computation mode determination. The second stage depicts the pairwise mapping process: candidate list generation based on matching descriptors, followed by optimizations including trivial mapping exclusion and block decomposition, and finally, the backtracking procedure used to derive the optimal mapping.

4. Benchmark Setup

While RMSD is defined between two molecular conformations, in practical applications, especially within automated pipelines, it is usually computed across multiple conformations. For instance, in docking workflows, multiple binding poses are often generated and must be compared with each other to identify distinct clusters. This step typically precedes more expensive stages such as rescoring or molecular dynamics, making early-stage correctness and robustness crucial. Therefore, a more scalable interface for cross-RMSD calculations is often more important. Tools

that support efficient, reliable cross-RMSD interfaces better support real-world use cases such as clustering, redundancy filtering, and structural diversity analysis.

Additionally, when RMSD tools are used repeatedly or integrated into long-running workflows, even minor issues, such as memory leaks, crashes, or incorrect output, can propagate and cause significant downstream errors. Therefore, we argue that benchmarking tools on their cross-RMSD functionality is not only representative of real usage scenarios but also a more comprehensive test of tool robustness and interface design.

In our benchmarking, we consider two complementary setups:

1. **Cross-RMSD Native Benchmark** – Tools are tested on their ability to compute all-pair RMSD values across a set of poses through their native interface.
2. **All-to-All Pairs RMSD Benchmark** – Tools are also tested on computing the same RMSD matrix using repeated two-pose calls to simulate scenarios where no cross-RMSD interface is available.

Tools will be evaluated along three criteria:

- **Reliability:** Success rate across tasks, accounting for errors, crashes, indefinitely long runtime, or invalid outputs.
- **Correctness:** Agreement with reference calculations using naïve but accurate RMSD implementations.
- **Performance:** Execution time, measured only on cases where all tools succeed to ensure fair comparison.

This setup allows us to assess both the core computational correctness and the practical utility of RMSD tools in scalable scientific applications.

To ensure a fair and meaningful comparison across tools, we extended the functionality of *DockRMSD* in two key ways. First, we modified the tool to support cross-RMSD computation directly from a single multi-conformer input file. This significantly reduces the number of redundant pairwise calls and mitigates file I/O overhead, aligning *DockRMSD*'s interface more closely with tools like *obrms* and *FlashRMSD* that natively support cross-RMSD calculations.

Second, we addressed limitations in *DockRMSD*'s file parsing. The original implementation only supported a narrow subset of MOL2 files, rejecting valid inputs that deviated from expected formatting. We revised the file reading logic to accommodate a broader range of MOL2 variants by relaxing strict constraints and improving parser robustness. These changes eliminate unnecessary preprocessing steps and ensure compatibility with more diverse datasets, improving *DockRMSD*'s utility in real-world workflows.

The resulting extended version, supporting both cross-RMSD input handling and enhanced MOL2 compatibility, is referred to as *DockRMSDExt* in our benchmarks. This ensures that performance and reliability comparisons across tools reflect differences in computational design, rather than constraints imposed by tool interfaces or input formatting.

4.1 Benchmarking Environment and Tools

To ensure fair and reproducible comparison across RMSD calculation tools, all benchmarks were conducted on a consistent hardware and software environment with the following specifications:

- **CPU:** AMD EPYC 9654 96-Core Processor
- **RAM:** 504 GB DDR4
- **Operating System:** Ubuntu 22.04 LTS (64-bit)
- **Storage:** NVMe SSD
- **Python Version:** 3.12.9 (used for automation, validation, and timing)

Each benchmarking task was run as a separate process to avoid system-level interference, and wall-clock times were measured using Python-based orchestration scripts. All tools were tested using their latest stable versions, compiled with default settings where applicable.

We evaluated the following tools:

- **obrms**
- **FlashRMSD (Level 3)**
- **FlashRMSDNaive**
 - FlashRMSD tool with naïve flag set, iterates over all possible mappings after layer data matching (**Figure 5**)
- **DockRMSD**
- **DockRMSDExt**

In this benchmark, we exclude *spyRMSD* due to its prohibitively slow performance and prior evidence of inefficiency [1, 2], focusing instead on faster tools for runtime evaluation.

5. Results

5.1 Cross-RMSD Native Benchmark

This benchmark focuses on evaluating each tool’s capability to compute all-to-all RMSD values across multiple conformations of the same molecule using their native cross-RMSD interfaces, where available. This use case is central to workflows that require clustering or structural deduplication prior to downstream analysis or simulation.

As mentioned before, *DockRMSD* doesn’t provide a native interface for such calculations, thus, we’ll compare other tools against each other.

For this benchmark, each tool was provided with a single MOL2 file containing multiple conformations of the same molecule. The expected output was a complete pairwise RMSD matrix of size $N \times N$, where N is the number of conformations in the input. Only the upper triangular part (excluding the diagonal) was used for performance analysis, as RMSD matrices are symmetric. To assess correctness, outputs were compared against results from *FlashRMSDNaive*, which performs exhaustive symmetry correction without heuristics. Minor floating-point differences

were allowed within a predefined tolerance (0.001). Any discrepancies beyond this threshold were flagged and analyzed.

To prevent excessive runtimes from affecting the benchmark, a per-call timeout of 60 seconds was set. Any individual RMSD computation that exceeded this limit was recorded as a timeout failure. However, for naïve calculations, the timeout was set to 180 seconds.

Runtime was measured for successful runs only, using wall-clock time recorded externally via orchestration scripts. This benchmark isolates and evaluates tools specifically on their native ability to handle structured, multi-conformer input efficiently and correctly.

Out of 45,706 total samples, 45,543 were completed successfully across all tools. For the remaining 163 samples, only timeout-related failures were encountered—no runtime crashes or output corruption were observed. We also verified that all outputs from the tools were numerically identical for the successful cases.

Table 2. Runtime summary of symmetry-corrected RMSD calculation tools on cross-RMSD benchmark (45,543 samples)

Tool	Mean (s)	Std (s)	Min (s)	Max (s)
FlashRMSD	0.0137	0.0099	0.0041	0.4596
FlashRMSDNaive	0.0736	2.3091	0.0074	169.3351
DockRMSDExt	0.0510	0.8490	0.0043	55.0944
obrms	0.0571	0.7833	0.0206	47.0439

As shown in Table 2, *FlashRMSD* outperformed all other tools in terms of runtime, completing tasks approximately 4 times faster than its nearest competitor on average.

For the 163 samples where one or more tools failed, we analyzed the output of *FlashRMSD* on the same cases. Notably, *FlashRMSD* failed for only 7 samples, all of which also failed in other tools. For the remaining cases where only other tools failed, *FlashRMSD* completed successfully, and its output matched with the succeeding tools.

Table 3. FlashRMSD runtime on samples that failed in other tools.

Failed Tool	Number of failures	FlashRMSD runtime report		
		Mean (s)	Min (s)	Max (s)
FlashRMSDNaive	43	1.8886	0.0064	49.7958
DockRMSDExt	118	0.4810	0.0056	49.7958
obrms	36	2.3881	0.0063	49.7958

As seen in Table 3, *FlashRMSD* handled most of these challenging samples well, maintaining reasonable runtimes. However, a single outlier pushed its maximum runtime to 49.8 seconds, which was close to the timeout threshold. This suggests the tool is generally robust, with rare edge cases that may require monitoring.

5.2 All-to-All Pairs RMSD Benchmark

This benchmark evaluates the behavior and performance of RMSD calculation tools when used in pairwise mode, computing RMSD values between all unique pairs of conformations. Unlike the native cross-RMSD benchmark, this approach requires invoking the tool separately for each pose pair, simulating the fallback strategy often required by tools that lack native cross-RMSD support.

For a molecule with N conformers, this results in $N(N - 1)/2$ individual RMSD computations. All tools were orchestrated via automated scripts to execute these comparisons sequentially, and per-call runtimes were collected. For this benchmark, a timeout of 5 seconds per call was set; any computation exceeding this limit was considered a timeout failure.

The objectives of this benchmark are threefold:

- To enable a direct comparison with the original *DockRMSD*, which does not support native cross-RMSD and must operate in this mode by design.
- To evaluate robustness and failure rates across specific pairwise comparisons, especially in challenging edge cases.
- To identify and showcase individual pose pairs for which certain tools fail, providing insight into tool stability and error patterns.

All available tools, including those with native cross-RMSD support, were evaluated in this benchmark to ensure a uniform baseline for comparison. As in the cross-RMSD benchmark, *FlashRMSDNaive* was used as the reference for correctness verification.

Out of 45,706 total samples, 42,406 were successfully processed by all tools, including the original implementation of *DockRMSD*. However, when excluding *DockRMSD*, the number of successful samples increases to 45,558. This discrepancy is due to the file parsing limitations of the original *DockRMSD* implementation, as discussed earlier.

On all samples where any two tools produced results, their outputs were in agreement in terms of correctness. To evaluate whether our modified version—*DockRMSDExt*—can reliably replace *DockRMSD* in broader benchmarks, we compared the two implementations on the 42,406 samples that both completed successfully.

Table 4. Runtime comparison of DockRMSD and DockRMSDExt on all-to-all pairs benchmark (42,406 samples)

Tool	Mean runtime over all calls (s)	Mean of per-sample averages (s)	Std over all calls (s)	Std of per-sample averages (s)
DockRMSD	0.00573	0.00562	0.0439	0.0367
DockRMSDExt	0.00571	0.00560	0.0442	0.0368

As shown in Table 4, the runtime performance of *DockRMSD* and *DockRMSDExt* is nearly identical. In fact, the revised version is marginally faster on average. This indicates that the improvements to file parsing in *DockRMSDExt* do not introduce any runtime penalty, validating its use in place of the original implementation.

Moreover, the original *DockRMSD* failed on approximately 7% of the total dataset due to strict file parsing issues—failures that are fully resolved in *DockRMSDExt*. Therefore, we will use *DockRMSDExt* in all further benchmarks as a reliable and representative version of *DockRMSD*. We conducted the same benchmark as in the previous section, with one key difference: we evaluated both per-call runtimes across all pose pairs and per-sample average runtimes separately to capture different aspects of tool performance.

Table 5. Runtime summary of symmetry-corrected RMSD calculation tools on all-to-all pairs benchmark (1,458,326 pairs)

Tool	Mean (s)	Std (s)	Min (s)	Max (s)
FlashRMSD	0.00435	0.00176	0.00150	0.06144
FlashRMSDNaive	0.00557	0.06241	0.00164	4.93368
DockRMSDExt	0.00607	0.04947	0.00170	4.94237
obrms	0.02072	0.02414	0.01431	2.47477

As shown in Table 5, *FlashRMSD* consistently outperforms other tools in terms of runtime on this benchmark. Notably, the minimum runtime for *obrms* is significantly higher than the other tools, reflecting the inherent overhead associated with being part of a larger, more complex codebase.

A more comprehensive view of runtime distributions across all tools can be seen in Fig. 6, which presents the box-and-whisker plot of per-call runtimes for all 1,458,326 comparisons.

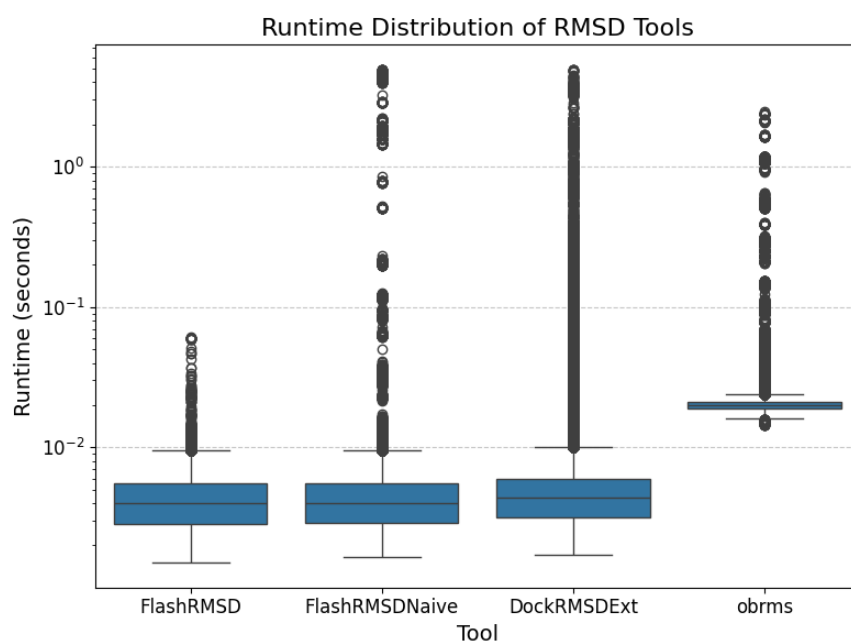


Fig. 6. Box and whiskers plot of runtimes of symmetry-corrected RMSD calculation tools (1,458,326 pairs)

Table 6. Per-sample average runtime summary of symmetry-corrected RMSD calculation tools on all-to-all pairs benchmark (45,558 samples)

Tool	Mean (s)	Std (s)	Min (s)	Max (s)
FlashRMSD	0.00435	0.00174	0.00162	0.04436
FlashRMSDNaive	0.00544	0.05885	0.00188	4.72553
DockRMSDExt	0.00593	0.04068	0.00191	3.50721
obrms	0.02063	0.02335	0.01563	2.38896

The results in Table 6 further support the conclusion that *FlashRMSD* outperforms other tools in terms of per-sample average runtime. This demonstrates that the complex atom featurization used in our algorithm, originally introduced to optimize cross-RMSD calculations, does not introduce any runtime overhead when applied to pairwise RMSD computations. On the contrary, *FlashRMSD* remains the most efficient across both benchmark modes.

Finally, there were 148 samples where one or more tools failed during the all-to-all pairwise benchmark. *FlashRMSD* failed on the fewest samples — 5 in total and consistent with previous results, all other tools also failed on those 5 samples.

Table 7. FlashRMSD runtime on pairs that failed in other tools.

Failed Tool	Number of failed samples	Number of failed pairs	FlashRMSD runtime report		
			Mean (s)	Min (s)	Max (s)
FlashRMSDNaive	40	1370	0.1530	0.0017	3.7507
DockRMSDExt	106	2932	0.0656	0.0018	3.7507
obrms	9	324	0.1101	0.0021	2.1288

As shown in Table 7, *FlashRMSD* handled these challenging samples successfully, maintaining reasonable runtime performance even in cases where other tools failed.

6. Case Studies

In this section, we’ll dive into benchmark results focusing on interesting molecules discussed in [1, 3], and also two new challenging examples identified during our current benchmarks.

CCD/PE3, CCD/33O

The molecules PE3 and 33O, previously discussed in [1], are known to consistently cause failures in the original *DockRMSD* implementation. Both structures consist of chains of alternating carbon and oxygen atoms, creating symmetric topologies that introduce multiple valid atom mappings during alignment.

These systems are particularly interesting because they expose limitations in tools that rely heavily on strict atom ordering or lack robust symmetry handling. In both cases, all tested tools, except for *DockRMSD*, successfully completed the RMSD calculation within the time limit. *DockRMSD* consistently exceeded the 5-second timeout, failing to return results.

Table 8. Comparison of RMSD calculation tools on DockRMSD breaking samples. Per-pair average runtimes are presented in seconds.

Tool	PE3 (per-pair average) (s)	33O (per-pair average) (s)
FlashRMSD	0.00282	0.00615
FlashRMSDNaive	0.00313	0.00563
obrms	0.02026	0.02033

As shown in Table 8, all successful tools returned results in a fraction of a second. The *FlashRMSD* and *FlashRMSDNaive* runtimes are nearly identical, but notably, *FlashRMSDNaive* performs slightly faster than the optimized implementation in the case of **33O**. This rare case emphasizes that while general optimizations are effective, atom featurization and initial pruning strategies are critical for performance consistency. Poorly suited heuristics or inadequate pruning, especially in highly symmetric cases, can lead to exhaustive search behavior even in otherwise optimized tools.

CCD/60C

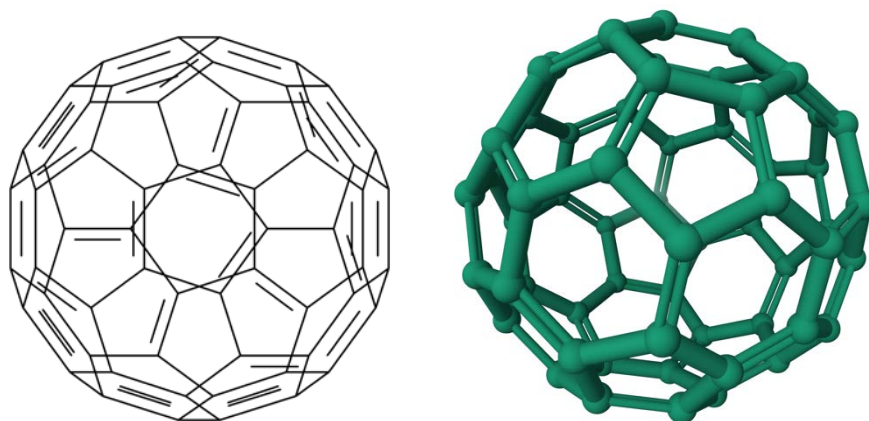


Fig. 7. 60C (buckminsterfullerene) molecules 2D (left) and 3D (right) structures.

The molecule **60C** (Fig. 7), previously analyzed in [3] for comparison between *DockRMSD* and *obrms*, serves as a valuable case for evaluating tool performance under extreme symmetry. Here, we extend the analysis by including benchmark results from the *FlashRMSD* and *FlashRMSDNaive* tools.

Structurally, **60C** features **12** pentagonal and **20** hexagonal faces arranged in a fullerene-like topology. A critical detail is that every edge of a pentagonal face is shared with a hexagonal face. This edge-sharing relationship creates a unique fingerprint for certain bonds; specifically, edges that bridge a pentagon and a hexagon are uniquely identifiable, as they cannot be matched to bonds lying solely between two hexagons.

As a result, when attempting to match two conformers of **60C**, any mapping that aligns a bond connecting a pentagon and a hexagon in the template must align with the corresponding bond in the reference. This significantly constrains the mapping space and leads to $2 \times 60 = 120$ possible

mappings — a manageable number, in contrast to estimates in [3]. However, the challenge lies in efficiently searching and pruning this space.

Despite this manageable mapping space, the *FlashRMSDNaive* tool failed to compute RMSD for any pose pairs, highlighting the limitations of exhaustive, non-pruned search methods in symmetric systems. The other tools, however, successfully completed the calculations and yielded the following average runtimes:

- *FlashRMSD*: 5.8 ms
- *DockRMSD*: 12.3 ms
- *obrms*: 37.6 ms

These results demonstrate that *FlashRMSD* outperforms both *DockRMSD* and *obrms*, achieving approximately **2** and **6.5** times better runtimes, respectively. The case of **60C** underscores the importance of efficient pruning and symmetry-aware mapping strategies, even in search spaces that are theoretically tractable. Without such optimizations, tools can still struggle or fail under the computational weight of redundant mappings.

BIRD/PRDCC_900031

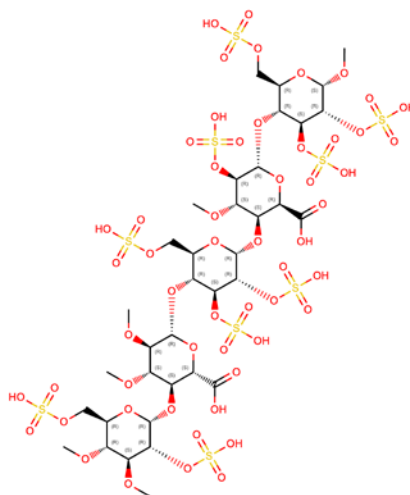


Fig. 8. PRDCC_900031 (heparin pentasaccharide) molecules 2D structure.

The molecule **PRDCC_900031** (Fig. 8) serves as a prime example where all key design features of the *FlashRMSD* tool contribute directly to performance. At a glance, the molecule appears to have a symmetric scaffold due to its ring-chain architecture and repetitive **SO₄** (sulfate) or **COOH** substituents. However, a closer inspection reveals that the core scaffold is not symmetric: the rings contain alternating carbon and oxygen atoms in a way that breaks symmetry.

Thanks to its advanced atom featurization, *FlashRMSD* is able to quickly detect this and identify a trivial atom mapping, effectively ruling out unnecessary branches during backtracking. This dramatically improves performance.

The real complexity arises from the nine **SO₄** and two **COOH** groups attached to the leaf atoms of the backbone. Each **SO₄** group can be matched in 3! (6) different ways, and each **COOH** group can be matched in 2! (2) ways, leading to a theoretical explosion of $2^2 6^9 = 40,310,784$

possible mappings across the entire molecule. While other tools treat this as a flat, unstructured mapping problem, *FlashRMSD*'s level-3 optimization decomposes the problem: each symmetrical group mentioned above is treated as an independent subtree, allowing mappings to be computed separately and then combined. This reduces the mapping search space from 2^{26^9} to just $2 \times 2 + 9 \times 6 = 58$ evaluations, a drastic and principled reduction.

All other tools failed to compute cross-RMSD in a reasonable time. *FlashRMSDNaive*, despite correctly accounting for symmetry, was forced to iterate through the full 2^{26^9} mappings, completing in 46.9 seconds. In contrast, *FlashRMSD* completed the same calculation in just 8.9 milliseconds, clearly demonstrating the power of intelligent symmetry decomposition.

We also evaluated all-to-all pairwise RMSD performance. *DockRMSD* succeeded on only 4 out of 36 pairs, while *obrms* failed on all. This case illustrates that clever partitioning of symmetric substructures can make the difference between exponential runtime and milliseconds.

CCD/7AZ, CCD/FWQ

These molecules are special because, independently, they managed to fit into a 5-second window, but in the cross-RMSD benchmark, the total runtime was bigger than 60 seconds. They both have a similar structure and represent a special case of symmetries – a big macrocycle with trailing similar components from macrocycle nodes. These kinds of samples are the subject of investigation as how they can be effectively analyzed.

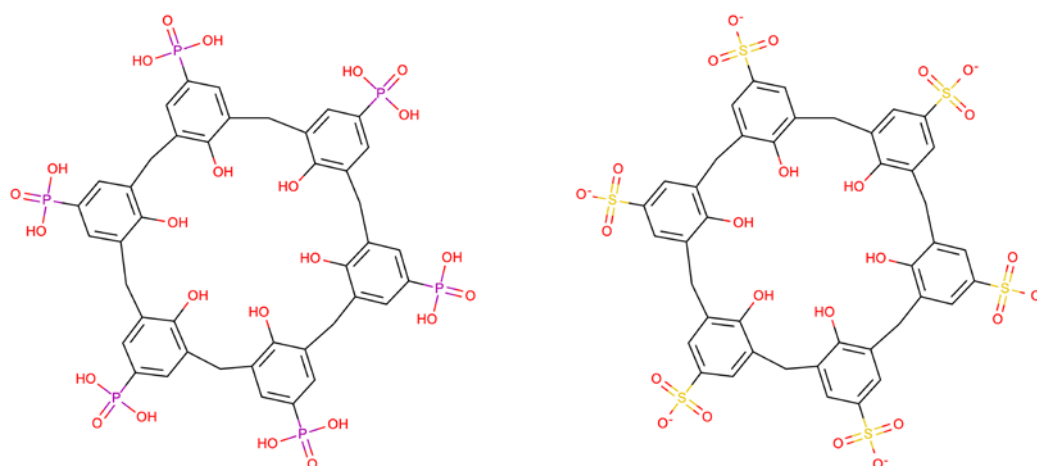


Fig. 9. 7AZ (left) and FWQ (right) molecules 2D structures.

Fig. 9 shows that both molecules share a common motif: a large macrocyclic core with branching, symmetry-repeating fragments extending from multiple macrocycle nodes. These fragments exhibit local similarity, but are distributed across the molecular structure in ways that significantly increase the number of potential atom mappings. These examples suggest a new class of test cases that require new approaches in future RMSD tools.

7. Conclusions

This work presents *FlashRMSD*, a symmetry-corrected RMSD calculation tool designed for accuracy, efficiency, and robustness in both standalone and large-scale automated workflows. Alongside *FlashRMSD*, we introduce a comprehensive benchmark dataset comprising thousands of molecular pose comparisons, specifically structured to evaluate tool performance under realistic and challenging scenarios.

Through systematic benchmarks, including native cross-RMSD calculations and all-to-all pairwise comparisons, we demonstrate that *FlashRMSD* consistently outperforms existing tools in terms of runtime, reliability, and correctness. It exhibits superior scalability, maintaining low variance across diverse molecular structures, and handles failure-prone or highly symmetric cases with resilience. Importantly, the optimizations introduced for cross-RMSD efficiency do not introduce overhead in simpler pairwise use cases.

Our benchmark suite also highlights structural motifs that pose challenges to current RMSD tools, such as highly symmetric systems, macrocyclic architectures, and molecules with repetitive substructures or symmetric side chains. These special cases, analyzed in detail, provide insight into where existing tools struggle and where future development should focus.

We make both *FlashRMSD* and the full benchmark dataset publicly available to facilitate reproducible evaluation and guide future development of RMSD tools. We hope this contribution will support more reliable and scalable structural comparison workflows in molecular modeling, docking, and related fields.

Appendix

Data and Code Availability

The benchmark dataset developed for this study is publicly available via Zenodo at <https://doi.org/10.5281/zenodo.15097621>. It includes over 45,000 small molecules from the CCD and BIRD repositories, complete with multi-conformer and per-pose files, as well as a results.csv file containing ground truth cross-RMSD values.

The source code for the *FlashRMSD* tool, along with the modified tool *DockRMSDExt*, is available on GitHub at <https://github.com/altunyanv/FlashRMSD>. Both the dataset and the code are released under open-source licenses to facilitate reproducibility and further development in symmetry-corrected RMSD calculations.

References

- [1] V. Altunyan, “Comparative analysis of symmetry corrected rmsd calculation tools in molecular docking”, *Vestnik RAU*, vol. 1, pp. 25-36, 2024.
- [2] R. Meli and P. C. Biggin, “syrmsd: symmetry-corrected RMSD calculations in Python”, *Journal of Cheminformatics*, vol. 12, no. 49, 2020. <https://doi.org/10.1186/s13321-020-00455-2>

- [3] E.W. Bell and Y. Zhang, “DockRMSD: an open-source tool for atom mapping and RMSD calculation of symmetric molecules through graph isomorphism”, *Journal of Cheminformatics*, vol. 11, no. 40, 2019. <https://doi.org/10.1186/s13321-019-0362-7>
- [4] N. M. O’Boyle, M. Banck, C.A. James, C. Morley, T. Vandermeersch and C. R. Hutchison, “Open Babel: An open chemical toolbox.”, *Journal of Cheminformatics*, vol. 3, no. 33, 2011. <https://doi.org/10.1186/1758-2946-3-33>
- [5] J. D. Westbrook, C. Shao, Z. Feng, M. Zhuravleva, S. Velankar and J. Young, “The chemical component dictionary: complete descriptions of constituent molecules in experimentally determined 3D macromolecules in the Protein Data Bank”, *Bioinformatics*, vol. 31, no. 8, pp. 1274–1278, 2015.
- [6] RDKit: Open-source cheminformatics. [Online]. Available: <https://www.rdkit.org>
- [7] P. Tosco, N. Stiefl, G. Landrum, “Bringing the MMFF force field to the RDKit: implementation and validation”, *Journal of Cheminformatics*, vol. 6, no. 37, 2014. <https://doi.org/10.1186/s13321-014-0037-3>
- [8] D. R. Koes, M.P. Baumgartner and C.J. Camacho, “Empirical scoring with smina from the CSAR 2011 benchmarking exercise”, *Journal of Chemical Information and Modelling*, vol. 53, pp. 1893-1904, 2013.
- [9] B.D. McKay and A. Piperno, “Practical graph isomorphism, II”, *Journal of Symbolic Computation*, vol. 60, pp. 94-112, 2014.

FlashRMSD . Արդյունավետ մոտեցում սիմետրիայով ճշգրտված RMSD հաշվարկի համար և համապարփակ բենչմարք վերլուծություն

Վահագն Ն. Ալթունյան

Երևանի պետական համալսարան, Երևան, Հայաստան
e-mail: altunyanv@gmail.com

Ամփոփում

Արմատ միջին քառակուսային շեղումը (RMSD) առանցքային չափում է մոլեկուլային կառուցվածքների նմանությունը գնահատելու համար: Սակայն սիմետրիկ մոլեկուլների դեպքում առաջանում են կոմբինատոր բարդություններ, որոնք խանգարում են հաշվարկի գործընթացին: Թեպետ հասանելի են մի շարք գործիքներ, որոնք RMSD-ի հաշվարկում հաշվի են առնում սիմետրիաները, բոլորն էլ ունեն իրենց սահմանափակումները՝ կապված արագության, ճշգրտության կամ կիրառելիության

հետ: Այս հոդվածում մենք ներկայացնում ենք FlashRMSD գործիքը՝ նոր, արագ և արդյունավետ մոտեցում սիմետրիայով ճշգրտված RMSD հաշվարկի համար: Բացի այդ, մենք ներկայացնում ենք մոլեկուլային կառուցվածքների բազա RMSD գործիքների գնահատման և գործող մեթոդների համեմատական վերլուծության համար:

Բանալի բառեր՝ սիմետրիայով ճշգրտված RMSD, FlashRMSD, մոլեկուլային դոկինգ:

FlashRMSD: Эффективный подход к вычислению RMSD с учётом симметрии и расширенный бенчмарковый анализ

Ваагн Н. Алтунян

Ереванский государственный университет, Ереван, Армения
e-mail: altunyanv@gmail.com

Аннотация

RMSD является важным показателем для оценки сходства молекулярных структур. Однако при работе с сильно симметричными молекулами возникают комбинаторные сложности, которые затрудняют процесс вычислений. Хотя существует ряд инструментов с открытым исходным кодом для вычисления RMSD с учетом симметрии, каждый из них имеет ограничения по скорости, точности или удобству использования. В данной статье мы представляем FlashRMSD — новый, быстрый и эффективный метод вычисления RMSD с учетом симметрии. Также мы представляем обширный набор молекулярных структур для оценки инструментов вычисления RMSD и проводим сравнительный анализ существующих методов с нашим решением.

Ключевые слова: RMSD с коррекцией симметрии, FlashRMSD, молекулярный докинг.

Կանոններ հեղինակների համար

ՀՀ ԳԱԱ ԻԱՊԻ «Կոմպյուտերային գիտության մաթեմատիկական խնդիրներ» պարբերականը տպագրվում է 1963 թվականից: Պարբերականում հրատարակվում են նշված ոլորտին առնչվող գիտական հոդվածներ, որոնք պարունակում են նոր՝ չհրատարակված արդյունքներ:

Հոդվածները ներկայացվում են անգլերեն՝ ձևավորված համապատասխան «ոճով» (style): Հոդվածի ձևավորման պահանջներին ավելի մանրամասն կարելի է ծանոթանալ պարբերականի կայքէջում՝ <http://mpcs.sci.am/>:

Rules for authors

The periodical “Mathematical Problems of Computer Science” of IIAP NAS RA has been published since 1963. Scientific articles related to the noted fields with novel and previously unpublished results are published in the periodical.

Papers should be submitted in English and prepared in the appropriate style. For more information, please visit the periodical's website at <http://mpcs.sci.am/>.

Правила для авторов

Журнал «Математические проблемы компьютерных наук» ИПИА НАН РА издается с 1963 года. В журнале публикуются научные статьи в указанной области, содержащие новые и ранее не опубликованные результаты.

Статьи представляются на английском языке и оформляются в соответствующем стиле. Дополнительную информацию можно получить на веб-сайте журнала: <http://mpcs.sci.am/>.

The electronic version of the periodical “Mathematical Problems of Computer Science” and rules for authors are available at

<http://mpcs.sci.am/>

Phone: (+37460) 62-35-51
Fax: (+37410) 28-20-50
E-mail: mpcs@sci.am
Website: <http://mpcs.sci.am/>

Ստորագրված է տպագրության՝ 23.05.2025

Թուղթը՝ օֆսեթ:

Հրատարակված է ՀՀ ԳԱԱ Ինֆորմատիկայի և ավտոմատացման
պրոբլեմների ինստիտուտի կողմից
Ծավալը՝ 103 էջ: Տպաքանակը՝ 100
ՀՀ ԳԱԱ ԻԱՊԻ Համակարգչային պոլիգրաֆիայի լաբորատորիա
Երևան, Պ. Սևակի 1
Հեռ. +(374 60) 623553
Գինը՝ անվճար

Подписано в печать 23.05.2025

Офсетная бумага.

Опубликовано Институтом проблем
информатики и автоматизации НАН РА

Объём: 103 страниц. Тираж: 100

Лаборатория компьютерной
полиграфии ИПИА НАН РА.

Ереван, П. Севака 1

Тел.: +(374 60) 623553

Цена: бесплатно

Signed in print 23.05.2025

Offset paper

Published by the Institute for
Informatics and Automation
Problems of NAS RA

Volume: 103 pages

Circulation: 100

Computer Printing Lab
of IIAP NAS RA

Yerevan, 1, P. Sevak str.

Phone: +(374 60) 623553

Free of charge